

2022

ACOUSTIC AND OPTICAL IMAGING TECHNIQUES FOR CHARACTERIZING ANIMAL DISTRIBUTIONS IN THE PELAGIC OCEAN

Benjamin Grassian
University of Rhode Island, bgrassian@gmail.com

Follow this and additional works at: https://digitalcommons.uri.edu/oa_diss

Recommended Citation

Grassian, Benjamin, "ACOUSTIC AND OPTICAL IMAGING TECHNIQUES FOR CHARACTERIZING ANIMAL DISTRIBUTIONS IN THE PELAGIC OCEAN" (2022). *Open Access Dissertations*. Paper 1381.
https://digitalcommons.uri.edu/oa_diss/1381

This Dissertation is brought to you by the University of Rhode Island. It has been accepted for inclusion in Open Access Dissertations by an authorized administrator of DigitalCommons@URI. For more information, please contact digitalcommons-group@uri.edu. For permission to reuse copyrighted content, contact the author directly.

ACOUSTIC AND OPTICAL IMAGING TECHNIQUES FOR
CHARACTERIZING ANIMAL DISTRIBUTIONS IN THE PELAGIC OCEAN

BY

BENJAMIN GRASSIAN

A DISSERTATION SUBMITTED IN PARTIAL FULFILLMENT OF THE
REQUIREMENTS FOR THE DEGREE OF
DOCTOR OF PHILOSOPHY
IN
OCEANOGRAPHY

UNIVERSITY OF RHODE ISLAND

2022

DOCTOR OF PHILOSOPHY DISSERTATION
OF
BENJAMIN GRASSIAN

APPROVED:

Dissertation Committee:

Major Professor Chris Roman

Melissa Omand

Lora Van Uffelen

Karen Wishner

Brenton DeBoef

DEAN OF THE GRADUATE SCHOOL

UNIVERSITY OF RHODE ISLAND

2022

ABSTRACT

Biological processes in midwater habitats—ocean areas between the sunlit surface layers and seafloor—are critical drivers of ocean biogeochemical cycling, oxygen availability, fish population dynamics, and ecological interactions over a wide range of scales. Achieving high-resolution observations of the environmental and biological heterogeneity in the ocean’s interior is important for understanding the status and evolution of the earth system at large. Traditional ocean sampling platforms (e.g. net systems, moored and shipboard sensors), are often unable to resolve marine biota at fine (cm-m) scales and over submesoscale (sub-km to kms) survey areas comparable to the relevant variability in their physical environment. Shipboard mounted acoustic echosounders are commonly used to resolve biological data in the open ocean but record coarse measurements below 300m depth, due to acoustic attenuation, and do not collect matching environmental data. Existing towed sensor platforms are limited in their spatial and temporal resolutions due to constraints from tow cable dynamics, and autonomous platforms such as AUVs and gliders are often limited by their speed and endurance.

The development of sensor-based field surveys that can achieve concurrent biological and environmental measurements over large sampling spaces at fine scales allows for improved characterization of these ecosystems. Studies employing these modern survey tools have shown that biological assemblages in marine ecosystems are often characterized by extreme spatial and temporal heterogeneity, and respond to fine environmental gradients, submesoscale physical processes (e.g. eddies, fronts, and internal waves), diel rhythms, and ephemeral opportunities for resource exploitation. This thesis work seeks to both derive techniques supporting the use of new imaging and acoustic sensor platforms to achieve detailed biological-environmental coupled datasets and to use the data to assess the linkages between

animal habits and local hydrography in diverse midwater habitats. Collectively the results from this project will help to further the technology-enabled exploration of the vast but difficult to observe midwater habitat and will contribute several novel characterizations of biological-environmental coupled dynamics in diverse epi and mesopelagic ecosystems.

ACKNOWLEDGMENTS

My graduate school journey has been long, strange, and challenging. When deciding to pursue an 'interdisciplinary' project, I had been warned that it would be easy for me to 'fall through the cracks.' With the help of my advisor, committee, colleagues and friends, I was able to not only get what I came for but conduct work that I am deeply curious and passionate about. In the end I feel extremely fortunate for the circuitous path that led to this work.

Chris Roman took a chance on me and has had my back ever since. He is someone I can easily look up to for both his professional and personal accomplishments. He is a visionary, with a vast skillset and broad intellectual bandwidth. He is also a great person with a lovely family. I am grateful for his commitment to me, as he has many people and projects that rely on him. I am grateful for the unique perspective into the oceans he offered me. Without him none of this work would have been possible.

I want to acknowledge my labmates, Kris Krasnosky and Dave Casagrande. They have been with me throughout my PhD journey. They each have contributed to my work and expanded my perspective in immeasurable ways. They are brilliant and unique people. I admire their playfulness and I enjoyed getting to join in on the many serious and less serious projects they undertook.

I am grateful for Melissa Omand, who has been a strong supporter of me during my time at URI. She is a researcher whose creativity and understanding of the oceans I aspire to. She has always been gracious in offering me a place to talk through my work, and her collaboration significantly expanded the results of my projects. She went above and beyond to assist me, and I learned a great deal from working alongside her. I am enormously grateful for her support and friendship.

Joe Warren and Lora Van Uffelen both provided me a jumpstart into the

acoustics world. Joe helped me crack open the Wire Flyer acoustic data, and his collaboration propelled us forward and helped us navigate through some hairy acoustic questions. Lora Van Uffelen is a wonderful teacher who provided me training in acoustics theory and who worked with me over the summer, helping get me out the door. I am very grateful she was able to join my committee and she has been an amazing resource for me during my last few years here.

Karen Wishner and Dawn Outram got me started in zooplankton work at URI. I loved spending time on the microscope with Dawn and learning zooplankton IDs. Karen has been a supporter of my work throughout my time here and I am grateful for her valuable perspective and expansive knowledge of the deep sea.

I want to thank all my friends aboard the E/V Nautilus. Working on the E/V Nautilus opened up the deep sea to me and was some of the most rewarding and fun times I had in graduate school. I am forever grateful for my Nautilus friends and mentors, like Renny, Trevor, Nicole, and Jess, and many more.

I also want to thank Lars N. Anderson and Kelly Benoit-Bird, both researchers who I admired from afar. Towards the end of my work, I was lucky enough to have conversations with them that helped contextualize my work and empowered me in my approaches. Lars helped me greatly to decode the spectral information from the system, which I am eager to explore further.

Lastly, I want to thank my friends and family. My partner Al and my friends like Corinne, Steph, and Natali have brought so much joy in to my life. They have always believed in me. I am lucky to have such good people in my life. My dad and my sister Alex helped me realize my interest in the sciences and have been constant supporters of me. I would like to also acknowledge my cat Buckley, my best companion who has been by my side since my undergraduate years in Miami. She is a fiercely loyal companion who brings love into my life everyday.

PREFACE

This dissertation is arranged in manuscript format and is presented as 3 chapters. **Chapter 1** focuses on establishing stereo image processing methods to describe the occurrence and evolution of a thin layer formed by the pelagic red crab, *Pleuroncondes planipes* from data collected in the eastern Tropical Pacific oxygen minimum zone offshore of Baja California, Mexico in Jan/ Feb 2018. This species is abundant in pelagic habitats throughout the eastern Pacific, with an estimated biomass of 215,000 - 611,000 metric tonnes supporting ecologically and commercially important oceanic predators including sharks, tunas, whales, and squids. *Pleuroncondes planipes* has both pelagic and benthic phases partitioned by life cycle stage. Pelagic populations can often be found in dense swarms at the surface or in midwaters, with variable diel habits and apparent vertical migration patterns suggested from net tow abundances that have not been observed in detail. Using in situ optical and environmental measurements, this project derives detailed characterization of a *P. planipes* thin layer and its rapid dispersal. The hypothesis that the thin layer distribution and dispersal corresponded to the location and timing of environmental and ecological features was investigated. Analysis of the crab thin layer contributes new understanding of the short-lived and rapid migration behaviors of *P. planipes* in their pelagic phase, and shows dispersal timing linked to the migration timing of a specific deep (400-500m) scattering layer. The chapter 1 analysis shows the coupling of the crab thin layer to a locally stratified isopycnal with an internal wave propagating through it, and also demonstrates alteration to the water column stratification distribution corresponding to the arrival of the deep migrating layers and crab thin layer dispersal. Collectively this work contributes new understanding of the pelagic habits of *P. planipes*, a first documentation of a micronekton aggregation meeting thin layer criteria, and suggests alteration to the

epi-pelagic physical and ecological structure over short (instantaneous to 2 hour) time intervals.

Chapter 2 sought to develop a new methodology to collect detailed concurrent hydrographic and acoustic sections in the midwater environment (0-1000 meters) with the Wire Flyer profiling vehicle and a dual-frequency split-beam echosounder (Simrad EK80 with 70 and 200 kHz transducers) . The Wire Flyer is able to provide high-resolution repeat profiling (0-2.5 m/sec up and down velocity) within specified water column depth bands (typically 300-400 m) and is controlled by a topside connection to an acoustic modem for up/down link communications. A unique aspect of the echosounder on this platform is the decision to have the transducers pointed lateral to the vehicle's movement, as opposed to the more traditional downward (or upward) transducers on ships and most other systems. An advantage of the side-looking arrangement is that the data being collected are orthogonal to the movement of the platform which provides collection of third-dimension data as the vehicle moves forward and vertically. A main objective of this chapter was to collect, process, and analyze 3-dimensional acoustic data with expectations that coherent scattering layers and patches would be resolved and demonstrate varying associations with the environmental sections.

This project provided initial characterization of the acoustic data collected by the system (noise floor, interference sources, diverging per-element power trends, and range-dependent trends) and implemented techniques to remove these sources of noise and power trends. From the derived data, submesoscale oceanographic phenomenon were visualized in detail showing coupling between fine scale horizontal oxygen gradients and biological distributions, scatterer distributions partitioned across a shallow water front, and coherent athwartship biological and gas plume patches. This work has proven the systems capabilities for simultaneously

recording biological and environmental information in the 0 to 1000 m region.

Chapter 3 of the dissertation implements techniques to quantify scattering layers acoustically in Wire Flyer sections for the purpose of defining biological assemblages and describing their submesoscale distributions within the environment. The methods for this chapter focus largely on implementing a detection routine for scattering layers and singles targets exploiting the side-looking acoustic aspect and statistical analysis of detected scattering layers. The analysis of thin layer shapes examined the extent to which planktonic thin layer shapes reflect the vertical adjacency of phytoplankton and zooplankton assemblages, as has been shown previously. Regression analysis identified environmental features influencing the distribution of the 70 and 200 kHz acoustic scattering layers, contributing insights into differing ecological zonation in the midwater habitat among the functional groups, and offering statistical analysis of the signal fidelity of the acoustically derived biological metrics. Modeling approaches were used to simulate the side-looking data and describe potential mechanisms for the observed profile layer shapes. Collectively this leverages the Wire Flyer datasets to perform analysis of scattering layer distributions and the influence of environmental variables that will further understanding of animal habits within the midwater environment.

Table 1. Summary of field work for datasets used in the thesis. The related figures are marked in the last ‘figures’ column

Main Platform	Secondary	Ship	Start Date (UTC)	End Date (UTC)	Start Lat Lon	End Lat Lon	Figures
Stereo Camera	Shipboard EK60	R/V <i>Sikuliaq</i>	31-Jan-2017-20:25:47	31-Jan-2017-22:15:10	21.435, -117.591	21.435, -117.591	1-8
Stereo Camera	Shipboard EK60	R/V <i>Sikuliaq</i>	31-Jan-2017-23:26:10	01-Feb-2017-01:03:17	21.435, -117.591	21.435, -117.591	1-8
Wire Flyer EK80	None	R/V <i>Atlantis</i>	03-Nov-2018-00:03:22	03-Nov-2018-09:47:16	8.846, -84.211	8.998, -84.462	21
Wire Flyer EK80	None	R/V <i>Falkor</i>	20-Jan-2019-04:16:20	20-Jan-2019-09:55:50	5.161, -87.423	4.971, -87.420	12
Wire Flyer EK80	Shipboard EK60	R/V <i>Falkor</i>	24-Jan-2019-02:10:45	24-Jan-2019-14:58:27	8.494, -85.454	9.144, -85.440	18
Wire Flyer EK80	Towfish EK60	R/V <i>Endeavor</i>	23-Sep-2019-23:12:50	24-Sep-2019-11:56:07	37.989, -73.891	37.994, -73.862	12,13,16-18,20,22-24

TABLE OF CONTENTS

ABSTRACT	ii
ACKNOWLEDGMENTS	iv
PREFACE	vi
TABLE OF CONTENTS	x
LIST OF FIGURES	xv
LIST OF TABLES	xxiii

MANUSCRIPT

1 Multi-Sensor Observation of a Rapidly Dispersing Micronekton Thin Layer	1
1.1 Abstract	2
1.2 Introduction	2
1.3 Materials and procedures	5
1.3.1 Data collection	5
1.3.2 Stereo image processing	6
1.3.3 Acoustic data	8
1.3.4 Buoyancy frequency analysis	8
1.4 Results	9
1.4.1 Coverage and imaging results:	9
1.4.2 Thin layer distribution	9
1.4.3 Thin layer dissociation	10
1.4.4 Acoustic scattering layers	11
1.4.5 Evidence for scattering layer compositions	12

	Page
1.5 Discussion	13
1.5.1 Micronekton thin layer evolution	13
1.5.2 Rapid dispersion and migration event	13
1.5.3 Camera avoidance	14
1.5.4 Applications and improvements of image processing methods	15
1.6 Conclusions	16
1.7 Figures	16
List of References	24
2 High resolution measurements of the epi- and mesopelagic ocean by a profiling vehicle equipped with environmental sensors and a broadband echosounder	27
2.1 Abstract	28
2.2 Introduction	29
2.3 Materials and procedures	32
2.3.1 Echosounder integration	33
2.3.2 Echosounder data processing	36
2.3.3 Acoustic scattering layers as recorded in the horizontal .	39
2.3.4 Concurrent shipboard echosounding	39
2.4 Assessment	40
2.4.1 Tracking diel migration	41
2.4.2 Shallow water front	42
2.4.3 Oxygen minimum zone vertical boundaries	44
2.4.4 Cold seep plume	44

	Page
2.5 Discussion	45
2.5.1 Echosounder calibration	45
2.5.2 Pressure effects on transducers	46
2.5.3 Echosounder orientation and scatterer directivity	47
2.6 Summary	48
2.7 Figures	49
List of References	61
3 Diverse Biological Information from Side-Looking Acoustic Survey Data with Concurrent Hydrographic Measurements in the Pelagic Ocean	69
3.1 Introduction	70
3.2 Materials and Procedures	73
3.2.1 Wire Flyer Profiling Vehicle	73
3.2.2 Baltimore Canyon Survey	74
3.2.3 Model Side-Looking Echosounder Pings	74
3.2.4 2D Metric for Scattering Layers	75
3.2.5 Edge Layer Shapes from Benoit Bird et al. 2009	76
3.2.6 1D Phytoplankton Model	77
3.2.7 Multivariate Linear Regression Models	78
3.2.8 Run Length Analysis	79
3.3 Assessment	80
3.3.1 Model Side-Looking Echosounder Ping Results	80
3.3.2 2D Metric for Scattering Layer Results	81
3.3.3 Edge Layer Shape Metric Results	82

	Page
3.3.4 1D Phytoplankton Model Results	83
3.3.5 Multivariate Linear Regression Model Results	83
3.3.6 Run Length Distributions	84
3.4 Discussion	84
3.4.1 Aspects of the Custom Metric	84
3.4.2 Efforts to Assess Layer Shapes	86
3.4.3 Environmental Predictors of the Scattering Layer Distri- butions	86
3.4.4 Interpretation of Run Length Data	87
3.4.5 Taxonomic Information	88
3.4.6 Spectral Information and System Noise	88
3.5 Summary	89
3.6 Acknowledgments	90
3.7 Figures	91
List of References	103

APPENDIX

.1 Appendix	108
.1.1 Chapter 1 Software Overview	108
.1.2 Ch1 Lighting Normalizations	108
.1.3 Ch1 Strobe illumination decimation	109
.1.4 Ch1 Ambient illumination decimation	111
.1.5 Ch1 Image Segmentation	111
.1.6 Ch1 Feature Detection	114

	Page
.1.7 Ch1 Stereo Matching and Definition of Paired Regions of Interests	114
.1.8 Ch1 Manual Identification and Data Processing	115
.1.9 Chapter 2 Software Overview	115
List of References	126
BIBLIOGRAPHY	127

LIST OF FIGURES

Figure		Page
1	Survey location offshore of Baja California, Mexico	17
2	Stereo camera profiling system. A) Schematic showing the side-looking stereo imaging volume. B) The stereo camera profiling system on deck.	17
3	Example stereo matched and segmented Regions of Interest (ROI) from an image pair inside the crab thin layer. The top panel shows processed stereo matching information for the right and left camera. The bottom panel shows a single bounded Region of Interest (bottom left) and detected keypoint features used for stereo matching (bottom right).	18
4	Example segmented image regions with taxonomic details. A) Segments identified as <i>Pleuroncondes planipes</i> representative of the variability in animal orientation and behavior. Detected animals ranged from 1.2 to 4.8 m distances from the camera. B) Example segmented image regions capturing other broadly identifiable taxa, including: a cestid ctenophore, copepods, shrimp, cydippid and beroe ctenophores, chaetognaths, polychaete worms, medusae, and fishes.	19

5	Measurements from sequential stereo camera profiling overlaid on 120 kHz acoustic scattering volume recorded from a ship-board echosounder. A) Stereo image profile paths for two sequential deployments as white line plots overlaid on 120 kHz Sv echogram with 5dB contours highlighting discrete acoustic scattering layers. Black rectangles define data subsets plotted in lower panels. B) Mean <i>Pleuroncondes planipes</i> abundance per imaging volume from bins of four image pairs shown as bubble plot size overlaid on 120 kHz Sv echograms for the midday imaging profile and C) repeated profiling over dusk. D) Chlorophyll-a fluorescence recorded by stereo camera profiler with <i>Pleuroncondes planipes</i> mean abundance data from imagery and Sv 8dB contours for midday profile and E) repeated profiling over dusk. D, E) <i>Pleuroncondes planipes</i> mean abundance from binned imaging data with Chlorophyll fluorescence data and 120 kHz Sv contours. F) Proportion of <i>Pleuroncondes planipes</i> individuals defined as vertically swimming from the mean ROI aspect ratio plotted as the color fill of the the abundance bubble plots and overlaid on the 120 kHz Sv contours for the midday profile, and G) repeated profiling. H) <i>Pleuroncondes planipes</i> abundances derived from the raw imaging sequence over time for for the midday profile subset and I) the repeating profiling at dusk.	20
6	Buoyancy frequency (N2) plotted against density with crab abundance information shown as bubble plots and color for camera profiles during repeat profiling at dusk	21
7	Maximum crab abundance per profile versus buoyancy frequency at the depth of the maximum crab abundance depth.	22
8	120kHz-38 kHz delta MVBS data for annotated scattering layers. Annotated acoustic scattering layer definitions for 1m x 10 ping cells nearby to imagery profiles shown on 120 kHz MVBS. Histograms of delta MVBS 120 kHz-38 kHz values for the four scattering layers.	23
9	Wire Flyer towing diagram and sampling trajectory (reproduced from [18])	49

Figure		Page
10	Wire Flyer mechanical details showing the repackaged EK80 electronics, the transducers inset into the foam flotation on the top of the vehicle and a photo of the Wire Flyer at sea. The oxygen sensor and fluorometer are mounted on the port side of the vehicle, out of view in this image.	50
11	Schematic of the input power filter.	50
12	Comparison of the input power filtering. The plots show a histogram of the received signal levels over range for a section of the water column with little biomass. In both cases the high end of signal range is similar.	51
13	Wire Flyer side-looking acoustic survey. (a) Sample of detailed side looking 70 kHz data showing patchiness. (b) The typical sampling pattern alternating frequencies on the up and down profiles. (c) Alternating pings by depth or time within a profile.	52
14	Process diagram outlining the Wire Flyer acoustic processing pipeline.	53
15	Schematic illustrating the fate of a side looking ping. The signal is attenuated over range due to the transmission loss terms and falls below the noise floor at range. The TVG amplification of the received backscatter signal, to compensate for the transmission loss, generates a non-uniform noise floor over range.	54
16	3D rendering of the Wire Flyer acoustic data showing side-looking acoustic data "unwrapped" along the vehicle path. . . .	54
17	Section plots showing Scattering Volume averaged between 5 and 35 meters range and the Wire Flyer survey path for the a) 200 kHz and b) 70 kHz profiles.	55
18	Downward diel migration at the New England shelf break front. (a) Shipboard 38 kHz shown in gray with the side looking Wire Flyer 70 kHz data shown in color and thresholded at the lower end. (b) 200 kHz Wire Flyer and shipboard data.	56
19	Downward diel migration at the Costa Rica Margin. (a) Shipboard 38 kHz shown in gray with the side looking Wire Flyer 70 kHz data shown in color and thresholded at the lower end. (b) 200 kHz Wire Flyer and shipboard data.	57

Figure	Page
20	Transect across a frontal feature at the New England Shelf. Overlays of (a) density, (b) oxygen, (c) salinity, and (d) temperature all show good agreement with the concentration in acoustic scattering. 58
21	Wire Flyer transect at the lower oxycline in the Costa Rica Margin (GMT-6) (a) 70 kHz Wire Flyer acoustic data from with the oxygen concentration contours overlaid. (b) Scatter plot of oxygen measurements from all of the Wire Flyer profiles indicating the minimum depth and variability amongst the profiles over the length of the transect. These data were collected prior to the final power filter, so the overall signal range is limited by the higher noise floor. 59
22	Wire Flyer acoustic transect at a cold seep plume in the Baltimore Canyon 60
23	Wire Flyer survey waypoints overlaid on Google Earth bathymetry. The major portion of the observed shallow water front is indicated by the green waypoints 91
24	Environmental and layer shape associated per-profile metrics from the 70 and 200 kHz custom metric data (red line plots) plotted alongside the chlorophyll layer shape data (blue) for the complete Baltimore Canyon Survey. The 200 kHz scattering layer reaches maximum intensities at the front. The 70 kHz layer shape data types track the downward migrating layer at dusk. 92
25	Simulated side-looking echosounder Power and Sv data (Theta = 18 deg, SL = 15 dB, NL=-146 dB, AbsCo=20 dB/km) matches the Wire Flyer data. A) Receive level distribution for a homogeneous scattering layer of -120 dB Target Strength across range angle cells. B) Modelled Power and Sv ping data for scattering layers of -120 and -150 dB Target Strength. C) Wire Flyer 100 ping power echogram showing bounded scattering feature. The colored bars atop show the 20 pings averaged for comparison to the model power data. D) Simulated power pings for TS=-120 dB and TS=-150 dB overlaid on Wire Flyer 20 ping power averages showing good alignment at far ranges. 93

Figure		Page
26	Modelled Scattering Volume for two scattering layers with TS=-120 and TS=-150 dB on the left panels, and the difference between the Sv for the high minus low TS pings on the right panel, under increasing Noise Levels (-120 dB top row, -150 dB middle row, -400 dB bottom row).	94
27	Averaged Wire Flyer Sv data from the Baltimore Canyon deployment demonstrating the raw and detrended Sv curves over range. A) Averaged 0-25% (blue) and 75-100% (red) Sv quartile averages. The difference between the high and low quantiles with an average value added back is shown in black and represents the detrended Sv data. B) The raw difference between the upper and lower Sv quantiles matches the logarithmic decay observed in the simulated Sv data.	95
28	Comparison of the custom metric, Sv, and MVBS signals. A) Custom metric normalized to sampling range plotted as black line over the 3-dimensional Sv data. The custom metric effectively traces contours in Scattering Volume across scattering layers. B) Normalized custom metric data plotted alongside normalized MVBS. The custom metric signal is smoother and captures more of the scattering layer intensity gradients.	96
29	70 and 200 kHz Wire Flyer echogram sections showing the custom metric data type versus MVBS derived from the full sampling range. The custom metric demonstrates better detection of the major scattering layers.	97
30	Pairwise linear regressions for layer shape based data types derived from the 70 kHz custom metric (left panels) and 70 kHz MVBS (right panels). The top panel shows chlorophyll layer shapes plotted against the scattering layer shapes. The second row shows the scattering layer depth plotted against the scattering layer shape. The third row shows the chlorophyll layer depth plotted against the scattering layer shape. The last row shows the chlorophyll layer shape as a function of the scattering difference above and below the chlorophyll layer.	98

Figure	Page
31	Pairwise linear regressions for layer shape based data types derived from the 200 kHz custom metric (left panels) and 200 kHz MVBS (right panels). The top panel shows chlorophyll layer shapes plotted against the scattering layer shapes. The second row shows the scattering layer depth plotted against the scattering layer shape. The third row shows the chlorophyll layer depth plotted against the scattering layer shape. The last row shows the chlorophyll layer shape as a function of the scattering difference above and below the chlorophyll layer. 99
32	1D phytoplankton model results. A) The simulated diffusivity profile. B) Phytoplankton model output for 10 days of run time. The phytoplankton starting distributions are shown in green. The final distributions are shown in red and demonstrate a dispersed lower gradient. C) Example 200 kHz chlorophyll profile demonstrating a similar shape to the model output. 100
33	Run length data section plots derived from the 70 kHz Scattering Volume profiles. A) Total number of runs detected per ping. The most abundant runs were observed in pings delineating the lower boundary of the mixed layer associated scattering layer and the migrating assemblage departing the surface at dawn. B) Average run length data (percentage of sampling range). Long runs visible in the color scale at lengths beyond that expected for individual animals corresponds directly to the dense nighttime scattering layer. C) Selection criteria showing the classification of valid single target data. Pings in black exceed the maximum run length criteria and denote the dense scattering layers. Ping data show in red and blue did not exceed the minimum run length size and number of runs per ping respectively. D) Valid single target data corresponds to the boundaries of the dense scattering layers and a unique region within the canyon. E) Oxygen section shows intermediate water mass distributions matching the mesopelagic single target distributions. 101

Figure	Page
34	Frequency dependent Scattering Volume data from active and passive mode Wire Flyer profiles. The top two rows and bottom two rows show Sv(f) data from the 70 kHz channel and 200 kHz channel respectively. The left and right panels show Sv(f) data collected during passive and active acoustic profiling respectively. The colored line plots show Sv(f) data for all pings in the profiles while the blue line plots show the average Sv(f) response shapes. The active mode Sv(f) demonstrates similar response shapes to the passive noise spectrum with elevated amplitude. 102
.35	Results of the two step image lighting normalization. A) Raw image from the color camera in the stereo pair. B) Flattened image data after subtracting the signed strobe lighting representation. C) Foreground isolated image data after subtracting the calculated ambient background lighting. 109
.36	Fixed lighting gradient calculated for the strobe lighting. Quadrant gain variation is evident and reflects the composite sensor design. 110
.37	Images generated by the sliding window ambient lighting correction. A) Ambient lighting generated for an image near the surface. B) Nearby ambient lighting images generated for images 10 m apart. C) Scalar mean intensity representation of the ambient lighting images generated for a whole profile. 112
.38	Bounding contours detected and reprojected from the stereo image pair. 113
.39	Screenshot of manually identified Pleuroncondes planipes image region pairs segmented autonomously. 116
.40	Comparison between Simrad's VBS data, the processed Sv Continuous Wave data, and the processed Sv Frequency Modulated data before installation of the input power filter. 123
.41	Per element power plots showing deviating trends among the sectors. 123
.42	Per element power point clouds showing non-stationary and diverging trends. 124

Figure	Page
.43	Comparison between Simrad’s VBS data, the processed Sv Continuous Wave data, and the processed Sv Frequency Modulated data after installation of the input power filter. 124
.44	Per element power plots showing largely consistent trends among the sectors. 125
.45	Per element power point clouds showing consistent power distributions 125

LIST OF TABLES

Table		Page
1	Summary of field work for datasets used in the thesis. The related figures are marked in the last ‘figures’ column	ix
2	Wire Flyer sensors and parameters	33

MANUSCRIPT 1

Multi-Sensor Observation of a Rapidly Dispersing Micronekton Thin Layer

by

Benjamin Grassian¹, Christopher Roman², Melissa Omand³

*Prepared for submission to Deep Sea Research Part I: Oceanographic Research
Papers*

¹Ph.D. Candidate, Graduate School of Oceanography, The University of Rhode Island, Narragansett RI 02882. Email: bgrassian@gmail.com

²Professor of Oceanography, Graduate School of Oceanography, The University of Rhode Island, Narragansett RI 02882. Email: croman2@uri.edu

³Associate Professor of Oceanography, Graduate School of Oceanography, The University of Rhode Island, Narragansett RI 02882. Email: momand@uri.edu

1.1 Abstract

Ocean midwaters—areas between the sunlit surface layers and seafloor—comprise the largest habitat on Earth but are among the least understood marine environments. Available sampling platforms (e.g. net systems, moored and shipboard sensors), are often unable to resolve the environmentally-coupled distributions of marine biota throughout the water column over the relevant scales. A deep profiling (1000 m rated) stereo camera was operated in tandem with a split-beam five channel fisheries echosounder to record midwater scattering layers in detail across the oxygen minimum zone (OMZ) offshore of Baja California. A computer vision software library was developed to batch process the collected water column imagery and the derived biological information was interpolated with environmental sensor and acoustic backscatter measurements. A large aggregation of the micronekton squat lobster *Pleuroncodes planipes* (red crab) was described in the imaging and acoustic data. During midday hours, the micronekton were distributed in an intense thin layer 2 m in vertical extent and having a maximum abundance of roughly $10 \text{ individuals m}^{-3}$. The thin layer distribution was tightly coupled to the 1026 kg m^{-3} isopycnal associated with a high-frequency internal wave. At dusk the crabs redistributed upwards suddenly as a specific mesopelagic scattering layer with a daytime settling depth of 600-800 m migrated through the micronekton thin layer near the surface.

1.2 Introduction

The spatial and temporal dynamics of animal distributions in pelagic ecosystems are patchy and vary over a broad range of scales related to heterogeneity in the environment, resources, and opportunities for biological and trophodynamic interactions [1]. Describing the distributions of marine populations within their physical environment over the relevant spatiotemporal scales is a fundamental re-

quirement for understanding the structure of pelagic ecosystems and the many factors driving their heterogeneity [2]. Plankton and micronekton populations are often highly aggregated over day- night cycles in the epi and meso-pelagic ocean, and nekton and top predators respond to prey patch patterns [3, 4]. The need for high resolution field surveys that record detailed concurrent information on the in situ distributions and identity of organisms within their local physical environments has steered the development of a range of sensor-based tools for optical and acoustic sensing [5]. Sensor-based water column surveys are capable of recording fine scale in situ structures that would be integrated by net tow samples [6].

Optical sampling has proven to be an especially valuable technique for surveys of planktonic animals [5, 7]. In situ imaging systems can record detailed taxonomic and behavioral information at fine scales and without bias against fragile gelatinous organisms that do not survive net tows [8, 9]. Modern plankton imaging systems collect large and feature-rich datasets that can be processed by autonomous methods [10, 11]. Deriving consistent, efficient, and accurate biological information from large image datasets remains challenging and lacks generalized procedures [12]. The image processing and computer vision problems of accurately counting and identifying animals from image data are often tackled by solutions that are specific to a particular system or deployment and can require extensive human-in-the-loop processing to establish training data [13]. Stereo imaging techniques that use paired exterior-facing camera sensors allow for measurements over large 3-dimensional sample volumes and are often applied to benthic surveys (Gibson et al. 2016). In the pelagic setting, stereo imaging systems can be used to quantify larger micronekton and nekton taxa while still resolving larger-size plankton and particles close to the camera. Without relying on collimated light sources or vehicle-bounded sample spaces, the traditional camera setup is more utilitarian but

not specifically optimized for the plankton. These systems are useful for assessments of the broader midwater community that incorporates larger micronekton taxa often missed by dedicated plankton imaging platforms.

Acoustic techniques in particular have provided substantial insight into the ubiquity and variability of Diel Vertical Migrating (DVM) behaviors by mesopelagic animals, thought to be driven by an efficiency between food availability at the surface layers and the risk of visually-cued predators [14, 15, 4]. Observations of the migrating behaviors of animals establish important mechanisms for connectivity between the surface and deep ocean over daily cycles, affecting the timing and pace of biogeochemical fluxes and ecological interactions in the ocean [16, 17, 18]. Acoustic echosounding can record cm scale measurements over extremely large (100 m) ranges away from the system. In contrast to imaging techniques, the derivation of bioacoustic quantities is formal, more well-posed and comparable, but provides coarser taxonomic information for single targets and coherent scattering layers. The use of multi-frequency and broadband echosounder systems expands the ability to distinguish distinct scatterer classifications but must rely on empirically derived scattering model information and typically can provide only broad classifications (e.g. zooplankton, fish) without ground-truth information from net collections or imaging data.

Sensor-based sampling techniques have enabled observation and study of extreme spatial heterogeneity in plankton distributions [19]. A particularly ubiquitous feature noted within acoustic and imaging systems is the existence of thin aggregations or layers of organisms [20, 21, 22]. The common criteria used to define thin layers are described by a peak intensity 3 times higher than the background signal and where the full width half maximum of the signal describes a vertical distribution of less than 5 m [23]. Certain micronekton species aggre-

gate in vertically-compressed swarms that meet the common criteria for thin layer aggregations.

Here we describe the occurrence and evolution of a thin layer formed by the pelagic red crab, *Pleuroncondes planipes*. This species is abundant in pelagic habitats throughout the eastern Pacific, with an estimated biomass of 215,000 - 611,000 metric tonnes supporting ecologically and commercially important oceanic predators including sharks, tunas, whales, and squids [24]. *P. planipes* has both pelagic and benthic phases partitioned by life cycle stage [25], but the habits appear exchangeable. Pelagic populations can often be found in dense swarms at the surface or in midwater, with variable diel habits and apparent vertical migration patterns suggested from net tow abundances that have not been observed in detail. Rapid migrations performed into the water column by a portion of densely compacted benthic populations on the continental shelf and slope have been recorded by hydro acoustic studies [26], and it is thought that younger benthopelagic adults migrating into a pelagic setting at night is common [27], but data are lacking on the fine scale vertical distribution and redistribution of offshore aggregations that retain pelagic habits over daily cycles.

1.3 Materials and procedures

1.3.1 Data collection

A 1000 m depth rated tethered stereo camera profiler was deployed in the eastern tropical Pacific (ETP) Oxygen Minimum Zone (OMZ) offshore of Baja California in 2017 (Figure 1). Cruise work was conducted from the RV Sikuliaq in January-February of 2017 as part of a project assessing the ecophysiology and zonation of animal aggregations throughout the OMZ environment. The goal of the camera work was to collect high resolution water column stereo imagery to describe the in situ distributions of zooplankton, micronekton, and nekton within

the epi and mesopelagic ocean. Datasets from two sequential deployments recorded an abundant pelagic aggregation of the squat lobster *Pleuroncodes planipes* and were analyzed in detail.

The camera system provided high resolution, 2752 x 2200 pixels, 16 bit images (Figure 2). One camera in the pair was a black and white camera and the other was color. Measurements from a suite of environmental sensors (CTD, Chl, Turbidity, Oxygen) mounted with the camera were also recorded. Lighting was provided by a pair of 200J strobes synced to the camera acquisition. The system was deployed on a standard CTD wire using a heave compensated winch while the ship held position with dynamic positioning. Shipboard acoustic measurements were collected simultaneously using a 5-channel fisheries echosounder system (Simrad EK60 split-beam Sonar with 18, 38, 70, 120, and 200 kHz transducers) mounted on the hull of R/V *Sikuliaq*. The derived acoustic, imaging, and environmental measurements were fused to generate multi-resolution biological-physical datasets for analysis of *Pleuroncodes planipes* and scattering layer distributions within the physical environment.

1.3.2 Stereo image processing

A software library to batch-process water column imagery was written in C++ using the OpenCV computer vision library. The software is configurable by the user, and multithreaded to operate on several image pairs simultaneously. The goals of this image processing library were to normalize the image data collected in the epi- and mesopelagic ocean and extract stereo-pair objects from 1000s of paired images).

Initially, a two step lighting correction was performed to remove lighting gradients resulting from the fixed strobe illumination and the variable photic conditions near the surface (shallower than 100m) at daylight hours. To correct for the

strobe illumination, a representative strobe lightfield was generated from averaging a subset of the images profiles, determined by image statistic (the mean and standard deviation of the image intensities) with lower quantiles corresponding to largely empty scenes. The histograms of these empty-scene images were translated to signed zero-mean intensity images and averaged, generating the strobe lightfield which was subtracted from the raw image profiles. These corrected images were further processed to remove the variable ambient illumination by pixel-wise median filtering among sequential images.

Following the lighting correction an image segmentation method was used to identify objects in the images. Each object was defined by a Region of Interest (ROI) which contained the boundary of the object and a list of keypoint features (Figure 3). ROIs in matching stereo image pairs were compared to identify the subset of ROIs which could be associated with each other and then reprojected in 3D using the stereo camera calibration. The final list of matched objects and interpolated depth and environmental data for each dive was then stored alongside a directory of the segmented images.

Pleuroncondes planipes individuals were manually identified from the total set of segmented ROIs and sorted into a separate directory of classified animal groups. A script then read through the directory of classified images and assigned taxonomic labels to the original data file based off the classification directory structure (Figure 4). Aspect ratios (height over width) were calculated from the ROI bounding boxes to provide a proxy metric for individual animal orientation. An aspect ratio value of ≥ 0.9 was selected to label vertically swimming individuals. Individuals sitting passively in the water were oriented more horizontally and had aspect ratios generally ≤ 0.75 . The ROI areas, determined in square millimeters, were calculated from the bounded pixel area and the calibrated pixel size. The assigned

ROI size was determined at the median range from the camera calculated from the subset of keypoints less than 2 standard deviations from the median value for all detected keypoints within the ROI. Crab abundances within the stereo volume (roughly 10 m^3) were calculated for each stereo pair, and then averaged in bins of four sequential image pairs to smooth the data and obtain an abundance profile.

1.3.3 Acoustic data

Shipboard acoustic measurements were collected while deploying the stereo imaging system using a 5-channel fisheries echosounder system (Simrad EK60 split-beam Sonar with 18, 38, 70, 120, and 200 kHz transducers) mounted on the hull of the R/V *Sikuliaq*. Continuous Wave acoustic Scattering Volume (Sv) and Mean Volume Backscattering Strength (MVBS) measurements was calculated from the raw data files in R. Backscatter information from the 120 kHz and 38 kHz channels was used to examine scattering layers in the upper 400 m of the water column, and major scattering layers of interest were manually defined from the 120 kHz Sv echogram. Delta MVBS (120 kHz MVBS -38 kHz MVBS) values were calculated to assess the broad frequency-dependant scatterer characteristics for the annotated scattering layers below 5m depth using 10 ping integration cells and a lower Sv threshold of -90 dB. These values overlapped the imaging profiles and the annotated scattering layer definitions.

1.3.4 Buoyancy frequency analysis

Buoyancy (Brunt–Väisälä) frequency, N^2 , was calculated for all camera profiles to analyze the distribution and potential influence of the water column stratification on the observed micronekton thin layer and scattering layer dynamics ([28]). Several smoothing and binning operations for the buoyancy frequency calculation were tested without significantly altering the trends observed in the stratification

profiles. The selected buoyancy frequency calculation followed [29]. Temperature and salinity data were filtered into 3 meter bins and density profiles were interpolated using cubic splines before the calculation of N^2 . A regression between the peak crab abundance and the in situ stratification at the corresponding depth was created for profiles before the occurrence of the layer migration with a peak crab abundance of greater than 5 individuals per the imaging volume.

1.4 Results

1.4.1 Coverage and imaging results:

Stereo image datasets from two consecutive deployments of the stereo camera profiler contained abundant *Pleuroncondes planipes* aggregations. The first deployment provided a single profile containing 410 image pairs, with a sustained observation (roughly 5 mins) of the crab thin layer at midday (Figure 5a,b). The subsequent deployment consisted of one truncated and 15 full repeating profiles in depth bands from 75 to 200 m, and 15m to 200m for the last 6 profiles, totaling 4,594 image pairs (Figure 5a,c). A total of 2,447 crabs from 10,458 ROIs and 2,600 crabs and 104,570 ROIs were identified from the 1st and 2nd deployments respectively. The majority of the ROIs were small particles, many of which resulted in mismatched pairs, and plankton detected within two meters from the camera center.

1.4.2 Thin layer distribution

Pleuroncondes planipes occupied a thin layer during daylight hours tracking the 1026 kg/m^3 isopycnal around 145 m depth. The midday stereo camera profile demonstrated the maximum *Pleuroncondes planipes* densities, reaching 80 individuals in the imaging volume at the thin layer (Figure 5 b,h). Vertical excursions in the camera profile path show a rapid drop off in crab abundance over short 2 m depth changes. Very few individuals were recorded above, and even fewer

below the thin layer. Acoustic Sv 120 kHz also was higher for the thin layer during this time, reaching roughly -55 dB. During the repeat profiling, the maximum crab abundances again occurred between 140-150m depth for the duration of the daylight observation (Figure 5c). *Pleuroncodes planipes* were completely absent at depths beginning several meters below their peak abundance while there was a consistent presence of individuals and smaller aggregations at shallower depths above their thin layer aggregation. A slight secondary peak abundance was observed in the intermediary profiles from 17:50 to 18:30 at the chlorophyll maximum at 80m depth. The maximum crab abundances recorded in the thin layer at this time was reduced from the midday profile, reaching 39 individuals in the imaging volume (Figure 5i).

The thin layer vertical distribution corresponded to a local peak in buoyancy frequency, N^2 , at the 1026 kg/m³ isopycnal (Figure 6). The calculated N^2 profiles had vertical structure, i.e. the location and relative magnitude of peaks and minima, that was largely conserved for the first 11 profiles when the crab thin layer was maintained. A high frequency internal wave propagating through the tracked isopycnal caused a small vertical oscillation in the crab thin layer depth distribution roughly 2-3 meters in amplitude. In the following profiles, the fine scale vertical structure in N^2 was diminished with fewer and lower frequency peaks in the density gradient, before higher-frequency N^2 structure reappeared in the final profile. A relationship between the maximum crab abundance and the in situ stratification intensity at the depth of the peak abundance was observed, where higher buoyancy frequencies corresponded to greater maximum crab densities (Figure 7).

1.4.3 Thin layer dissociation

The presence of the thin layer remained stable until 19:00, in the 12th profile. The *Pleuroncondes planipes* thin layer abruptly dispersed before the 12th profile

while a shallower distribution occurred with no crabs recorded below 100m depth (Figure 5c). An abundant aggregation was observed briefly near the surface in profiles 12-13 during the rapid crab redistribution. In the last profiles, the aggregation occurring around the chlorophyll maximum at 80 m depth appears to ‘descend’ over the profile sequence, settling at depths near the original occurrence of a thin layer but with a broader and more diffuse vertical distribution. The acoustic data suggested a reformation of a thin layer starting at 21:00 (Figure 5a).

Distinct orientation characteristics of *Pleuroncondes planipes* individuals coincided with the dissociation timing of the crab thin layer aggregation (Figure 5f,g). An increase in the proportion of vertically oriented individuals was observed for the last recorded instance of the the thin layer aggregation and for the shallower aggregation in the following profile which had 60-80 percent vertical individuals at the peak abundance. Smaller aggregations and individuals recorded between the thin layer and the chlorophyll maximum also had a high proportion of vertically oriented individuals during the early migrating layers ascent through the 75 m-150 m depth band. Aggregations recorded in the last sequence of four profiles capturing descending crab distributions did not demonstrate the high proportion of vertically oriented individuals found in the preceding imaging profile. The orientation information suggested a short-lived escape-response-like vertical swimming behavior in response to the ascent of deep migrators followed by a slower descent of horizontally oriented individuals.

1.4.4 Acoustic scattering layers

The acoustic backscatter from the shipboard echosounder closely matched the *Pleuroncondes planipes* distributions derived from the imagery. The thin layer observed in the image data occurred as a matching oscillating feature in the acoustic Sv data that disappears at 19:00. The acoustic echogram also identified two

coherent deeper scattering layers that ascended through the crab thin layer during the repeat camera profiling. A scattering layer ascended slowly through the micronekton thin layer at 17:00 local time departing from a diffuse distribution at a daytime settling depth around 200 m seen for the prior two hours. A large scattering layer with a daytime settling depth between 300-400 m ascended more rapidly and arrived at the thin layer. Scatterers aggregated broadly around the chlorophyll maximum at 80 meters during nighttime hours with slightly partitioned scattering layers visible 20 meters above and below the main aggregation.

1.4.5 Evidence for scattering layer compositions

The delta MVBS (120kHz - 38 kHz) values calculated from data cells corresponding to the two migrating layers and the large nighttime aggregation at the chlorophyll maximum demonstrated unique unimodal distributions (Figure 8). The two migrating layers had non-overlapping 25-75 quartiles, with the 1st and 2nd migrating layer having median delta MVBS values of +7.7 and -3.3. The mixed aggregation had an intermediary delta MVBS value slightly elevated from the 2nd migrating layer with a median value of -1.3. Unequal variance t-tests showed significant difference in the delta-MVBS sample means between the three annotated scattering layers. The assumption that delta MVBS largely describes size-dependent assemblages composition information, with positive delta MVBS values indicative of zooplankton dominated scattering layers and fishes and nekton resulting in zero or negative centered delta MVBS values, would suggest a zooplankton dominated 1st migrating layer and a deeper migrating layer containing midwater fishes and large invertebrates.

1.5 Discussion

1.5.1 Micronekton thin layer evolution

Direct observations of micronekton aggregations are uncommon relative to phytoplankton and zooplankton assemblages. This study provided direct observation of the evolution of a *Pleuroncondes planipes* pelagic aggregation meeting the criteria for a thin layer during a day-night transition. The thin layer was initially comprised of horizontally oriented individuals with outstretched pleopods showing minimal swimming behavior. The micronekton thin layer persisted during daylight hours closely tracking the 1026 kg m^3 isopycnal while oscillating with an internal wave. A 2-3 fold decrease in peak abundance then occurred from the midday profile to the subsequent deployment beginning roughly two hours before sunset. A local peak in buoyancy frequency was present at the thin layer depth for the duration of its occurrence. Local stratification may have contributed to the formation and/or maintenance of the aggregation at the particular isopycnal, as the thin layer depth provided a sharp lower boundary in the vertical distributions of the detected crabs. Interestingly, the observed fine scale water column stratification structure was reduced and lost during the dispersal of the thin layer. The timing of the observed changes in water column structure and biological migrations might suggest mixing mechanisms linking these events, but that remains speculative because the dataset is non-Lagrangian and thus advective processes may be incorporated in the apparent environmental and biological distributions.

1.5.2 Rapid dispersion and migration event

The micronekton thin layer underwent a rapid dissociation accompanied by a short-lived migration event. Rapid migrations have been observed acoustically for benthopelagic *P. planipes* aggregations but have not been directly observed for pelagic aggregations [26]. An interesting result was the apparent response of

the crab layer to the ascending migration of a specific scattering layer, and the maintenance of the thin layer aggregation during the ascent of an earlier migrating layer. These observations suggested that a transition in the epipelagic distributions of *P. planipes* can be initiated by the timing of select migrating layers that cues the rapid alteration of *P. planipes* vertical distributions and behavior. Furthermore, these observations support an emerging understanding of the importance of dynamic behavioral responses driven by encounters between predators and prey in restructuring the zonation of animals in pelagic ecosystems ([30, 31]). While the identity of the deep scattering layer composition was not well resolved by the imaging data, the frequency dependant scattering characteristics suggested that this layer was largely comprised of micronekton fishes and larger soft-bodied organisms that settled at the chlorophyll maximum during nighttime hours. The acoustic observation of a reformed thin layer near the original micronekton layer depth roughly three hours after the initial dispersal suggested a short-lived migration into and out of the densely populated 0-100m depth band after dusk. The recording of the micronekton thin layer dispersal and redistribution at high temporal resolutions supports other findings showing the role of critical time windows at dusk diminishing spatial segregation of populations and providing pronounced and ephemeral alterations to pelagic ecosystem structure ([17]).

1.5.3 Camera avoidance

It is likely that avoidance behaviors led to an undersampling of larger nekton species and decreased the ability to resolve the variable community compositions over space and time from the imaging data alone. Size spectral analysis of imaged animals and particles within the distinct scattering layer did not show significant differences, likely reflecting both the avoidance behavior of larger animals and potential biases in the image processing pipeline configured to optimize extraction of

the squat lobster individuals. Observations of the squat lobsters did not appear to be substantially affected by avoidance due to the camera and strobe, as evidenced by the maintenance of the thin layer aggregation during repeated camera profiling and the vertical orientation of *P. planipes* individuals only showing escape response behaviors at limited times in response to ecological factors.

1.5.4 Applications and improvements of image processing methods

The image processing pipeline constructed for this study addressed the basic steps necessary for batch-processing water column stereo imagery datasets to derive biological information in the 3D imaging volume. Stereo imaging as a water column survey technique is readily available with off the shelf cameras and lighting systems, but the processing of this data presents unique challenges with variable background intensity gradients, scale dependant resolution, and the need to apply paired image segmentation and stereo matching routines. This study demonstrates the high resolution biological data obtainable by addressing these processing requirement using relatively simple methods. Similar approaches to semi-autonomous stereo image processing could be applied to process unexploited datasets available from stereo imaging systems on ROVs and AUVS collected during blue water operations. Stereo imaging datasets collected from these systems during midwater transits are largely ignored, in part due to a lack of processing pipelines and standard operating procedures like those existing for epibenthic fauna. An underlying goal of the construction of the image processing methods used for this study was to explore simple but robust automated techniques to derive useful information from water column stereo imaging datasets. The implemented image processing methods demonstrated skill for quantification of hard-bodied micronekton. Implementing more sophisticated image segmentation procedures and the optimization of the camera configuration to increase depth of field and image

contrast would improve the detection and identification of particles, plankton, and nekton. The coupled acoustic and optical dataset compiled for this study has potential value for refining scattering model descriptions for pelagic squat lobsters ([32]). The in situ orientation information for identified *P. planipes* individuals can be used to better describe the predicted target strength.

1.6 Conclusions

This study combined optical, environmental and acoustic measurements to describe the distribution and redistribution of a *P. planipes* thin layer with details that could not be obtained by single sensor survey approaches. The stereo imaging profiler allowed for visual identification, abundance calculations, and behavioral analysis of individuals within a 3-dimensional sampling space. The concurrent environmental measurements allowed for the derived biological quantities to be assessed within the local hydrographic context. Acoustic backscatter from a shipboard echosounder recorded scattering layer distributions synoptically across a large range of depths, providing information on distribution and migration timing of deeper scattering layers while also providing a ground truth for the biological information derived from the semi-automated image processing methods.

1.7 Figures

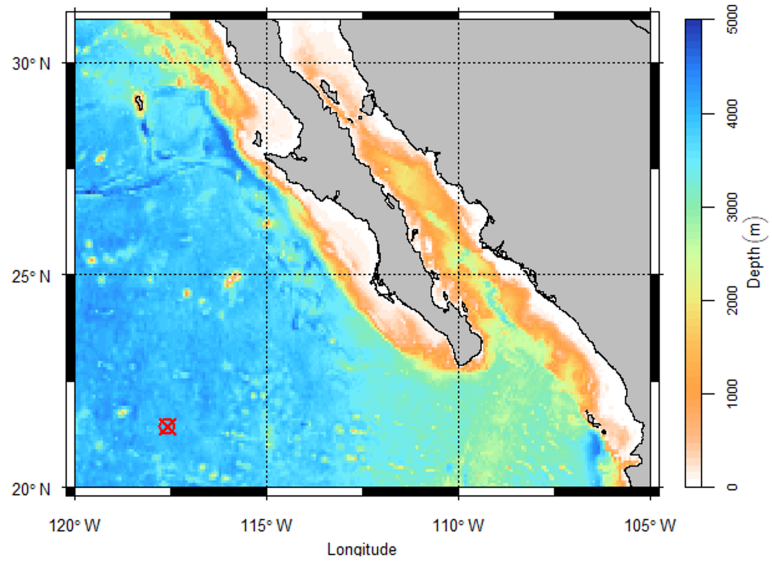


Figure 1. Survey location offshore of Baja California, Mexico

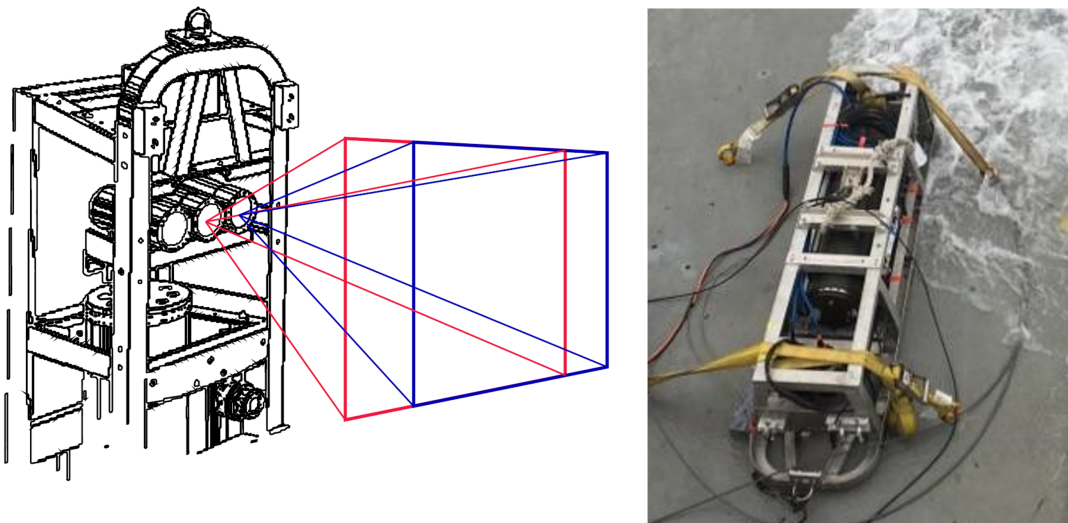


Figure 2. Stereo camera profiling system. A) Schematic showing the side-looking stereo imaging volume. B) The stereo camera profiling system on deck.

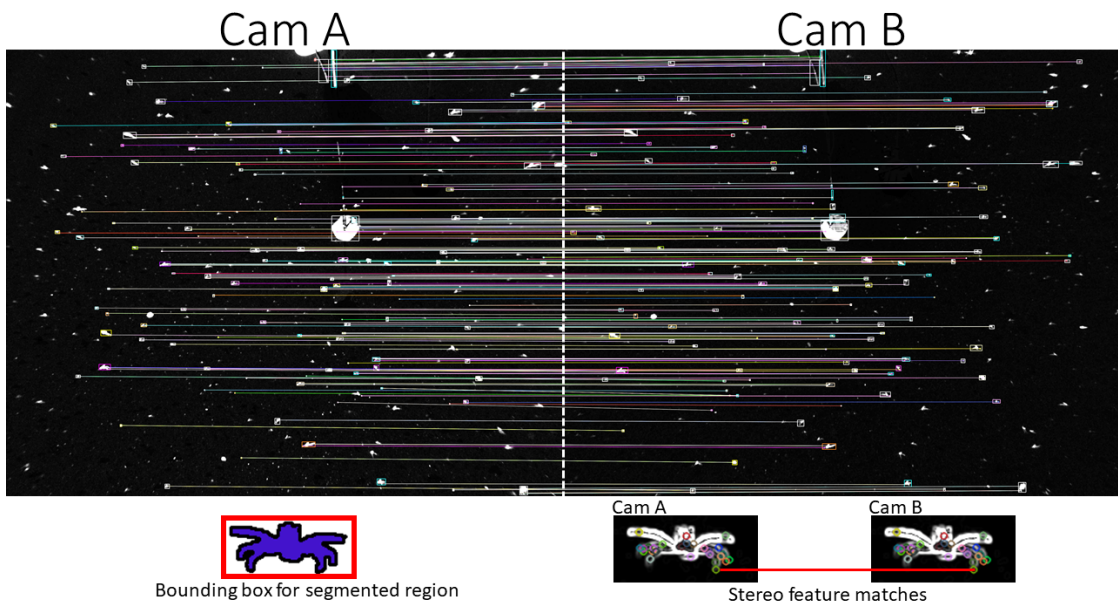


Figure 3. Example stereo matched and segmented Regions of Interest (ROI) from an image pair inside the crab thin layer. The top panel shows processed stereo matching information for the right and left camera. The bottom panel shows a single bounded Region of Interest (bottom left) and detected keypoint features used for stereo matching (bottom right).

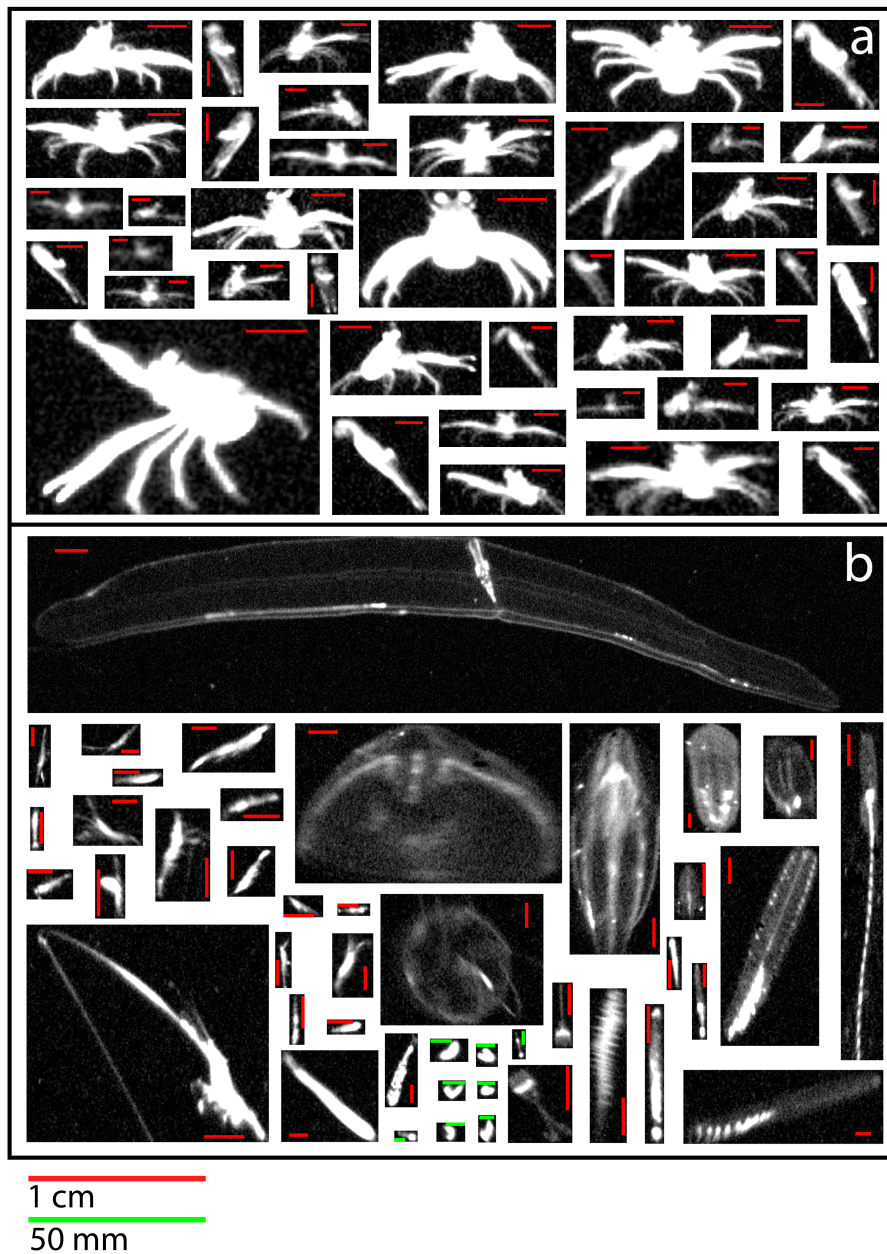


Figure 4. Example segmented image regions with taxonomic details. A) Segments identified as *Pleuroncondes planipes* representative of the variability in animal orientation and behavior. Detected animals ranged from 1.2 to 4.8 m distances from the camera. B) Example segmented image regions capturing other broadly identifiable taxa, including: a cestid ctenophore, copepods, shrimp, cydippid and beroe ctenophores, chaetognaths, polychaete worms, medusae, and fishes.

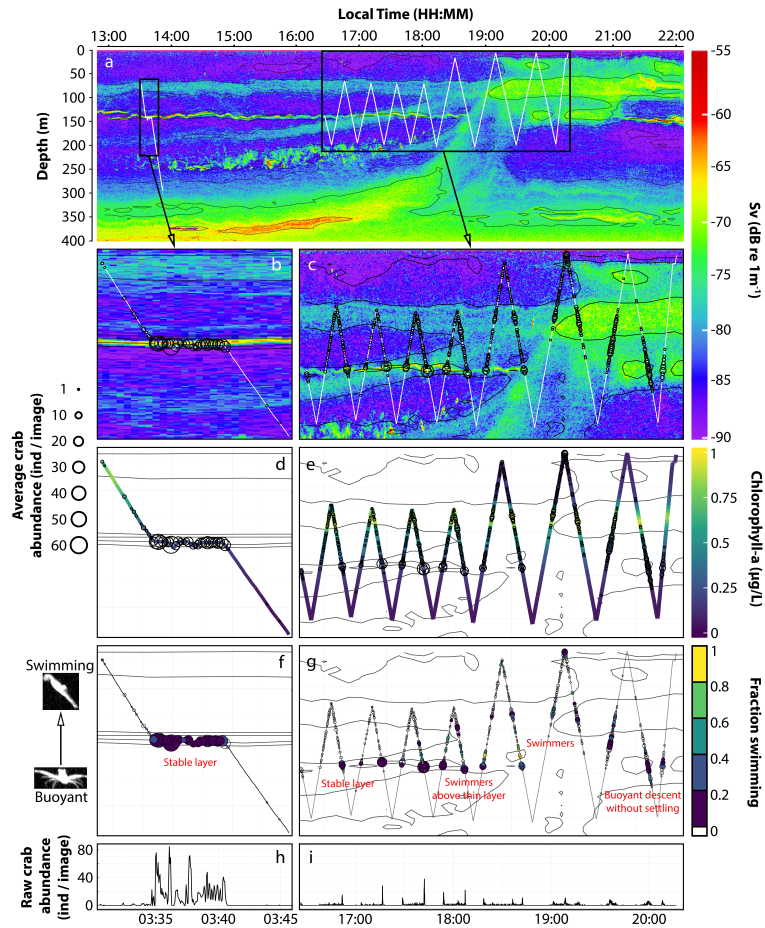


Figure 5. Measurements from sequential stereo camera profiling overlaid on 120 kHz acoustic scattering volume recorded from a shipboard echosounder. A) Stereo image profile paths for two sequential deployments as white line plots overlaid on 120 kHz Sv echogram with 5dB contours highlighting discrete acoustic scattering layers. Black rectangles define data subsets plotted in lower panels. B) Mean *Pleuroncondes planipes* abundance per imaging volume from bins of four image pairs shown as bubble plot size overlaid on 120 kHz Sv echograms for the midday imaging profile and C) repeated profiling over dusk. D) Chlorophyll-a fluorescence recorded by stereo camera profiler with *Pleuroncondes planipes* mean abundance data from imagery and Sv 8dB contours for midday profile and E) repeated profiling over dusk. D, E) *Pleuroncondes planipes* mean abundance from binned imaging data with Chlorophyll fluorescence data and 120 kHz Sv contours. F) Proportion of *Pleuroncondes planipes* individuals defined as vertically swimming from the mean ROI aspect ratio plotted as the color fill of the the abundance bubble plots and overlaid on the 120 kHz Sv contours for the midday profile, and G) repeated profiling. H) *Pleuroncondes planipes* abundances derived from the raw imaging sequence over time for for the midday profile subset and I) the repeating profiling at dusk.

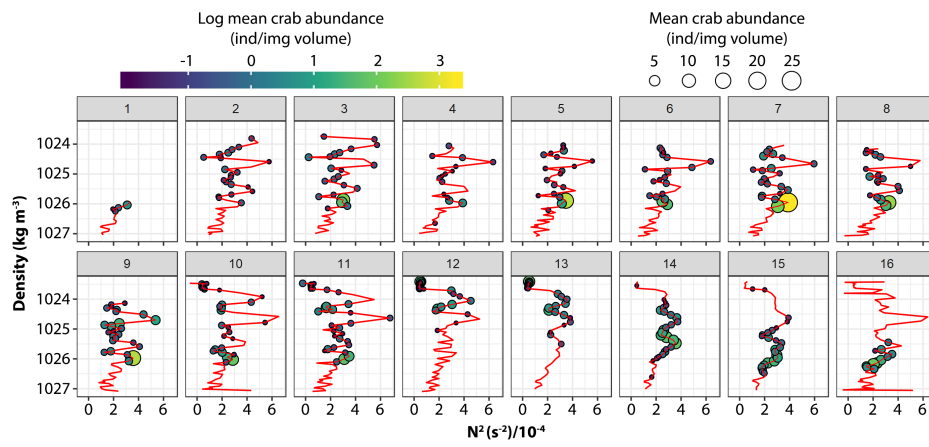


Figure 6. Buoyancy frequency (N^2) plotted against density with crab abundance information shown as bubble plots and color for camera profiles during repeat profiling at dusk

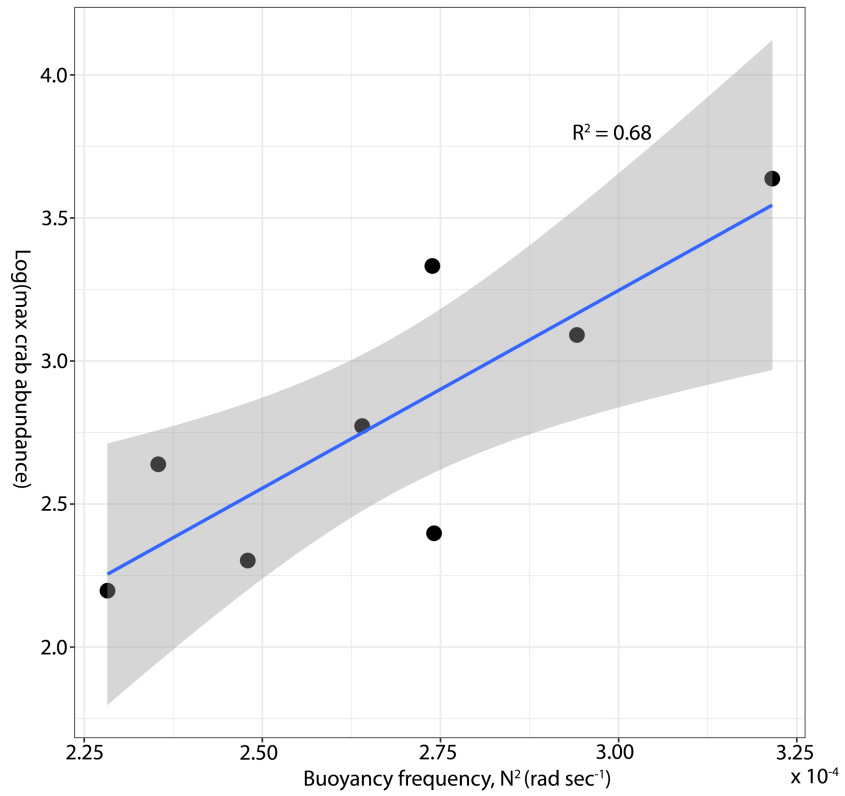


Figure 7. Maximum crab abundance per profile versus buoyancy frequency at the depth of the maximum crab abundance depth.

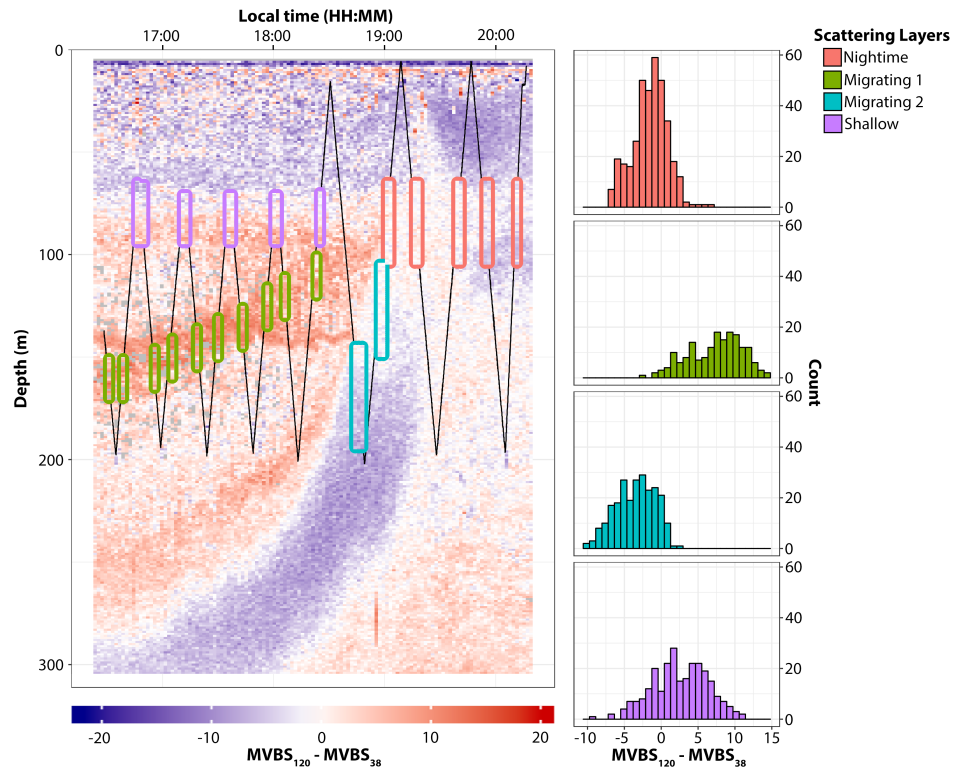


Figure 8. 120kHz-38 kHz delta MVBS data for annotated scattering layers. Annotated acoustic scattering layer definitions for 1m x 10 ping cells nearby to imagery profiles shown on 120 kHz MVBS. Histograms of delta MVBS 120 kHz-38 kHz values for the four scattering layers.

List of References

- [1] L. Haury, J. McGowan, and P. Wiebe, “Patterns and processes in the time-space scales of plankton distributions,” in *Spatial pattern in plankton communities*. Springer, 1978, pp. 277–327.
- [2] L. Legendre and S. Demers, “Towards dynamic biological oceanography and limnology,” *Canadian Journal of Fisheries and Aquatic Sciences*, vol. 41, no. 1, pp. 2–19, 1984.
- [3] K. J. Benoit-Bird, B. C. Battaile, S. A. Heppell, B. Hoover, D. Irons, N. Jones, K. J. Kuletz, C. A. Nordstrom, R. Paredes, R. M. Suryan, *et al.*, “Prey patch patterns predict habitat use by top marine predators with diverse foraging strategies,” *PloS one*, vol. 8, no. 1, p. e53348, 2013.
- [4] T. A. Klevjer, X. Irigoien, A. Røstad, E. Fraile-Nuez, V. M. Benítez-Barrios, and S. Kaartvedt, “Large scale patterns in vertical distribution and behaviour of mesopelagic scattering layers,” *Scientific Reports*, vol. 6, no. 1, pp. 1–11, 2016.
- [5] P. H. Wiebe and M. C. Benfield, “From the hensen net toward four-dimensional biological oceanography,” *Progress in Oceanography*, vol. 56, no. 1, pp. 7–136, 2003.
- [6] D. Holliday, R. Pieper, C. Greenlaw, and J. Dawson, “Acoustical sensing of small-scale vertical structures in zooplankton assemblages,” *Oceanography*, vol. 11, no. 1, pp. 18–23, 1998.
- [7] M. E. Sieracki, M. Benfield, A. Hanson, C. Davis, C. H. Pilskaln, D. Checkley, H. M. Sosik, C. Ashjian, P. Culverhouse, R. Cowen, *et al.*, “Optical plankton imaging and analysis systems for ocean observation,” *Proc. Ocean Obs*, vol. 9, pp. 21–25, 2010.
- [8] A. Remsen, T. L. Hopkins, and S. Samson, “What you see is not what you catch: a comparison of concurrently collected net, optical plankton counter, and shadowed image particle profiling evaluation recorder data from the north-east gulf of mexico,” *Deep Sea Research Part I: Oceanographic Research Papers*, vol. 51, no. 1, pp. 129–151, 2004.
- [9] L. Corgnati, S. Marini, L. Mazzei, E. Ottaviani, S. Aliani, A. Conversi, and A. Griffa, “Looking inside the ocean: Toward an autonomous imaging system for monitoring gelatinous zooplankton,” *Sensors*, vol. 16, no. 12, p. 2124, 2016.
- [10] C. S. Davis, S. M. Gallager, M. Marra, and W. K. Stewart, “Rapid visualization of plankton abundance and taxonomic composition using the video plankton recorder,” *Deep Sea Research Part II: Topical Studies in Oceanography*, vol. 43, no. 7-8, pp. 1947–1970, 1996.

- [11] P. F. Culverhouse, R. Williams, M. Benfield, P. R. Flood, A. F. Sell, M. G. Mazzocchi, I. Buttino, and M. Sieracki, “Automatic image analysis of plankton: future perspectives,” *Marine Ecology Progress Series*, vol. 312, pp. 297–309, 2006.
- [12] M. C. Benfield, P. Grosjean, P. F. Culverhouse, X. Irigoien, M. E. Sieracki, A. Lopez-Urrutia, H. G. Dam, Q. Hu, C. S. Davis, A. Hansen, *et al.*, “Rapid: research on automated plankton identification,” *Oceanography*, vol. 20, no. 2, pp. 172–187, 2007.
- [13] P. González, E. Álvarez, J. Díez, Á. López-Urrutia, and J. J. del Coz, “Validation methods for plankton image classification systems,” *Limnology and Oceanography: Methods*, vol. 15, no. 3, pp. 221–237, 2017.
- [14] A. De Robertis, J. S. Jaffe, and M. D. Ohman, “Size-dependent visual predation risk and the timing of vertical migration in zooplankton,” *Limnology and Oceanography*, vol. 45, no. 8, pp. 1838–1844, 2000.
- [15] D. Bianchi and K. Mislan, “Global patterns of diel vertical migration times and velocities from acoustic data,” *Limnology and Oceanography*, vol. 61, no. 1, pp. 353–364, 2016.
- [16] A. R. Longhurst and W. G. Harrison, “The biological pump: profiles of plankton production and consumption in the upper ocean,” *Progress in Oceanography*, vol. 22, no. 1, pp. 47–123, 1989.
- [17] K. J. Benoit-Bird and M. A. McManus, “A critical time window for organismal interactions in a pelagic ecosystem,” *PLoS One*, vol. 9, no. 5, p. e97763, 2014.
- [18] T. B. Kelly, P. C. Davison, R. Goericke, M. R. Landry, M. D. Ohman, and M. R. Stukel, “The importance of mesozooplankton diel vertical migration for sustaining a mesopelagic food web,” *Frontiers in Marine Science*, vol. 6, p. 508, 2019.
- [19] A. T. Greer, R. K. Cowen, C. M. Guigand, and J. A. Hare, “Fine-scale planktonic habitat partitioning at a shelf-slope front revealed by a high-resolution imaging system,” *Journal of Marine Systems*, vol. 142, pp. 111–125, 2015.
- [20] M. McManus, A. Alldredge, A. Barnard, E. Boss, J. Case, T. Cowles, P. Donaghay, L. Eisner, D. Gifford, C. Greenlaw, *et al.*, “Characteristics, distribution and persistence of thin layers over a 48 hour period,” *Marine Ecology Progress Series*, vol. 261, pp. 1–19, 2003.
- [21] J. M. Sullivan, P. L. Donaghay, and J. E. Rines, “Coastal thin layer dynamics: consequences to biology and optics,” *Continental shelf research*, vol. 30, no. 1, pp. 50–65, 2010.

- [22] A. T. Greer, A. D. Boyette, V. J. Cruz, M. K. Cambazoglu, B. Dzwonkowski, L. M. Chiaverano, S. L. Dykstra, C. Briseño-Avena, R. K. Cowen, and J. D. Wiggert, “Contrasting fine-scale distributional patterns of zooplankton driven by the formation of a diatom-dominated thin layer,” *Limnology and Oceanography*, vol. 65, no. 9, pp. 2236–2258, 2020.
- [23] M. M. Dekshenieks, P. L. Donaghay, J. M. Sullivan, J. E. Rines, T. R. Osborn, and M. S. Twardowski, “Temporal and spatial occurrence of thin phytoplankton layers in relation to physical processes,” *Marine Ecology Progress Series*, vol. 223, pp. 61–71, 2001.
- [24] B. A. Seibel, B. E. Luu, S. N. Tessier, T. Towanda, and K. B. Storey, “Metabolic suppression in the pelagic crab, pleuroncodes planipes, in oxygen minimum zones,” *Comparative Biochemistry and Physiology Part B: Biochemistry and Molecular Biology*, vol. 224, pp. 88–97, 2018.
- [25] D. Aurioles-Gamboa, “Inshore-offshore movements of pelagic red crabs pleuroncodes planipes (decapoda, anomura, galatheidae) off the pacific coast of baja california sur, mexico,” *Crustaceana*, pp. 71–84, 1992.
- [26] C. J. Robinson and J. Goómez-Gutieérrez, “The red-crab bloom off the west coast of baja california, mexico,” *Journal of plankton research*, vol. 20, no. 10, pp. 2009–2016, 1998.
- [27] C. M. Boyd, “The benthic and pelagic habitats of the red crab, pleuroncodes planipes,” 1967.
- [28] B. Cushman-Roisin and J.-M. Beckers, “Stratification,” in *International Geophysics*. Elsevier, 2011, vol. 101, pp. 347–364.
- [29] S. M. Gallagher, H. Yamazaki, and C. S. Davis, “Contribution of fine-scale vertical structure and swimming behavior to formation of plankton layers on georges bank,” *Marine Ecology Progress Series*, vol. 267, pp. 27–43, 2004.
- [30] S. S. Urmy, K. J. Benoit-Bird, J. P. Ryan, and J. K. Horne, “Mesopelagic predator-prey interactions revealed by joint passive and active acoustic observations,” *The Journal of the Acoustical Society of America*, vol. 146, no. 4, pp. 2899–2899, 2019.
- [31] S. S. Urmy and K. J. Benoit-Bird, “Fear dynamically structures the ocean’s pelagic zone,” *Current Biology*, vol. 31, no. 22, pp. 5086–5092, 2021.
- [32] R. Kubilius, E. Ona, and L. Calise, “Measuring in situ krill tilt orientation by stereo photogrammetry: examples for euphausia superba and meganyctiphanes norvegica,” *ICES Journal of Marine Science*, vol. 72, no. 8, pp. 2494–2505, 2015.

MANUSCRIPT 2

**High resolution measurements of the epi- and mesopelagic ocean by a
profiling vehicle equipped with environmental sensors and a
broadband echosounder**

by

Benjamin Grassian¹, Christopher Roman², Joe Warren³, Dave Casagrande⁴

Prepared for submission to Limnology and Oceanography: Methods

¹Ph.D. Candidate, Graduate School of Oceanography, The University of Rhode Island, Narragansett RI 02882. Email: bgrassian@gmail.com

²Professor of Oceanography, Graduate School of Oceanography, The University of Rhode Island, Narragansett RI 02882. Email: croman2@uri.edu

³Associate Professor, School of Marine and Atmospheric Sciences, Stony Brook University, Southampton, NY, 11968, USA. Email: jwarren@uri.edu

⁴Marine Development Engineer, Graduate School of Oceanography, The University of Rhode Island, Narragansett RI 02882. Email: dcasa@uri.edu

2.1 Abstract

Collecting detailed surveys of the environmental and biological heterogeneity in the epi and mesopelagic ocean is important for understanding the basic processes that govern these expansive habitats and influence the earth system at large. Common ocean sampling platforms (e.g. net systems, moored and shipboard sensors), are often unable to resolve marine biota at scales comparable to the variability existing in their physical environment. Newer approaches using mobile robotic systems carrying suites of environmental sensors have enabled detailed interrogation of the fine and sub-mesoscale distribution of animals, and have provided more context for the water column structure. We have integrated a dual-frequency split-beam echosounder (Simrad EK80 with 70 and 200 kHz transducers) into the Wire Flyer profiling vehicle to achieve concurrent hydrographic and acoustic sections in the midwater environment (0-1000 meters) at novel scales. The Wire Flyer provides high-resolution repeat profiling (0-2.5 m/sec up and down velocity) within specified water column depth bands typically spanning 300-400m. This system can provide acoustic backscatter data at depths unavailable to shipboard surveys due to attenuation limits and can be operated in tandem with conventional shipboard echosounders to provide overlapping acoustic coverage with concurrent hydrographic sections. The side-looking transducer orientation, as opposed to the traditional vertically oriented arrangement on ships, samples orthogonal to the vehicle's profiling survey path and provides a direct measurement of horizontal heterogeneity. The collected and processed data have proven the system's capacity to track migrating layers and resolve coherent biological patches and single targets in the horizontal, rising seafloor gas plumes, and scattering layer distributions tightly coupled to measured submesoscale features such as strong vertical oxygen gradients.

2.2 Introduction

The majority of the world's biomass resides within the mesopelagic region of the oceans [1, 2, 3]. The biological and physical processes in this habitat are dynamic and vary on multiple temporal and spatial scales [4, 5]. This has made effective sampling of the mesopelagic difficult [6], as traditional ocean sampling platforms (e.g. net systems, moored and shipboard sensors) are often unable to resolve marine biota at scales comparable to the variability in their physical environment. Ship-based surveys using direct (e.g. nets) or indirect (e.g. acoustic) sensors can typically monitor the near-surface (i.e. epipelagic) regions over smaller spatial and time scales, but they can be limited in their ability to sample smaller organisms (i.e. zooplankton) in deeper parts of the water column (> 200 m). Stationary sensor systems (e.g. moorings or buoys) can provide greater temporal resolution of these processes over longer time periods, but they are point samples and likely alias the patchy nature of the region.

The ability to measure deeper habitats is critical to understand a variety of fundamental and dynamic physical and biological ocean processes. The non-uniform migration of discrete scattering layers within the water column at daily rhythms helps drive the biological pump and underpins many of the ecological interactions in the open ocean. Frontal systems and submesoscale processes are often responsible for driving surface processes through nutrient enhancement [7] and coastal upwelling. Frontal systems are also common at shelf break environments where mixing between the epi- and meso-pelagic environment occurs [8]. Offshore, the importance of the massive mesopelagic fish community [9, 10] and their roles in the global carbon budget is a topic of growing interest [11, 12]. In addition, geologic features such as cold seeps support unique habitats [13] and chemical environments [14]. These processes and others are difficult to sample co-

herently with traditional instrumentation and methods (e.g. CTD casts, tow-yos and shipboard acoustics), and may be better captured using towed rapid profiling instruments (e.g. UCTD [15], SeaSoar [16], MVP [17], or Wire Flyer [18] that can resolve the appropriate spatiotemporal scales.

Acoustic sensors provide a way to remotely sample the marine environment at ranges of 10's to 1000's of meters at very high temporal resolutions (seconds). Acoustic echosounders are widely used tools to measure the abundance and distribution of marine organisms, especially zooplankton and fish [19]. The effective range of acoustic systems decreases with increasing frequency due to absorption, however higher frequencies, greater than 38 kHz, are most useful for measuring smaller lower trophic level organisms such as crustacean zooplankton. Additionally, the ensonified sample volume from ship-mounted systems increases with depth, which makes effective single target detection depth-dependant and more difficult for deeper scatterers [20]. For these reasons the depth that -based echosounders can effectively measure the abundance and distribution of marine organisms is limited. While lower frequency echosounders (typically below 38 kHz) can measure acoustic backscatter throughout much of the mesopelagic region these systems will not resolve weaker scatterers in deep environments due to signal attenuation. One solution to this problem is to bring the echosounders to the scattering features of interest by lowering and/or towing them from a ship [21, 22, 23, 24]. These systems often have incorporated multiple acoustic frequencies, environmental sensors and optical imagery to provide additional context to the acoustic data. The towed systems are typically operated in a tow-yo pattern to produce the water column coverage necessary to evaluate vertical distributions and produce hydrographic sections of environmental data. These ancillary data (e.g. temperature, salinity and oxygen) taken at depth are useful and are typically lacking in strictly

shipboard surveys. When using vertically oriented transducers on towed vehicles, some of the acoustic data will still remain outside of the depth range where the vehicle has been undulating and collecting environmental data.

Vertically-lowered, acoustic profilers have been used to profile with side-looking [25] and down-looking [26, 27] transducers. Using coincident acoustic and imaging volumes has proven effective in confirming single targets, such as fish with swim bladders, and scattering strength estimates [25]. Earlier vertically profiling acoustic systems, specifically the Tracor Acoustic Profiling System (TAPS) and Multifrequency Acoustic Profiling System (MAPS), have provided bioacoustical data at high (up to megahertz) frequencies with concurrent environmental measurements in the surface ocean [28]. These systems were configured to ensonify small horizontal sampling volumes (2-3 meters in horizontal range) in order to isolate recordings of zooplankton from larger scatters [29]. Sonar information collected in the horizontal orientation has been analyzed from TAPS at short meter scales [30] but point sample data is typically derived from these systems instead of analysis of backscatter returns over the full sampling range [31, 32, 33]. These systems were designed to examine fine vertical structures in the plankton and distribution patterns within the local environment, prioritizing innovative acoustic survey approaches over standardized techniques. Echosounders integrated into large [34, 35, 36] and mid-size [37] autonomous underwater vehicles (AUVs) have also been effective at collecting data beyond the range of shipboard systems. By using dual frequencies these systems are able to provide animal discrimination that is not achievable from shipboard systems due to frequency dependent attenuation (e.g. [38]). Lower power gliders are also able to carry echosounders [39, 40, 41]. Although somewhat constrained by power limitations, gliders fill a niche for multi-day observations and have many operational advantages over more demanding

ship and AUV operations.

In this paper we describe integrating a dual frequency (70 & 200 kHz) echosounder into the Wire Flyer towed vehicle [18]. The system utilizes the EK80 miniWBT echosounder in a similar manner as [41], but on a higher speed profiling vehicle with side-looking transducers. With the ability to quickly collect vertical profiles that are close in both time and space, our ability to study dynamic oceanographic (e.g. frontal systems, deep-sea vents, etc) or biological (animal zonation, deep scattering layer migration) processes can be improved. We present the integration of the acoustic system into the vehicle and present sample data that demonstrate a new ability to resolve acoustic scattering with high resolution and coincident hydrographic data within the mesopelagic.

2.3 Materials and procedures

The Wire Flyer towed profiling system is able to provide high horizontal resolution repeat profiling within a specified region of the water column [18] (Figure 9). The vehicle is autonomous and slides up and down a standard towed .322" CTD wire in an automatically controlled manner using the lift created by wing foils. A 2100 lb clump weight is towed below the lower profile depth to keep the tow wire taut, typically at 2-5 knots. The vehicle can achieve user specified up and down velocities ($0-2.5 \text{ m s}^{-1}$) while profiling down to 1000 meters. During deployments the vehicle is typically set to cover vertical bands of 300-400 meters positioned within the water column as needed. The profile cycles will generally repeat with one kilometer spacing.

The Flyer is equipped with the suite of environmental sensors (Table 2) to produce detailed hydrographic sections of the water column. A post processing routine accounts for the cable shape and vehicle layback behind the ship to place the data at the proper location (Latitude, Longitude, depth).

2.3.1 Echosounder integration

The EK80 miniWBT (Simrad Kongsberg) [42] is integrated into the Wire Flyer as a stand-alone sensor packaged in its own 1500 meter rated pressure housing 10. The 200 kHz ES200-7CDK-split $7^\circ \times 7^\circ$ and 70 kHz ES70-18CD, $18^\circ \times 18^\circ$ transducers are inset into the syntactic foam flotation on the top of the Wire Flyer with the beams oriented level and pointing sideways. They are mostly flush with the side of the vehicle and bordered by a retaining bezel to minimize flow disturbance. Testing with thin plastic coverings to make a completely flush fairing did not cause a change in signal quality, providing some indication that the level of flow induced signal noise is low.

The EK80 miniWBT electronics were removed from the standard splash-proof rectangular case and repackaged in a 106 mm diameter and 260 mm long cylindrical housing. In this configuration the four acoustic channel cards required additional ribbon cables to plug into the main transceiver backplane. The Mission Controller and storage card is also packaged with the system. This repackaging allows the system to be removed from the Flyer for testing and also keeps it away from radiated electrical noise inside the Wire Flyer’s main electronics housing. Each receiver card can be multiplexed to switch between two inputs, which provides eight total acoustic channels. The EK80 receives power and has RS422 communications with the main Raspberry Pi vehicle computer. A switching circuit allows the communications lines to be routed to either the vehicle computer or outside the

Table 2. Wire Flyer sensors and parameters

Sensor	Parameters	Sample rate
SBE 49 FastCAT	Temperature, conductivity, depth	16 Hz
Aanderra 4831F optode	Oxygen	0.5 Hz
Wetlabs FLbb-2K	Chlorophyll-a, turbidity (700 nm)	1 Hz

electronics housing via the deck cable so that the EK Mission Planner software can have a dedicated connection from an external computer. Due to the noise sensitivity of the sonar [41], power to the EK80 is filtered to achieve a roughly -50 dB noise reduction in the 75 kHz transducer band (Figure 11). We used a capacitance multiplier to increase the filter's RC while avoiding a large voltage drop over R1. The current through the resistor R1 is reduced by the T1 transistor gain, which is typically ≈ 100 . Selection of T1 impacts the filter's effectiveness and efficiency. The high bandwidth, at least 1 MHz, allows the filter to remove noise up to that frequency and the low voltage drop increases efficiency. The capacitance multiplier is followed by a second RC stage with a small resistor, R2, to remove any high frequency noise passing through or introduced by the transistor. Figure 12 shows a comparison with and without the power filter. This evaluation was made by looking at the distribution of the returns as a function of range in a region of the water column relatively devoid of acoustic scatterers. Since the test was done while towing, it also provides an assessment of the lower detection limit that also incorporates flow noise due to the vehicle's motion. With the EK80 running at a nominal 6 W the endurance of the Wire Flyer with the 800 Wh battery system is roughly 24 hours.

The EK80 mission files are planned and downloaded to the sonar prior to deployment. The mission plans are set up for a number of preset ensembles with ping patterns for each frequency. A linux-based sensor driver was written to interact with the EK80 via the RS422 communications interface. This driver connects to the EK80, sets the unit's time to match the vehicle's time and then sends the appropriate commands to ping particular ensembles. The ensemble pattern is set as part of the Flyer's overall mission plan, and the driver changes the pinging pattern as needed during a mission. The EK80 is configured to output real-time volume

backscattering strength (S_v) data for 20 range bins per ping. The driver records these messages as part of the standard data log and also flags other status messages indicating the state of the system. The logged S_v messages contain a timestamp from the EK80 that can be compared against the vehicle's time to correct for time drift within the sonar. These S_v data are also buffered in memory while operating and can be retrieved in snippets via the acoustic modem communications between the Wire Flyer and the ship side operator. This subsample of the data is useful to identify scattering aggregations and layers during a deployment. The full data are recorded on a large high speed USB flash drive in the EK80 electronics housing and retrieved for processing after a deployment.

The ping sequence is typically configured to alternate frequencies in the up and down directions (Figure 13b). The change in direction prompts the EK80 driver to switch the ping ensembles. In this pattern it is best to set the ensemble length longer than a single profile duration. If the ensemble completes the unit will pause and require the driver to resend a command to continue pinging. This exchange will create a gap of a few seconds in the data. Changing frequencies also causes a 8-10 second gap when the unit switches the multiplexer to the other channel on each card before resuming pinging at the new frequency (Figure 13c). When the Flyer is in a hold depth mode of level flight the pinging is typically set to alternate frequencies, executing a fixed number of pings at each frequency before switching.

A unique aspect of the echosounder on this platform is horizontal beam orientation, as opposed to the more traditional downward (or upward) transducers on ships and most other subsurface systems. An advantage of the side-looking arrangement is that the data are collected orthogonal to the movement of the platform, which creates an undulating ribbon of data as the vehicle moves forward and

vertically. The size of the ensonified sampling volume is also constant across the profile depth and is coincident with the environmental measurements. In addition, the echosounder data is from a region that is physically separated from the vehicle and cable wake or bow-wave where animals are more likely to exhibit natural behaviors as opposed to an avoidance reaction. Several echosounders have been previously deployed in a horizontally forward or side-looking configuration arrangement ([43, 44, 45, 46]). One disadvantage of this geometry is that the majority of fisheries acoustics literature considers data from downward-looking system. Thus, the interpretation of volume backscatter or target strength data from these side-looking systems will be more complicated than traditional ship surveys.

2.3.2 Echosounder data processing

The sonar was configured in Frequency Modulated (FM) mode, with a pulse length of 2048 μ s and a linear frequency sweep from 55-90 kHz and 185-255 kHz for the 70 and 200 kHz channels respectively. Simrad's broadband EK80 system outputs datagrams (.RAW file format) that encapsulate the system configuration and received acoustic information from both channels. To derive echocounting and echointegration values from the .RAW files, a software parser written in Matlab ingests the .RAW datagrams and calculates the Frequency Modulated (FM) pulse compressed and Continuous Wave (CW) versions of acoustic Power, Target Strength (TS) and Scattering Volume (S_v), and the angular positions. FM pulse compressed data are calculated by match filtering with the time-reversed complex conjugate of the original transmit chirp that is twice filtered at receive and recreated using the frequency sweep, slope, and filter values stored in the .RAW datagrams. The match filter power is used to derive pulse compressed versions of S_v and TS, and CW versions are derived using the raw power values and by appropriately scaling the effective pulse length. The CW values, while inaccurate for the

Frequency Modulated configuration, provide a dataset matching the mean volume backscatter strength calculated onboard the EK80 and are sufficient for on-the-fly mission adjustment and verification that the system is operating properly. The derived FM and CW echo integration and echocounting values are fused to the vehicle sensor information and stored in a data directory for post-processing.

The raw Sv data appeared to be dominated by the amplification of noise by the Time-Varying Gain (TVG) term, and a post-processing step was implemented to effectively 'flatten' the return over range. This post-processing step was applied differently for data collected before installation of the input power filter and for the higher SNR data collected following the power filter-installation (Figure 14). For the unfiltered data, the SV is detrended on a profile by profile basis by averaging all pings within that profile at depths unaffected by surface returns and median filtered to obtain a representative ping across range. This averaged ping is subtracted from each individual ping within that profile. The mean (Power/Sv/TS) value calculated from all pings within the survey is then added back as an offset. This processing step also alleviated the non-stationary power trends observed over the duration of the dive in the earlier datasets, often where deep profile sections have an increased power/ noise floor relative to the shallow 0-400m sections. This may be due to pressure effects on the transducers but we have not done a dedicated test. The higher SNR data collected after the installed power filter did not have the problem of a non-stationary noise floor/ power level across the duration of the dive, and these datasets were detrended as a single batch by averaging ping across all profiles at depths below 50m and adding back in an average value.

An additional post-processing step is performed to remove the roughly 1-4 pings that are interfered with every 30 seconds by the transmission from the acoustic modem used for vehicle and ship communications. The modem affected

pings were efficiently removed for the low SNR datasets with a median difference filter using the distal power values averaged from 50-100 m. In the higher SNR power filtered data, where the modem interference does not raise the noise floor as substantially and single targets are more often resolved at the distal ranges, the median difference filter was less effective and we instead removed the interfered pings manually. In future deployments, the stored timestamp marking the modem transmissions will allow us to remove these pings excluding the data within a small time window around the modem transmit timing.

When the vehicle is near the surface, scattering from the air-water interface can be observed in the data. This is the triangular region of high intensity scattering seen in Figure 13a. The surface-reflected region is excluded during post processing, as shown in Figure 16. This section can be calculated from the transducer beam angle, and varies by several meters with sea surface state. A triangle extending from the distal range at the surface is prescribed during processing and data within this region are automatically removed. An exclusion line from the full 100 m range at 50 meter depth back to the surface at a 5 m range is typically sufficient to remove the surface returns.

For data visualization, the processed Wire Flyer acoustic data can be range-averaged to render two-dimensional echograms similar to those obtained from shipboard systems. Since the range-averaged data occur along the vehicle's trajectory the coverage in the vertical is more sparse than a typical shipboard system, but the horizontal orientation should enable better statistics at a given depth. The 2-dimensional echograms are useful for directly comparison to the simultaneously collected environmental data. The acoustic data can also be rendered in full as a 3-dimensional point cloud. For most of the 3-dimensional Wire Flyer data presented here the 3-d acoustic Scattering Volume pointclouds were overlaid on co-registered

2-d echograms obtained by a downward-looking echosounder systems at the surface on the ship. The Wire Flyer Scattering volume data was thresholded at a lower bound to only show returns indicative of single scatterers, scattering layers, and acoustically-detectable hydrographic features.

2.3.3 Acoustic scattering layers as recorded in the horizontal

Horizontally insonified scattering layers record different synoptic information than from the vertical perspective (Figure 15). Compared to the vertical gradients, changes in backscatter intensity are typically smaller across the scattering layer horizontally, resulting in more constant backscatter over range. Due to spreading and absorption losses, the received backscatter decays logarithmically over the horizontal range and the signal intensity will fall below the noise floor at a certain distance (i.e. when the signal-to-noise ratio equals 0). When the signal loss terms are compensated by applying a TVG function (as is performed in the Sv and TS calculations), the noise floor is no longer fixed. By detrending the data over range (as described in the previous section), the signal excess is revealed. The balance between the scattering layer intensity and loss terms across the horizontal range explains the 'flame'-looking backscatter distribution seen in the 3-dimensional renders of the scattering layers. Within the layer the separation between the return scattering signal and the noise is greatest at short range, and then it decays with range until the return signal is at the noise level.

2.3.4 Concurrent shipboard echosounding

Downward looking acoustic data were recorded using hull-mounted or tow-fish based downward looking echosounder systems during several Wire Flyer deployments to provide standard acoustic echograms for comparison and groundtruth. A centerboard-mounted EK60 echosounder (operating at 38, 70, and 200 kHz)

recorded concurrent Continuous Wave (CW) acoustic data during deployments at the Costa Rica Margin in January 2019, and a dual-frequency (38 and 200 kHz EK80 miniWBT was deployed off the starboard side of the R/V *Endeavor* using a small towfish during deployments in Baltimore Canyon in September 2019. The transducers were located at a depth of approximately 5m and 1m below the surface for the R/V *Falkor* EK60 and the towfish systems respectively. These backscatter data were processed using a combination of Echoview and Matlab scripts. Surface and bottom exclusion zones were created to avoid noise from bubbles and bottom features and the background noise was removed following [47]. Volume backscattering strength values were integrated into 25 or 50 m horizontal by 1 m vertical bins and then exported. The 25 x 1 m towfish echogram, used to show the cold seep 2.4.4 was blurred using a Gaussian kernel after scaling the x-y echogram axes for the visualization. The downward looking acoustic data provided a ground truth and a comparison for the horizontally-beamed Wire Flyer data and were used to create the 3-dimensional data visualization products shown below.

2.4 Assessment

The Wire Flyer and integrated echosounder have been used on three cruises, allowing us to investigate several different scenarios where the overlapping environmental and acoustic data provide insight into the mesopelagic habitat. We show examples of salient oceanographic phenomenon recorded by the Wire Flyer in the following sections: diel vertical migration, shallow water front, deep oxycline associated assemblages, and a gaseous cold seep plume. These represent several broadly important biological and hydrographic features the Wire Flyer is uniquely suited to investigate.

2.4.1 Tracking diel migration

The massive Diel Vertical Migration (DVM) of animals at dawn and dusk is a near-ubiquitous biological phenomenon across the oceans that is well-studied using acoustic techniques. Shipboard acoustic observations of DVM around the globe has shown distinct regional heterogeneity in the timing and vertical redistribution of discrete scattering layers [48]. Variability in these migration events helps support and modify the ecological interactions and biogeochemical exchanges between surface and deep communities. The dynamics of scattering layer migrations appear to vary among species and their life histories, with some animal assemblages settling at depths that are physiologically driven (constrained by the oxycline), determined by phototaxis (a fixed depth at a specific illumination intensity), and influenced by food availability and predator avoidance. To understand how the spatiotemporal aspects of migrating biological layers are influenced by the local environmental gradients requires concurrent hydrographic measurements recorded over the relevant depths and temporal scales. Additionally, observing small migrating zooplankton layers requires high frequency acoustics that decay quickly over range and acoustic measurements that are not biased across the vertical sampling space. We show here two examples of DVM events captured in detail by the Wire Flyer (Figure 18, 19). Most notably the higher frequency echograms from ship or tow-based echosounders do not cover the full range of the migrating organisms. The Wire Flyer echograms are able to bring the higher frequency transducers to the depths of the scattering layers themselves, enabling their detection below the effective range of the shipboard measurements. Perhaps most importantly, the scattering layer features are similarly resolved and tracked at the surface by both systems suggesting that the differences in echosounder orientations (side vs down looking) is not problematic in terms of layer detection and tracking. Character-

istically "patchy" scattering layers have horizontal structure directly observed in the Wire Flyer data.

Most studies of mesopelagic deep scattering layers [1, 49, 50] rely on either one or two echosounder frequencies, typically 18 or 38 kHz. These frequencies allow recording of scattering layers at kilometer ranges from the surface. However, for most of the water column only larger (fish, squid) or strongly-scattering (swim-bladdered fish) organisms are detected. We know that the mesopelagic community is exceptionally diverse [6] and contains a variety of zooplankton and smaller organisms not well detected at these low frequencies (including the bristlemouth *Cyclothone* spp. which may be the most abundant vertebrate genus on the planet) [51]. Use of the Wire Flyer to explore these habitats can provide novel insights into the characteristics and movements of migrating layers. For many of the resonant (i.e. swim-bladdered fish) scatterers, it is likely that the size or shape of their swimbladder will change as the animals move vertically in the water column. It is however incredibly difficult to get individual target strength measurements from these layers as they migrate with traditional sampling methods, but it would be possible to track a migrating layer by having the Flyer adjust its profiling accordingly to provide repeated measurements of individual scatterer characteristics over large depth ranges. AUV and glider-based echosounders could also collect these data, however their ability to track migrating layers vertically would be more challenging without guidance from other sensing systems.

2.4.2 Shallow water front

The passive aggregation of plankton at oceanic fronts creates unique physical environments that catalyse biological interactions. Oceanic fronts promote enhanced biological activity and an associated redirection of foraging and motile behaviors. Submesoscale processes are often described from satellite or modelled

data ([52]). The idea that the surface ocean may be dominated by ephemeral submesoscale circulation processes that passively drive the distribution of primary producers or actively enhance primary production is becoming more prominent ([53, 54, 55]). High-resolution in situ assessments, alone and in combination with remote sensing and modelled information, have described nutrient distributions structured by filamentous submesoscale processes and the non-uniform responses to both the physical and ecological aspects of these features among identified taxa ([56, 57, 58]). The acoustic and environmental sections recorded by the Wire Flyer allow for near synoptic observation of the distribution of oceanic fronts and any associated redistribution of biological layers. In data recorded across a shallow water front off the New England Shelf Break, the division and aggregation of the biological layers is observed directly along the coherent edges of the front 20. The direct overlay of the environmental information and the biological layers provides observation of the coupling or lack of coupling between the environmental gradients imparted at the front and the distribution of biological layers. Turbulent features are visible in the environmental data across the front and corresponding horizontal patchiness is observed in the 200 kHz scattering data.

Environmental [59, 60, 61] and biological [62, 63, 64] measurements using towed vehicles or nets have been made across frontal zones for several decades. However, the vertical speeds of these towed samplers limits the horizontal spacing of the vertical profiles or the depth range which can be covered by the systems. The Wire Flyer platform produces data at a finer horizontal (order of kilometer) and vertical (cm) scale than any other current sensor system and offers a novel look at the processes occurring at the fronts. In addition, other oceanographic frontal features such as warm and cold core rings could also be better resolved with the increased sampling capabilities of the Wire Flyer system.

2.4.3 Oxygen minimum zone vertical boundaries

Oxygen data collected at the Costa Rica Margin (8.96N, 84.31W) show the potential of the system to capture small scale structure within the Oxygen Minimum Zone (OMZ) and across the upper and lower oxycline boundaries. Deep horizontally-distributed physical features like the lower oxycline have acoustic scattering distributions which closely match the concurrently recorded vertical oxygen gradients (Figure 21). The lower oxycline measurements recorded by the Wire Flyer consistently show an associated scattering layer tightly coupled to very fine scale variations in the oxygen environment. The correlation between the scattering layer depth and features of the oxygen profile has been observed using CTD casts (e.g. [65, 66]) but not with the level of detail seen here. This particular layer was persistent overnight and likely comprised of non-migrating animals whose depth is physiologically constrained at the lower oxycline [67, 68, 69]. As the distributions of the worlds OMZs are impacted in their extent and severity by ocean warming and climatic shifts, measurements capable of describing the settling depths and environments of migrating and non-migrating layers within the OMZ will prove valuable for discerning these animal habits as well as the anticipated impacts of the redistribution of the persistent oxygen boundaries.

2.4.4 Cold seep plume

Measurements from cold seep gas plumes on the New England Shelf break adjacent to the Baltimore Canyon produced 3-dimensional sections of salient hydrographic features 22. The Wire Flyer sensor measurements provide a detailed recording of not only the plume itself, but how the plume dynamics evolves and imparts structure to the water column in space and time. The larger overall structure of the gaseous plume, as well as wandering smaller-scale filaments, are well resolved in the 70 and 200 kHz data respectively. Compared to the 2-dimensional

measurements from the surface-bound towfish, the Wire Flyer data constrains the totality of the feature and the finer athwartship structures. The inherent geometry of the Wire Flyer acoustic survey data allows for it to fully capture these features in a matter somewhat similar to watercolumn imaging with multibeam sonar [70] but with a level of detail not easily achieved from a surface vessel due to attenuation limits.

2.5 Discussion

The integration of side-looking broadband echosounders into a rapidly profiling vehicle provides several advantages over other sensing systems used today. However, there are several issues, some common to any mesopelagic sampler and some unique to the Wire Flyer platform, that need further investigation.

2.5.1 Echosounder calibration

A key component of any acoustic echosounder system is the calibration [71] which allows for comparison of data between different sites and systems and, in some cases, identification and discrimination of individual scatterers. Given the Wire Flyer configuration, in situ calibrations with a standard target positioned athwartship of the vehicle would be very challenging to complete in most environments. However, the acoustic components can be separated from the Wire Flyer vehicle for an independent calibration using a hanging tethered sphere from a ship. A preliminary calibration provided poor coverage of the transducer surface (10 percent), but indicated moderate calibration values (i.e. mostly 1-4 dB differences between the uncompensated TS and compensated TS values) using the Simrad EK80 Client software. Uncalibrated data from the Wire Flyer can also be compared with ship-board or tow-fish echosounders to compare the relative values of backscatter strength of near-surface scattering layers and aggregations. How-

ever, the direct comparison of TS or other scattering parameters between these two systems would need to account for the backscatter directivity of most marine organisms. Even without a calibration, the data collected are useful for the identification of distinct scattering features in the ocean and relative comparisons of backscattering levels from these features.

2.5.2 Pressure effects on transducers

While the transducers used in the system are rated to 1500 meters depth, the Wire Flyer profiling repeatedly pressure cycles the sensors. To our knowledge this is the most stress (in terms of depth changes per time) these standard echosounder transducers have been exposed to. In survey data collected before the installation of an input power filter in the EK80 sensor package, the 70 kHz power from the individual transducer-elements varied over the course of a dive. These increasing or decreasing per-element power trends were pronounced when operating below 300 m and transitioning from deep to shallow depth bands, which suggests that the vehicle operating depth (pressure) may be a factor. We do not yet have data collected below 350 m using the input-power filtered echosounder setup, and cannot yet discern if these varying per-element trends are still evident. For the affected data, profile-specific TVG detrending, as described in the methods, alleviated most of the observed variability over time. A dedicated per-element test and analysis will need to be conducted to discern the effects of rapid pressure cycling in the 0-1000 m depth range. Additional analysis of a pressure induced impedance changes may also indicate a contribution to the nonstationary noise floor in the acoustic measurements over the duration of the survey [72].

2.5.3 Echosounder orientation and scatterer directivity

The majority of echosounder systems are deployed in near-vertical downward- (and to a lesser extent, upward-) looking configurations. Horizontally-oriented echosounders have been deployed on towed net systems and other platforms, but a major issue in the analysis of these side-looking data is whether the assumptions regarding target distribution, spacing, and other standards used to derive acoustic echo counting and echo integration quantities are still valid. The Wire Flyer acoustic data present an opportunity to reassess these assumptions for the horizontal-orientation perspective where a heterogeneous distribution of scatterers is observed within the beam pattern such as when profiling through scattering layers thinner than the beam width. Similarly, we have not yet derived frequency-dependent scatterer information (TS) for the broadband EK80 data, but we anticipate that standard scattering models will need to be modified (or re-calculated) for the geometry of this system.

As the Wire Flyer samples across dense scattering layers, the received backscatter signal is heavily attenuated over range. We assume the heavy attenuation of the acoustic returns while sampling within/ across dense scattering layers results in part from outgoing acoustic energy being scattered (in all directions) by the dense distributions of scatterers thus violating a key assumption in echo integration that most of the acoustic energy continues through scattering layers. If this assumption is violated, then analysis of our data may have to include multiple scattering theory such as what is done in the analysis of dense schools of fish where "shadow zones" exist below dense scattering aggregations. The loss of acoustic energy at the thin layer depths is increased by the horizontal beam direction which samples a dense scatterer distribution across the entire signal, as opposed to downward looking systems which sample across the vertically com-

pressed axis of these layers. If the signal loss due to enhanced extinction at dense scattering layers is better accounted for, quantification of scattering inhomogeneity or patchiness in the horizontal could be achieved, which remains an elusive measurement. Echo statistics [73, 74] may be a useful way of investigating the scattering characteristics of these layers.

2.6 Summary

The results from this project demonstrate a new acoustic survey capability to acquire environmental and acoustic sections in the 0-1000m region of the ocean at novel resolutions. The side-looking transducer orientation samples orthogonal to the vehicle's profiling survey path and provides a unique three dimensional acoustic dataset with coincident environmental data. This unique survey perspective enables observation of the spatial and temporal aspects of biological and physical scattering processes within the ocean. The survey resolution provided by the Wire Flyer can resolve dynamic features that would be aliased or unresolved by other available survey platforms. The 3-dimensional acoustic data collected by the Wire Flyer has also proven capable of resolving biological patchiness and rising seafloor gas plumes across both the horizontal and vertical sampling perspectives. Collectively the contributions from this project help to further the technology-enabled exploration of ocean ecosystems and the vast but difficult to observe mesopelagic habitat.

2.7 Figures

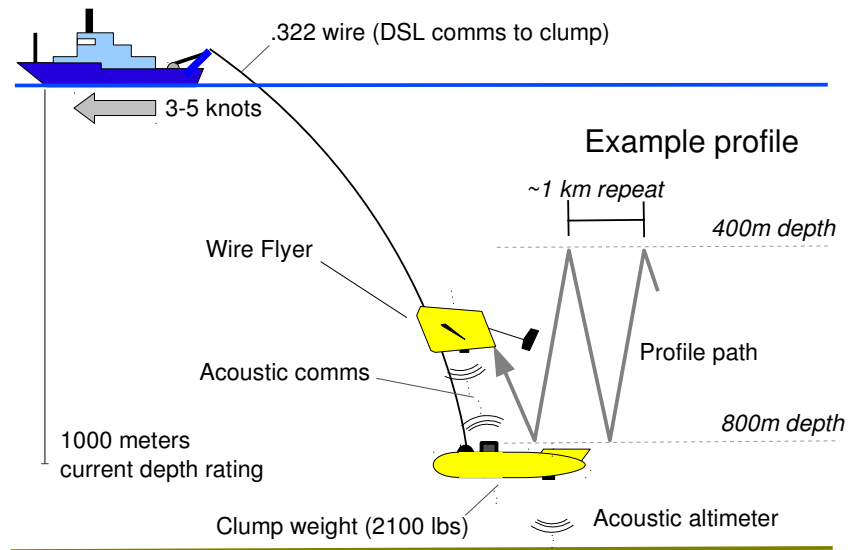


Figure 9. Wire Flyer towing diagram and sampling trajectory (reproduced from [18])

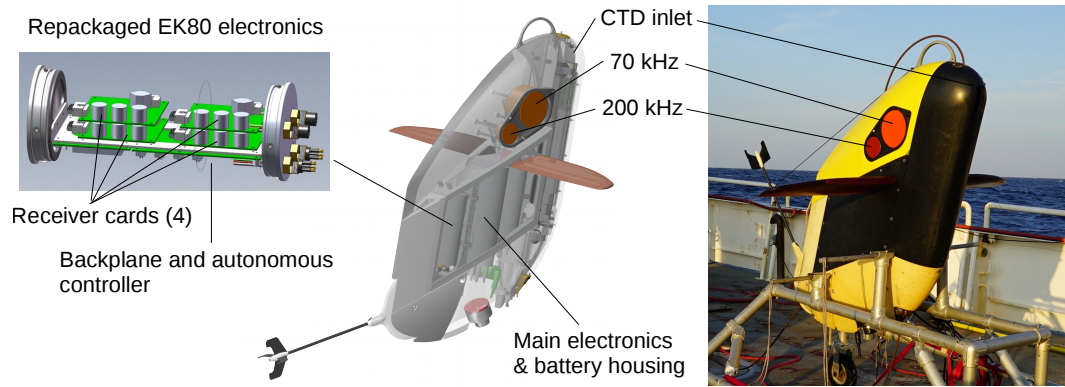


Figure 10. Wire Flyer mechanical details showing the repackaged EK80 electronics, the transducers inset into the foam flotation on the top of the vehicle and a photo of the Wire Flyer at sea. The oxygen sensor and fluorometer are mounted on the port side of the vehicle, out of view in this image.

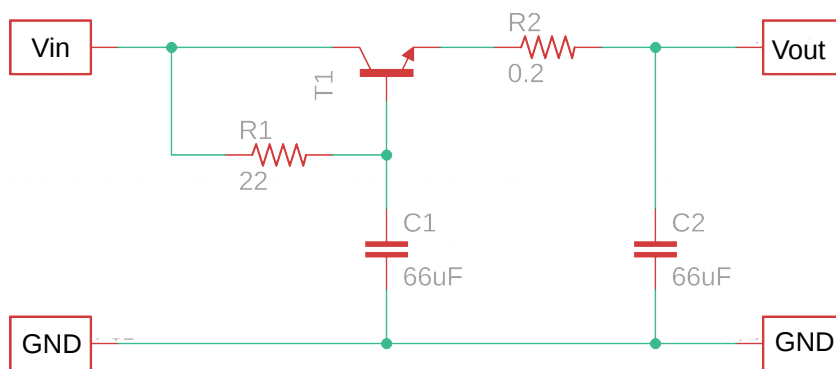


Figure 11. Schematic of the input power filter.

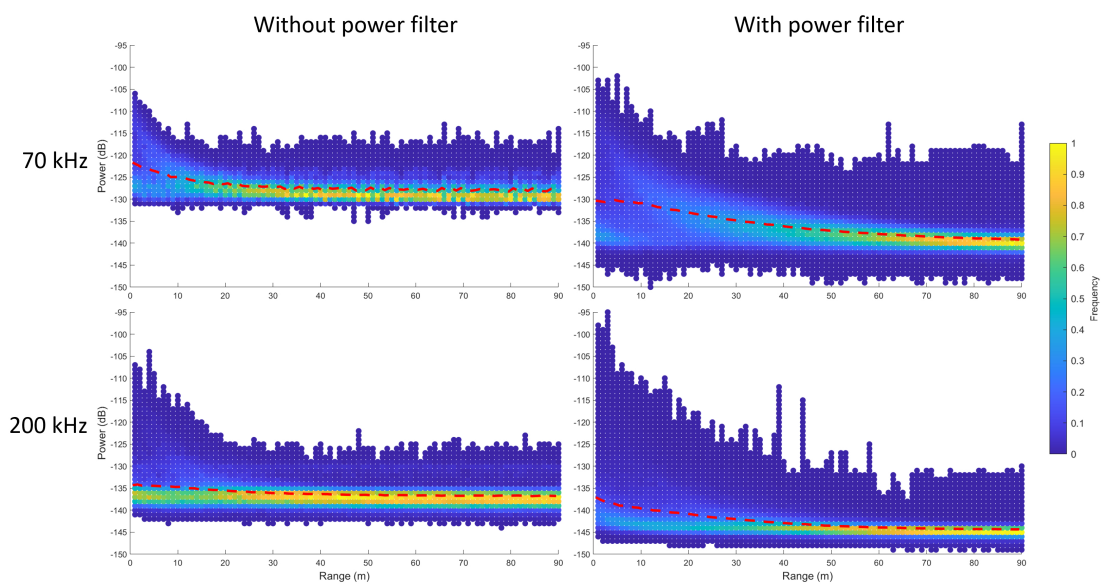


Figure 12. Comparison of the input power filtering. The plots show a histogram of the received signal levels over range for a section of the water column with little biomass. In both cases the high end of signal range is similar.

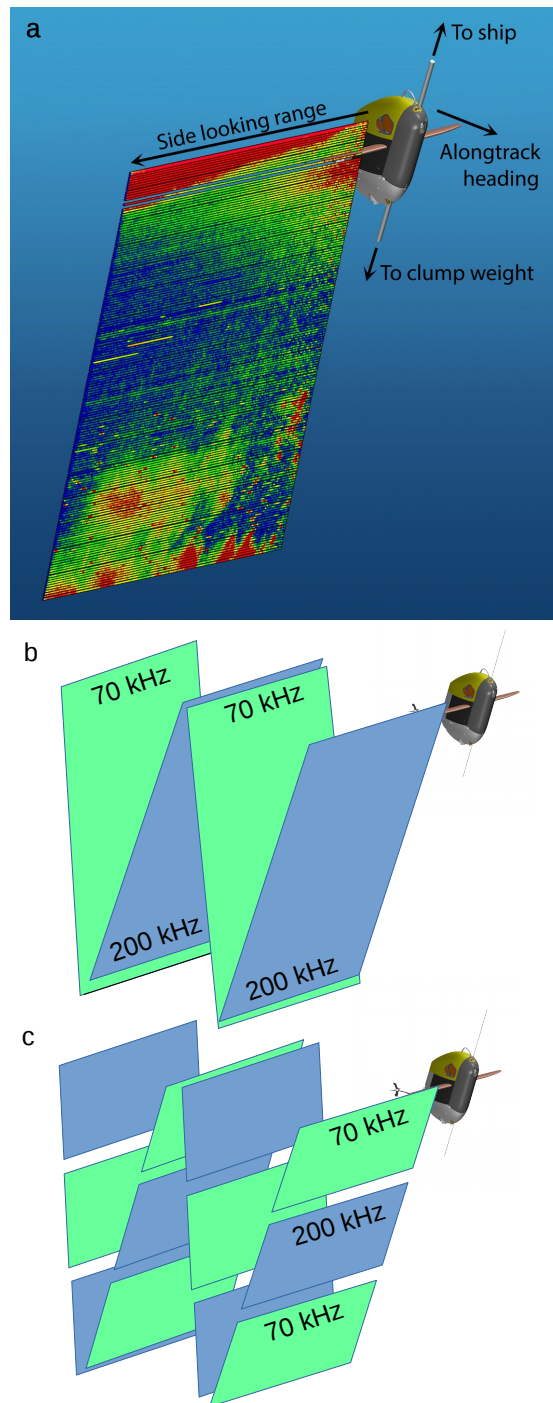


Figure 13. Wire Flyer side-looking acoustic survey. (a) Sample of detailed side looking 70 kHz data showing patchiness. (b) The typical sampling pattern alternating frequencies on the up and down profiles. (c) Alternating pings by depth or time within a profile.

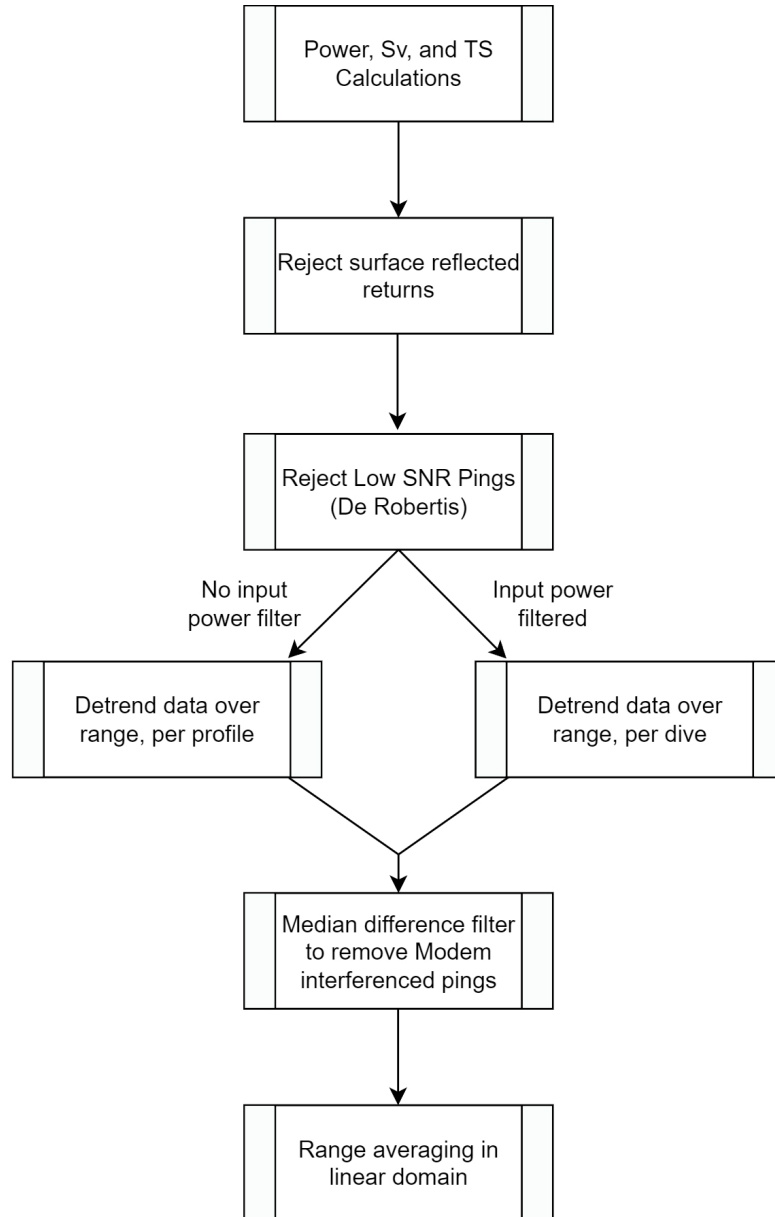


Figure 14. Process diagram outlining the Wire Flyer acoustic processing pipeline.

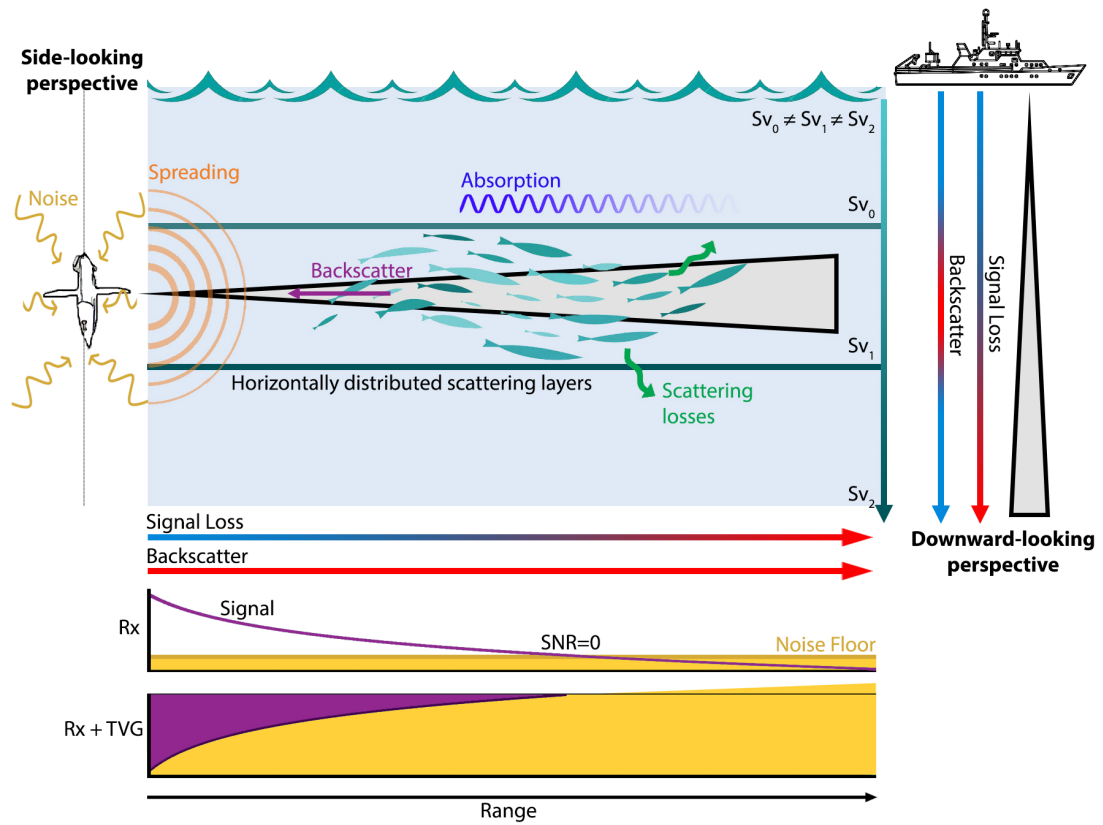


Figure 15. Schematic illustrating the fate of a side looking ping. The signal is attenuated over range due to the transmission loss terms and falls below the noise floor at range. The TVG amplification of the received backscatter signal, to compensate for the transmission loss, generates a non-uniform noise floor over range.

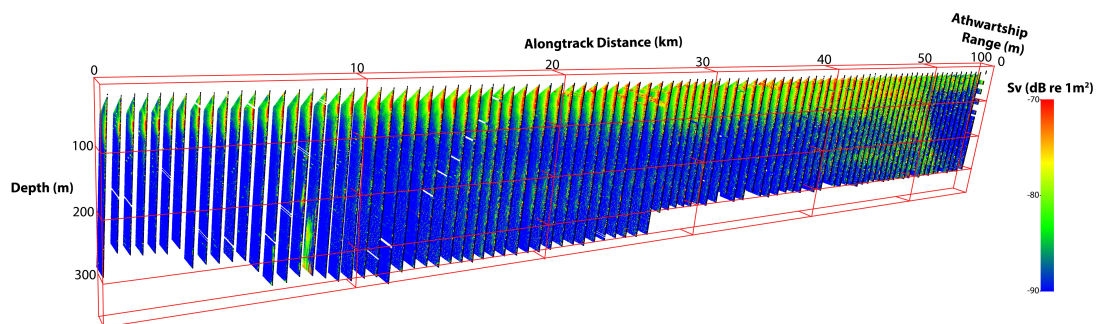
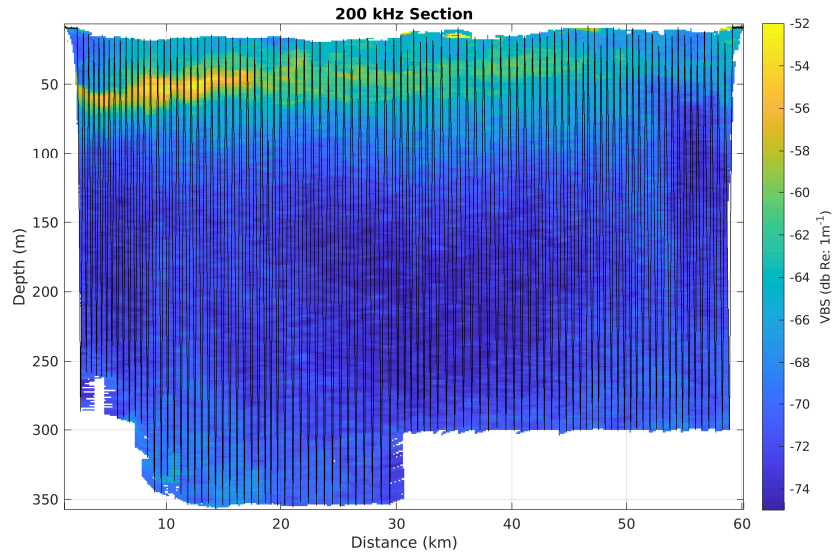
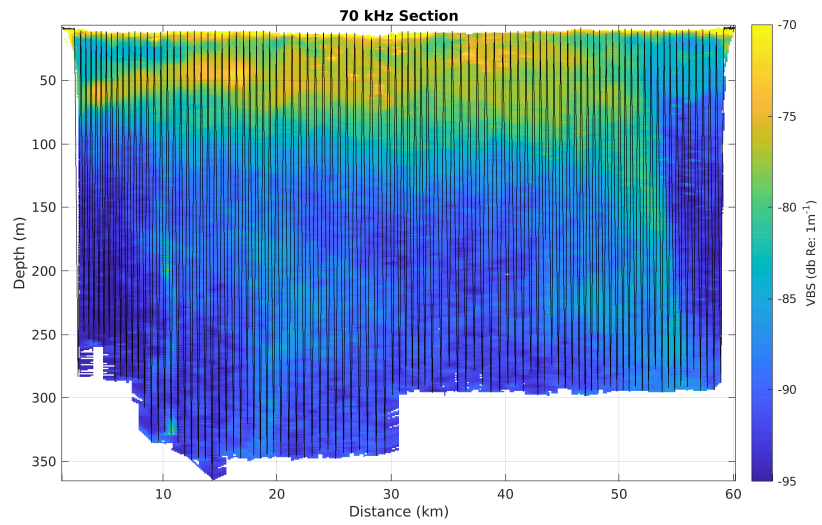


Figure 16. 3D rendering of the Wire Flyer acoustic data showing side-looking acoustic data "unwrapped" along the vehicle path.

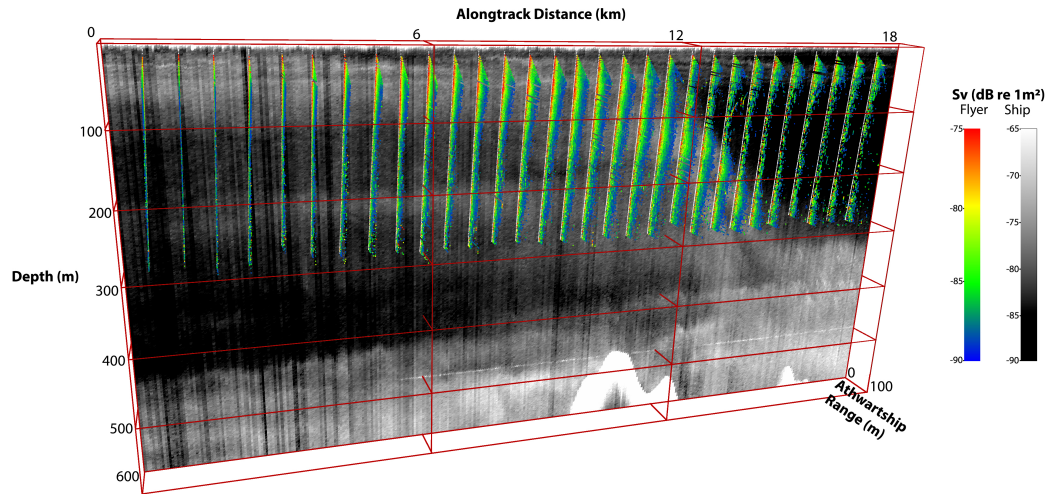


(a) Flyer 200 kHz

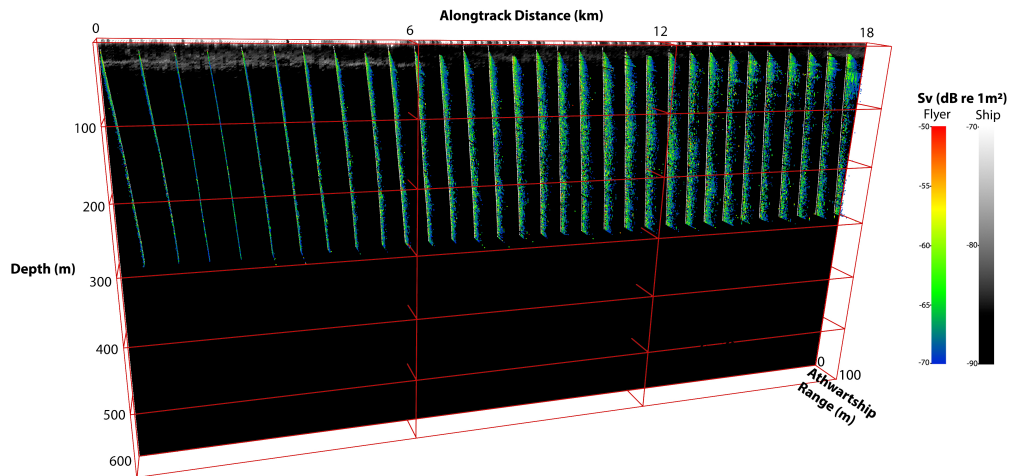


(b) Flyer 70 kHz

Figure 17. Section plots showing Scattering Volume averaged between 5 and 35 meters range and the Wire Flyer survey path for the a) 200 kHz and b) 70 kHz profiles.

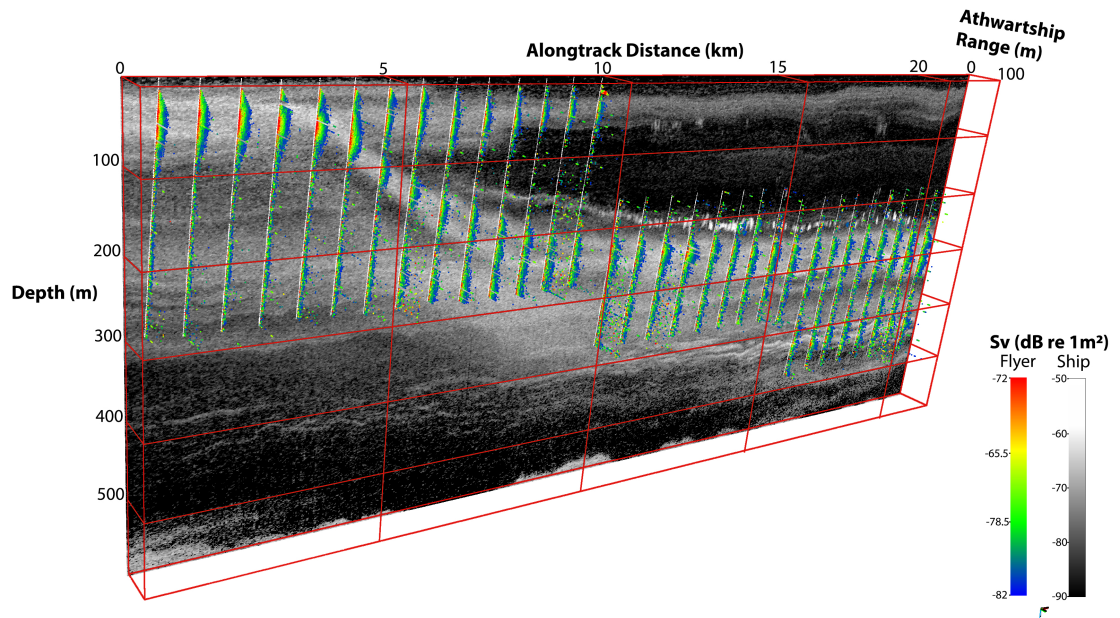


(a) Shipboard 38 and Wire Flyer 70 kHz

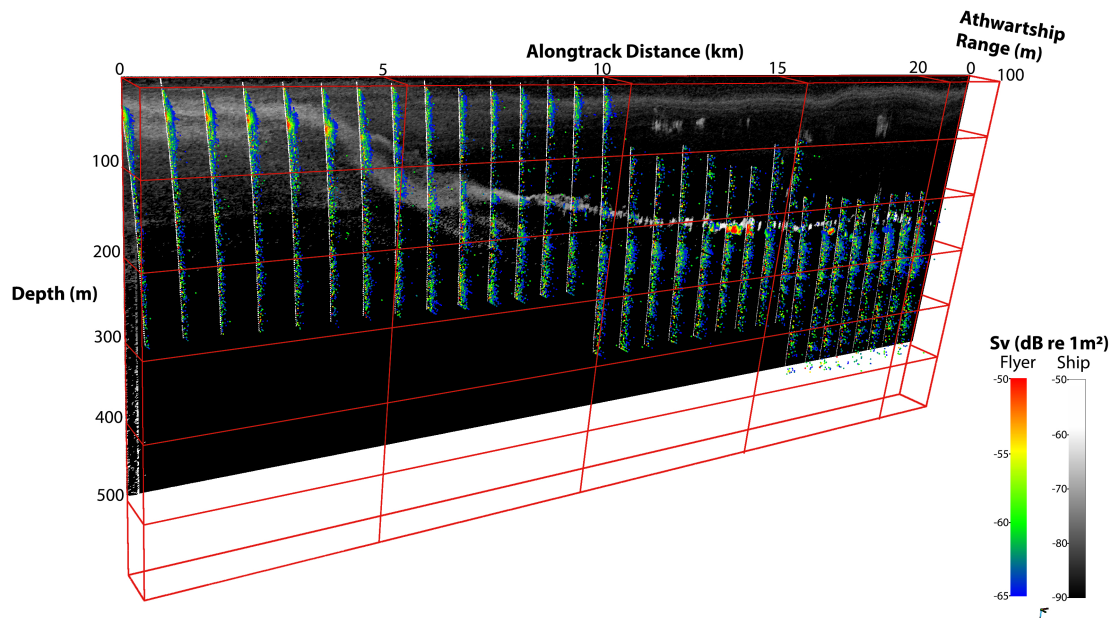


(b) Shipboard 200 and Wire Flyer 200 kHz

Figure 18. Downward diel migration at the New England shelf break front. (a) Shipboard 38 kHz shown in gray with the side looking Wire Flyer 70 kHz data shown in color and thresholded at the lower end. (b) 200 kHz Wire Flyer and shipboard data.



(a) Shipboard and Wire Flyer 70 kHz



(b) Shipboard and Wire Flyer 200 kHz

Figure 19. Downward diel migration at the Costa Rica Margin. (a) Shipboard 38 kHz shown in gray with the side looking Wire Flyer 70 kHz data shown in color and thresholded at the lower end. (b) 200 kHz Wire Flyer and shipboard data.

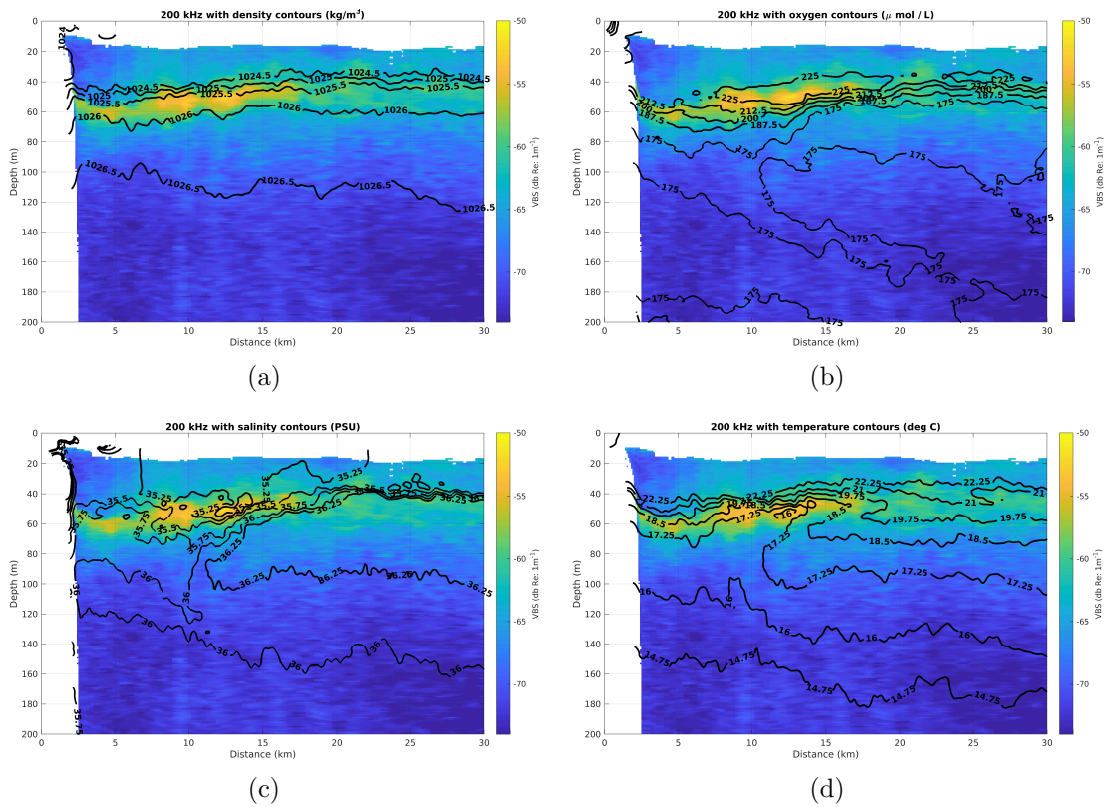


Figure 20. Transect across a frontal feature at the New England Shelf. Overlays of (a) density, (b) oxygen, (c) salinity, and (d) temperature all show good agreement with the concentration in acoustic scattering.

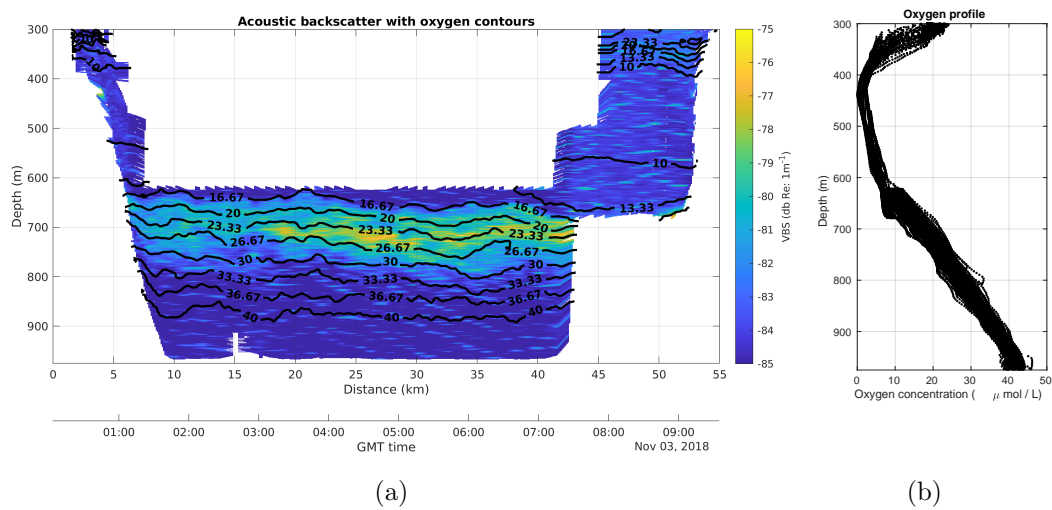


Figure 21. Wire Flyer transect at the lower oxycline in the Costa Rica Margin (GMT-6) (a) 70 kHz Wire Flyer acoustic data from with the oxygen concentration contours overlaid. (b) Scatter plot of oxygen measurements from all of the Wire Flyer profiles indicating the minimum depth and variability amongst the profiles over the length of the transect. These data were collected prior to the final power filter, so the overall signal range is limited by the higher noise floor.

List of References

- [1] S. Kaartvedt, A. Staby, and D. L. Aksnes, “Efficient trawl avoidance by mesopelagic fishes causes large underestimation of their biomass,” *Marine Ecology Progress Series*, vol. 456, pp. 1–6, 2012.
- [2] X. Irigoien, T. A. Klevjer, A. Røstad, U. Martinez, G. Boyra, J. L. Acuña, A. Bode, F. Echevarria, J. I. Gonzalez-Gordillo, S. Hernandez-Leon, *et al.*, “Large mesopelagic fishes biomass and trophic efficiency in the open ocean,” *Nature communications*, vol. 5, no. 1, pp. 1–10, 2014.
- [3] R. Proud, N. O. Handegard, R. J. Kloser, M. J. Cox, and A. S. Brierley, “From siphonophores to deep scattering layers: uncertainty ranges for the estimation of global mesopelagic fish biomass,” *ICES Journal of Marine Science*, vol. 76, no. 3, pp. 718–733, 04 2018. [Online]. Available: <https://doi.org/10.1093/icesjms/fsy037>
- [4] J. A. Koslow, P. Davison, A. Lara-Lopez, and M. D. Ohman, “Epipelagic and mesopelagic fishes in the southern california current system: Ecological interactions and oceanographic influences on their abundance,” *Journal of Marine Systems*, vol. 138, pp. 20–28, 2014.
- [5] E. Sinclair and P. Stabeno, “Mesopelagic nekton and associated physics of the southeastern bering sea,” *Deep Sea Research Part II: Topical Studies in Oceanography*, vol. 49, no. 26, pp. 6127–6145, 2002.
- [6] T. T. Sutton, M. R. Clark, D. C. Dunn, P. N. Halpin, A. D. Rogers, J. Guinotte, S. J. Bograd, M. V. Angel, J. A. A. Perez, K. Wishner, *et al.*, “A global biogeographic classification of the mesopelagic zone,” *Deep Sea Research Part I: Oceanographic Research Papers*, vol. 126, pp. 85–102, 2017.
- [7] K. L. Denman and T. M. Powell, “Effects of physical processes on planktonic ecosystems in the coastal ocean,” *Oceanogr. Mar. Biol. Ann. Rev*, vol. 22, pp. 125–168, 1984.
- [8] G. Gawarkiewicz and D. C. Chapman, “The role of stratification in the formation and maintenance of shelf-break fronts,” *Journal of Physical Oceanography*, vol. 22, no. 7, pp. 753–772, 1992.
- [9] P. Davison, D. Checkley Jr, J. Koslow, and J. Barlow, “Carbon export mediated by mesopelagic fishes in the northeast pacific ocean,” *Progress in Oceanography*, vol. 116, pp. 14–30, 2013.
- [10] M. A. St John, A. Borja, G. Chust, M. Heath, I. Grigorov, P. Mariani, A. P. Martin, and R. S. Santos, “A dark hole in our understanding of marine ecosystems and their services: perspectives from the mesopelagic community,” *Frontiers in Marine Science*, vol. 3, p. 31, 2016.

- [11] C. Robinson, D. K. Steinberg, T. R. Anderson, J. Arístegui, C. A. Carlson, J. R. Frost, J.-F. Ghiglione, S. Hernández-León, G. A. Jackson, R. Koppelman, *et al.*, “Mesopelagic zone ecology and biogeochemistry—a synthesis,” *Deep Sea Research Part II: Topical Studies in Oceanography*, vol. 57, no. 16, pp. 1504–1518, 2010.
- [12] T. R. Anderson and K. W. Tang, “Carbon cycling and poc turnover in the mesopelagic zone of the ocean: Insights from a simple model,” *Deep Sea Research Part II: Topical Studies in Oceanography*, vol. 57, no. 16, pp. 1581–1592, 2010.
- [13] E. K. Åström, M. L. Carroll, W. G. Ambrose Jr, A. Sen, A. Silyakova, and J. Carroll, “Methane cold seeps as biological oases in the high-arctic deep sea,” *Limnology and Oceanography*, vol. 63, no. S1, pp. S209–S231, 2018.
- [14] G. Aloisi, I. Bouloubassi, S. K. Heijs, R. D. Pancost, C. Pierre, J. S. S. Damsté, J. C. Gottschal, L. J. Forney, and J.-M. Rouchy, “Ch4-consuming microorganisms and the formation of carbonate crusts at cold seeps,” *Earth and Planetary Science Letters*, vol. 203, no. 1, pp. 195–203, 2002.
- [15] D. L. Rudnick and J. Klinke, “The Underway Conductivity Temperature Depth Instrument,” *Journal of Atmospheric and Oceanic Technology*, vol. 24, pp. 1910–1923, 2007.
- [16] R. Pollard, “Frontal surveys with a towed profiling conductivity/temperature/depth measurement package (SeaSoar),” *Nature*, vol. 323, p. 433–435, 1986.
- [17] A. W. Herman, B. Beanlands, M. Chin-Yee, A. Furlong, J. Snow, S. Young, and T. Phillips, “The Moving Vessel Profiler (MVP): In-situ sampling of plankton and physical parameters at 12 kts and the integration of a new laser/optical plankton counter,” in *Proceedings of Oceanology International*, vol. 102, 1998, pp. 123–135.
- [18] C. Roman, D. S. Ullman, D. Hebert, and S. Licht, “The Wire Flyer Towed Profiling System,” *Journal of Atmospheric and Oceanic Technology*, vol. 36, no. 2, pp. 161–182, 2019. [Online]. Available: <https://doi.org/10.1175/JTECH-D-17-0180.1>
- [19] J. Simmonds and D. N. MacLennan, *Fisheries acoustics: theory and practice*. John Wiley and Sons, 2008.
- [20] N. Diner, “Correction on school geometry and density: approach based on acoustic image simulation,” *Aquatic Living Resources*, vol. 14, no. 4, pp. 211–222, 2001.

- [21] E. J. Katz and W. E. Witzell Jr, “A depth controlled tow system for hydrographic and current measurements with applications,” *Deep Sea Research Part A. Oceanographic Research Papers*, vol. 26, no. 5, pp. 579–596, 1979.
- [22] R. J. Kloser, “Improved precision of acoustic surveys of benthopelagic fish by means of a deep-towed transducer,” *ICES Journal of Marine Science*, vol. 53, no. 2, pp. 407–413, 1996.
- [23] P. H. Wiebe, T. K. Stanton, C. H. Greene, M. C. Benfield, H. M. Sosik, T. C. Austin, J. D. Warren, and T. Hammar, “Biomaper-ii: an integrated instrument platform for coupled biological and physical measurements in coastal and oceanic regimes,” *IEEE Journal of Oceanic Engineering*, vol. 27, no. 3, pp. 700–716, 2002.
- [24] A. C. Lavery, T. K. Stanton, J. M. Jech, and P. Wiebe, “An advanced sensor platform for acoustic quantification of the ocean twilight zone,” *The Journal of the Acoustical Society of America*, vol. 145, no. 3, pp. 1653–1653, 2019. [Online]. Available: <https://doi.org/10.1121/1.5101063>
- [25] R. J. Kloser, T. E. Ryan, G. Keith, and L. Gershwin, “Deep-scattering layer, gas-bladder density, and size estimates using a two-frequency acoustic and optical probe,” *ICES Journal of Marine Science*, vol. 73, no. 8, pp. 2037–2048, 01 2016. [Online]. Available: <https://doi.org/10.1093/icesjms/fsv257>
- [26] A. Marouchos, M. Sherlock, R. J. Kloser, T. Ryan, and J. Cordell, “A profiling acoustic and optical system (paos) for pelagic studies; prototype development and testing,” *OCEANS 2016 - Shanghai*, pp. 1–6, 2016.
- [27] K. Haris, R. J. Kloser, T. E. Ryan, and J. Malan, “Deep-water calibration of echosounders used for biomass surveys and species identification,” *ICES Journal of Marine Science*, vol. 75, no. 3, pp. 1117–1130, 2018.
- [28] D. Holliday and R. Pieper, “Bioacoustical oceanography at high frequencies,” *ICES Journal of marine Science*, vol. 52, no. 3-4, pp. 279–296, 1995.
- [29] D. Holliday, R. Pieper, and G. Kleppel, “Determination of zooplankton size and distribution with multifrequency acoustic technology,” *ICES Journal of Marine Science*, vol. 46, no. 1, pp. 52–61, 1989.
- [30] K. J. Benoit-Bird and W. W. Au, “Echo strength and density structure of hawaiian mesopelagic boundary community patches,” *The Journal of the Acoustical Society of America*, vol. 114, no. 4, pp. 1888–1897, 2003.
- [31] M. R. Roman, D. V. Holliday, and L. P. Sanford, “Temporal and spatial patterns of zooplankton in the chesapeake bay turbidity maximum,” *Marine Ecology Progress Series*, vol. 213, pp. 215–227, 2001.

- [32] M. McManus, A. Alldredge, A. Barnard, E. Boss, J. Case, T. Cowles, P. Donaghay, L. Eisner, D. Gifford, C. Greenlaw, *et al.*, “Characteristics, distribution and persistence of thin layers over a 48 hour period,” *Marine Ecology Progress Series*, vol. 261, pp. 1–19, 2003.
- [33] K. J. Benoit-Bird, M. J. Zirbel, and M. A. McManus, “Diel variation of zooplankton distributions in hawaiian waters favors horizontal diel migration by midwater micronekton,” *Marine Ecology Progress Series*, vol. 367, pp. 109–123, 2008.
- [34] P. G. Fernandes, P. Stevenson, A. S. Brierley, F. Armstrong, and E. J. Simmonds, “Autonomous underwater vehicles: future platforms for fisheries acoustics,” *ICES Journal of Marine Science*, vol. 60, no. 3, pp. 684–691, 2003.
- [35] R. Patel, N. O. Handegard, and O. R. Godø, “Behaviour of herring (*clupea harengus* l.) towards an approaching autonomous underwater vehicle,” *ICES Journal of Marine Science*, vol. 61, no. 7, pp. 1044–1049, 2004.
- [36] C. Scalabrin, C. Marfia, and J. Boucher, “How much fish is hidden in the surface and bottom acoustic blind zones?” *ICES J. Mar. Sci.*, vol. 66, 06 2009.
- [37] M. A. Moline, K. Benoit-Bird, D. O’Gorman, and I. C. Robbins, “Integration of scientific echo sounders with an adaptable autonomous vehicle to extend our understanding of animals from the surface to the bathypelagic,” *Journal of Atmospheric and Oceanic Technology*, vol. 32, no. 11, pp. 2173–2186, 2015. [Online]. Available: <https://doi.org/10.1175/JTECH-D-15-0035.1>
- [38] K. J. Benoit-Bird, M. A. Moline, and B. L. Southall, “Prey in oceanic sound scattering layers organize to get a little help from their friends,” *Limnology and Oceanography*, vol. 62, no. 6, pp. 2788–2798, 2017. [Online]. Available: <https://aslopubs.onlinelibrary.wiley.com/doi/abs/10.1002/lno.10606>
- [39] D. Guihen, S. Fielding, E. J. Murphy, K. J. Heywood, and G. Griffiths, “An assessment of the use of ocean gliders to undertake acoustic measurements of zooplankton: the distribution and density of antarctic krill (*euphausia superba*) in the weddell sea.” *Limnology and Oceanography: Methods*, vol. 12, no. 6, pp. 373–389, 2014.
- [40] L. Suberg, R. B. Wynn, J. Van Der Kooij, L. Fernand, S. Fielding, D. Guihen, D. Gillespie, M. Johnson, K. C. Gkikopoulou, I. J. Allan, *et al.*, “Assessing the potential of autonomous submarine gliders for ecosystem monitoring across multiple trophic levels (plankton to cetaceans) and pollutants in shallow shelf seas,” *Methods in Oceanography*, vol. 10, pp. 70–89, 2014.

- [41] K. Benoit-Bird, C. Waluk, P. Welch, J. A. Barth, I. Wangen, P. McGill, C. Okuda, G. Hollinger, M. Sato, and S. Mccammon, “Equipping an underwater glider with a new echosounder to explore ocean ecosystems,” *Limnology and oceanography, methods*, 09 2018.
- [42] D. Demer, L. Andersen, C. Bassett, L. Berger, D. Chu, J. Condiotty, and G. Cutter, “Evaluation of a wideband echosounder for fisheries and marine ecosystem science,” *ICES Cooperative Research Report*, no. 336, 2017.
- [43] C. H. Greene, P. H. Wiebe, A. J. Pershing, G. Gal, J. M. Popp, N. J. Copley, T. C. Austin, A. M. Bradley, R. G. Goldsborough, J. Dawson, *et al.*, “Assessing the distribution and abundance of zooplankton: a comparison of acoustic and net-sampling methods with d-bad mocness,” *Deep Sea Research Part II: Topical Studies in Oceanography*, vol. 45, no. 7, pp. 1219–1237, 1998.
- [44] M. J. Underwood, E. García-Seoane, T. Klevjer, G. J. Macaulay, and W. Melle, “An acoustic method to observe the distribution and behaviour of mesopelagic organisms in front of a trawl,” *Deep Sea Research Part II: Topical Studies in Oceanography*, p. 104873, 2020.
- [45] R. O’Driscoll, J. Oeffner, O. Ross, A. Dunford, and P. McMillan, “Pilot acoustic survey for jack mackerel on the west coast new zealand (jma7),” *New Zealand Fisheries Assessment Report*, vol. 1, pp. 1–53, 2013.
- [46] C. G. Easson, K. M. Boswell, N. Tucker, J. D. Warren, and J. V. Lopez, “Combined edna and acoustic analysis reflects diel vertical migration of mixed consortia in the gulf of mexico,” *Frontiers in Marine Science*, 2020.
- [47] A. De Robertis and I. Higginbottom, “A post-processing technique to estimate the signal-to-noise ratio and remove echosounder background noise,” *ICES Journal of Marine Science*, vol. 64, no. 6, pp. 1282–1291, 2007.
- [48] D. Bianchi and K. Mislan, “Global patterns of diel vertical migration times and velocities from acoustic data,” *Limnology and Oceanography*, vol. 61, no. 1, pp. 353–364, 2016.
- [49] M. D’elia, J. D. Warren, I. Rodriguez-Pinto, T. T. Sutton, A. Cook, and K. M. Boswell, “Diel variation in the vertical distribution of deep-water scattering layers in the gulf of mexico,” *Deep Sea Research Part I: Oceanographic Research Papers*, vol. 115, pp. 91–102, 2016.
- [50] K. M. Boswell, M. D’Elia, M. W. Johnston, J. A. Mohan, J. D. Warren, R. Wells, and T. T. Sutton, “Oceanographic structure and light levels drive patterns of sound scattering layers in a low-latitude oceanic system,” *Frontiers in Marine Science*, vol. 7, p. 51, 2020.

- [51] J. S. Nelson, T. C. Grande, and M. V. Wilson, *Fishes of the World*. John Wiley and Sons, 2016.
- [52] L.-L. Fu and R. Ferrari, “Observing oceanic submesoscale processes from space,” *Eos, Transactions American Geophysical Union*, vol. 89, no. 48, pp. 488–488, 2008.
- [53] A. Pascual, S. Ruiz, A. Olita, C. Troupin, M. Claret, B. Casas, B. Mourre, P.-M. Poulain, A. Tovar-Sanchez, A. Capet, *et al.*, “A multiplatform experiment to unravel meso-and submesoscale processes in an intense front (alborex),” *Frontiers in Marine Science*, vol. 4, p. 39, 2017.
- [54] M. Lévy, P. J. Franks, and K. S. Smith, “The role of submesoscale currents in structuring marine ecosystems,” *Nature communications*, vol. 9, no. 1, pp. 1–16, 2018.
- [55] L. Rousselet, A. De Verneil, A. M. Doglioli, A. A. Petrenko, S. Duhamel, C. Maes, and B. Blanke, “Large-to submesoscale surface circulation and its implications on biogeochemical/biological horizontal distributions during the outpace cruise (southwest pacific),” *Biogeosciences*, vol. 15, no. 8, 2018.
- [56] J. Y. Luo, B. Grassian, D. Tang, J.-O. Irisson, A. T. Greer, C. M. Guigand, S. McClatchie, and R. K. Cowen, “Environmental drivers of the fine-scale distribution of a gelatinous zooplankton community across a mesoscale front,” *Marine Ecology Progress Series*, vol. 510, pp. 129–149, 2014.
- [57] N. Hernández-Hernández, J. Arístegui, M. F. Montero, E. Velasco-Senovilla, F. Baltar, Á. Marrero-Díaz, A. Martínez-Marrero, and Á. Rodríguez-Santana, “Drivers of plankton distribution across mesoscale eddies at submesoscale range,” *Frontiers in Marine Science*, vol. 7, p. 667, 2020.
- [58] L. Siegelman, M. O’toole, M. Flexas, P. Rivière, and P. Klein, “Submesoscale ocean fronts act as biological hotspot for southern elephant seal,” *Scientific reports*, vol. 9, no. 1, pp. 1–13, 2019.
- [59] R. W. Houghton, D. B. Olson, and P. J. Celone, “Observation of an anticyclonic eddy near the continental shelf break south of new england,” *Journal of Physical Oceanography*, vol. 16, no. 1, pp. 60–71, 1986.
- [60] M. A. Sundermeyer and J. R. Ledwell, “Lateral dispersion over the continental shelf: Analysis of dye release experiments,” *Journal of Geophysical Research: Oceans*, vol. 106, no. C5, pp. 9603–9621, 2001.
- [61] M. M. Rienecker and C. N. Mooers, “Mesoscale eddies, jets, and fronts off point arena, california, july 1986,” *Journal of Geophysical Research: Oceans*, vol. 94, no. C9, pp. 12 555–12 569, 1989.

- [62] T. Yamamoto and S. Nishizawa, “Small-scale zooplankton aggregations at the front of a kuroshio warm-core ring,” *Deep Sea Research Part A. Oceanographic Research Papers*, vol. 33, no. 11-12, pp. 1729–1740, 1986.
- [63] P. B. Ortner, P. H. Wiebe, L. Haury, and S. Boyd, “Variability in zooplankton biomass distribution in the northern sargasso sea: the contribution of gulf stream cold core rings,” *Fishery Bulletin*, vol. 76, no. 2, pp. 323–334, 1978.
- [64] P. H. Wiebe, N. J. Copley, and S. H. Boyd, “Coarse-scale horizontal patchiness and vertical migration of zooplankton in gulf stream warm-core ring 82-h,” *Deep Sea Research Part A. Oceanographic Research Papers*, vol. 39, pp. S247–S278, 1992.
- [65] A. N. Netburn and J. Anthony Koslow, “Dissolved oxygen as a constraint on daytime deep scattering layer depth in the southern california current ecosystem,” *Deep Sea Research Part I: Oceanographic Research Papers*, vol. 104, pp. 149 – 158, 2015. [Online]. Available: <http://www.sciencedirect.com/science/article/pii/S0967063715001107>
- [66] T. Klevjer, D. Torres, and S. Kaartvedt, “Distribution and diel vertical movements of mesopelagic scattering layers in the red sea,” *Marine Biology*, vol. 159, 08 2012.
- [67] K. F. Wishner, D. M. Outram, B. A. Seibel, K. L. Daly, and R. L. Williams, “Zooplankton in the eastern tropical north pacific: Boundary effects of oxygen minimum zone expansion,” *Deep Sea Research Part I: Oceanographic Research Papers*, vol. 79, pp. 122–140, 2013.
- [68] A. E. Maas, S. L. Frazar, D. M. Outram, B. A. Seibel, and K. F. Wishner, “Fine-scale vertical distribution of macroplankton and micronekton in the eastern tropical north pacific in association with an oxygen minimum zone,” *Journal of plankton research*, vol. 36, no. 6, pp. 1557–1575, 2014.
- [69] K. F. Wishner, B. A. Seibel, C. Roman, C. Deutsch, D. Outram, C. T. Shaw, M. A. Birk, K. A. S. Mislán, T. J. Adams, D. Moore, and S. Riley, “Ocean deoxygenation and zooplankton: Very small oxygen differences matter,” *Science Advances*, vol. 4, no. 12, 2018. [Online]. Available: <http://advances.sciencemag.org/content/4/12/eaau5180>
- [70] K. Colbo, T. Ross, C. Brown, and T. Weber, “A review of oceanographic applications of water column data from multibeam echosounders,” *Estuarine, Coastal and Shelf Science*, vol. 145, pp. 41–56, 2014. [Online]. Available: <https://www.sciencedirect.com/science/article/pii/S0272771414000900>
- [71] D. A. Demer, L. Berger, M. Bernasconi, E. Bethke, K. Boswell, D. Chu, R. Domokos, A. Dunford, S. Fassler, S. Gauthier, *et al.*, “Calibration of acoustic instruments.” 2015.

- [72] D. A. Demer and J. S. Renfree, “Variations in echosounder–transducer performance with water temperature,” *ICES Journal of Marine Science*, vol. 65, no. 6, pp. 1021–1035, 2008.
- [73] D. Chu and T. K. Stanton, “Statistics of echoes from a directional sonar beam insonifying finite numbers of single scatterers and patches of scatterers,” *IEEE journal of oceanic engineering*, vol. 35, no. 2, pp. 267–277, 2010.
- [74] T. K. Stanton, W.-J. Lee, and K. Baik, “Echo statistics associated with discrete scatterers: A tutorial on physics-based methods,” *The Journal of the Acoustical Society of America*, vol. 144, no. 6, pp. 3124–3171, 2018.

MANUSCRIPT 3

**Diverse Biological Information from Side-Looking Acoustic Survey
Data with Concurrent Hydrographic Measurements in the Pelagic
Ocean**

by

Benjamin Grassian¹, Christopher Roman², Melissa Omand³

*Prepared for submission to Deep Sea Research Part I: Oceanographic Research
Papers*

¹Ph.D. Candidate, Graduate School of Oceanography, The University of Rhode Island, Narragansett RI 02882. Email: bgrassian@gmail.com

²Professor of Oceanography, Graduate School of Oceanography, The University of Rhode Island, Narragansett RI 02882. Email: croman2@uri.edu

³Associate Professor of Oceanography, Graduate School of Oceanography, The University of Rhode Island, Narragansett RI 02882. Email: momand@uri.edu

3.1 Introduction

The majority of the world's biomass resides within the mesopelagic region of the oceans [1, 2, 3]. The biological and physical processes in this habitat are dynamic and vary on multiple temporal and spatial scales [4, 5]. This has made effective sampling of the mesopelagic ocean difficult, as traditional ocean sampling platforms (e.g. net systems, moored and shipboard sensors) are often unable to resolve marine biota at scales comparable to the variability in their physical environment [6]. Ship-based surveys using direct (e.g. nets) or indirect (e.g. acoustic) sensors can typically monitor the near-surface (i.e. epipelagic) regions over smaller spatial and time scales, but they can be limited in their ability to sample smaller organisms (i.e. zooplankton) in deeper parts of the water column (> 200 m). Stationary sensor systems (e.g. moorings or buoys) can provide greater temporal resolution of these processes over longer time periods, but they are point samples and likely alias the patchy nature of the region. To expand our understanding of pelagic ecosystems, field studies must be able to measure the local epi and mesopelagic hydrography concurrent to measurements of the resident populations [7, 8]. Physical gradients in the environment influence the processes of plankton aggregation, dispersal, and survival, helping to drive their heterogeneous distributions [9]. Biological structures in the pelagic environment are complex and plankton habits are diverse and not simple passive tracers of the physical gradients. Different populations demonstrate different responses to environmental conditions over different scales depending on their behavioral cues and life stage-specific dynamics, e.g. locomotion, diet, fecundity, and differential survival rates [10, 11]. Field studies must be able to simultaneously quantify the distributions of multiple trophic levels in the environment to differentiate between behavioral and physically mediated structures. Without quantifying the distributions of higher trophic levels includ-

ing especially micronekton, (small fish, crustaceans, and cephalopods that are the trophic link between zooplankton and top pelagic predators), key ecological questions concerning predator-prey interactions and their spatiotemporal overlap are not accessible [12]. Simultaneous measurements of phytoplankton, zooplankton, and micronekton are rare due to sampling constraints [13], but studies achieving these measurements have resolved novel biological dynamics that impart structure to pelagic ecosystems [10, 14, 15, 16, 17].

The dynamics and habits of micronekton are especially under-resolved relative to lower trophic levels [18], despite their key roles in pelagic habitats. Many micronekton species perform Diel Vertical Migration, migrating to surface waters to forage at night when predation pressures are reduced [19, 20] while other populations permanently reside at mesopelagic depths [21, 22]. Since primary production is absent in the mesopelagic, the migration rhythms of micronekton species establish a major conduit for the vertical transport of energy to the region [23]. Basin-scale studies have demonstrated regionally variable dynamics of the diel migrating pelagic component [24, 25] and detailed studies in local environments have begun to demonstrate the importance of behaviors between predator and prey in inducing vertical restructuring of pelagic populations and in promoting patchiness [26]. Survey approaches that can simultaneously measure the distributions of multiple trophic levels and hydrography from the surface ocean to mesopelagic depths offer ability to directly examine the roles the environment and predator-prey interactions play in structuring the inter-connected epi- and mesopelagic ecosystems.

Acoustic sensors provide a way to remotely sample the marine environment at ranges of 10's to 1000's of meters at very high temporal resolutions (seconds). Acoustic echosounders are widely used tools to measure the abundance and distribution of marine organisms, especially zooplankton and fish [27]. The effective

range of acoustic systems decreases with increasing frequency due to absorption, however higher frequencies, greater than 38 kHz are most useful for measuring smaller lower trophic level organisms such as crustacean zooplankton. Additionally, the insonified sample volume from ship-mounted systems increases with depth, which makes effective single target detection depth-dependent and more difficult for deeper scatterers [28]. For these reasons the depth ship-based echosounders can effectively measure the abundance and distribution of marine organisms is limited. While lower frequency echosounders (typically below 38 kHz) can measure acoustic backscatter throughout much of the mesopelagic region these systems will not resolve weaker scatterers in deep environments due to signal attenuation. One solution to this problem is to bring the echosounders to the scattering features of interest by lowering and/or towing them from a ship [29, 30, 31, 32]. In this paper we describe the analysis and data processing opportunities from side-looking acoustic data collected by the Wire Flyer towed profiling vehicle[33] integrated with a dual frequency (70 & 200 kHz) fisheries echosounder. The system utilizes the EK80 miniWBT echosounder in a similar manner as [33] but on a higher speed profiling vehicle with side-looking transducers. We demonstrate unique data types leveraging aspects of the side-looking orientation to target the measurement of dense scattering layers and inhomogeneous features. We analyze the acoustic data with respect to the environmental measurements and use modelling approaches to interrogate the distributions of scattering layers within the environment and examine whether known mechanisms related to the maintenance of plankton thin layers are evidenced in the multisensor dataset.

3.2 Materials and Procedures

3.2.1 Wire Flyer Profiling Vehicle

The Wire Flyer towed profiling system is able to provide high horizontal resolution repeat profiling within a specified region of the water column [34, 35]. The vehicle is autonomous and slides up and down a standard towed .322" CTD wire in an automatically controlled manner using the lift created by wing foils. A 2100 lb clump weight is towed below the lower profile depth to keep the tow wire taut. The vehicle can achieve user specified up and down velocities (0-2.5 m/s) while profiling down to 1000 meters. During deployments the vehicle is typically set to cover vertical bands of 300-400 meters positioned within the water column as needed. The profile cycles will generally repeat with one kilometer spacing.

The Flyer is equipped with the suite of environmental sensors to produce detailed hydrographic sections of the water column. The EK80 miniWBT (Simrad Kongsberg) is integrated into the Wire Flyer as a stand-alone sensor packaged in its own 1500 meter rated pressure housing. The system is dual channel with both 70 (Simrad ES70-18CD) and 200 (ES200-7CDK) kHz split beam transducers. For the presented dataset, the ping sequence was configured to alternate frequencies in the up (70 kHz) and down (200 kHz) profiling direction. The sonar was configured in Frequency Modulated (FM) mode, with a pulse length of 2048 μ s and a 'fast-ramping' linear frequency sweep from 55-90 kHz and 185-255 kHz for the 70 and 200 kHz channels respectively.

A unique aspect of the echosounder on this platform is the decision to have the transducers pointed laterally to the vehicle's movement, as opposed to the more traditional downward (or upward) transducers on ships and most other systems. An advantage of the side-looking arrangement is that the data being collected are orthogonal to the movement of the platform which provides collection of three-dimensional data as the vehicle moves forward and vertically. One disadvantage of

this geometry is that the interpretation of echoes from backscatter data is derived from assumptions made for downward and upward looking systems in the fisheries acoustic literature (Maclennan and Simmons). Thus, the interpretation of volume backscatter or target strength data from side-looking systems will be more complicated than traditional ship surveys. Since the range-averaged data occur along the vehicle's trajectory the coverage in the vertical is sparser than a typical shipboard system (meter vs cm scale), but the horizontal orientation should enable better statistics at a given depth.

3.2.2 Baltimore Canyon Survey

Field work on the R/V Endeavor in Sept 2019 targeting phosphorescent mussel assemblages associated with cold seeps around the Baltimore Canyon. The presented data was collected from a 13-hour Wire Flyer survey during nighttime hours through dawn (Sept 23rd 23:12 UTC – Sept 24th 11:55 UTC) following a transect path along axis of the continental shelf and across axis of the Baltimore Canyon that loops back onto a parallel transect roughly 2 km offshore (Figure 23). The full dataset comprised 188 individual profiles, 94 each for the 70 and 200 kHz channels and covered a total of 59 km alongtrack distance. Diverse biological and hydrographic features were recorded in the multisensor survey data, including coherent biological scattering layers, cold seep plumes detected acoustically, a shallow water oceanic front, and downward Diel Vertical Migration (DVM) at dawn.

3.2.3 Model Side-Looking Echosounder Pings

A 3D echosounder simulation was constructed to examine the received backscatter signal from a horizontally insonified scattering layer. The received power and Scattering Volume (Sv) were calculated by solving the sonar equation

across a conical acoustic beam extending 100m in range. The received sound intensity level (RL) was calculated for range and angle cells as a function of the source level (SL) and target strength (TS) for backscatter targets after accounting for the two-way spreading and absorption transmission loss (TL) terms. To simulate the beam pattern affect, a loss term was added to achieve a 3db reduction in power at half of the beam width. The received signal was scaled by the volume of each range angle cell to approximate the total contribution of scatterers that would be uniformly distributed in the cell. The total Power was calculated by summing the received sound intensity level RL across angle cells in the linear domain. A noise term (NL) was added to the received signal power in the linear domain to simulate stationary additive noise at the transducer. Scattering Volume was calculated by normalizing the received power by the beam area at range.

```

Beam simulator pseudo code: for i=1:dRange:Range
for j = 0:dTheta:Theta/2
RL (i, j) = 10∧[(SL(angle) -TL(range) + TS(angle, range))10]
RL (i, j) = RL * Beam Sector Volume(i,j)
end
Received Power(i) = 10*log10[Sum RL(i) + 10∧(NL/10)]
Scattering Volume = Received Power(i) Beam Sector Volume(i)
End

```

3.2.4 2D Metric for Scattering Layers

To enable direct analysis of the acoustically derived biological data with the environmental measurements, the 3-dimensional acoustic data needs to be reduced to a scalar value across range. The standard way to reduce the dimensionality of the acoustic data would be to average the Scattering volume (Sv) over range in the linear domain, converting the Sv data into Mean Volume Backscattering

Strength (MVBS) which represents the average backscattering intensity over the 100m sampling range and is proportional to animal density [36]. We explored other methods for reducing the dimensionality of the acoustic data with the highest fidelity to resolve the relative scattering layer intensities in the vertical and that may leverage the side-looking sampling aspect.

3.2.5 Edge Layer Shapes from Benoit Bird et al. 2009

The derived backscatter intensity and proxy profiles at scattering layers demonstrated asymmetric vertical gradients above and below the peak layer depth. The asymmetric ‘layer shapes’ were especially pronounced in the 200 kHz data, due at least in part to the smaller 7° beam width enabling measurements at tighter vertical resolutions. Profile layer shapes have been studied for phytoplankton and to a lesser extent zooplankton thin layers, which among several defining criteria are less than 5 m in vertical extent. Several viable formation mechanisms for thin layers and their observed shapes have been proposed including differential settling at stratified layers, convergence and vertical shear, passive diffusion, swimming behaviors, and vertical gradients in predation pressure [16, 37, 38, 10, 39]. The vertical extent of biological “layers” described by the chlorophyll and acoustic profiles from the Wire Flyer deployment in the Baltimore canyon exceeded the vertical thickness ascribed to thin layers.

We sought to derive information on the layer shapes for the chlorophyll fluorescence and 70 and 200 kHz acoustic profiles to determine if direct correlations to the environmental data and observable mechanisms related to thin layer formation were present (Figure 24). Our methodology for derivation of a layer shape metric followed [16] and provided a means to derive layer-specific data types without manual selection of the layer boundaries and against varying background intensities. In brief, the raw profiles are initially smoothed using a median filter, and the 1st

derivative is calculated and smoothed using a ‘loess’ filter. The intersection points defining the layer upper and lower boundaries are assigned from local maxima in the second derivative above and below the fluorescence or scattering peak depth. An upper and lower gradient value is calculated as the absolute value of the difference in the peak value and the value at 10% of peak with respect to the upper or lower baseline, divided by the difference in depth between the peak depth and the depths at the 10% upper or lower boundaries. The final layer shape value is calculated by subtracting the upper gradient divided by the value peak minus the lower gradient divided by the value peak.

3.2.6 1D Phytoplankton Model

To examine whether passive diffusion could produce the observed layer shape, we constructed a simple 1D model of phytoplankton vertical distributions over time in a 300 meter vertically stratified water column mirroring the stratification structure observed in the Baltimore Canyon. Our model resolution was configured with 1 meter depth bins with timestep increments of 1 minute. Starting phytoplankton distributions were modelled as gaussian curves centered at 100 meters with a sigma of 5 meters. An artificial diffusivity profile was created to mirror the inverse relationship to the recorded stratification profile structures, by establishing k values of 3×10^{-3} (highest k , least stratified), 1×10^{-5} (lowest k , maximum stratification), and 2×10^{-3} (intermediate diffusivity and stratification) for depths from 0-60 meters, 60-100 meters, and 100-300 meters respectively. The diffusivity profiles were smoothed using iterative moving average filters to reduce the sharpness of the interfaces. Phytoplankton flux was modelled as function of the vertical diffusivity gradient with constant growth and loss terms. The model was allowed to run for 10 days.

3.2.7 Multivariate Linear Regression Models

Multiple linear regression was used to examine the overall relationships between the acoustically derived biological information and the concurrently collected environmental data. Best-fit models were constructed separately for the 70 and 200 kHz datasets using unfiltered acoustic scattering metrics and environmental sensor data to maximize the model comparisons. Two models were derived for each channel using the range-averaged Mean Volume Backscatter Strength (MVBS) and the custom 2D metric for scattering layers. All profile data collected in the Baltimore Canyon before the start of Diel Vertical Migration were used for the multiple linear regressions to target only the nighttime distributions, 67 and 66 profiles for the 70 and 200 kHz respectively. For each of the four models, best-fit model selection was performed by stepwise forward selection using Akaike's information criteria (AICc) to determine the included explanatory variables[40]. Variable Inflation Factors (VIF) were calculated to assess collinearity among the explanatory variables. VIF values below 5 were considered minimally affected by collinearity and acceptable for inclusion in the model [41]. Explanatory variables were selected both using the AIC criteria to diagnose the goodness of fit of the model output against the number of predictor variables and using the VIF and independent pairwise testing to determine the strongest explanatory variables that minimized collinearity. Outlier data points with large influence on the model results were identified using Cook's Distance criteria, and outliers with Cooks Distance values > 0.025 were removed from the dataset for the final models analyzed [42]. Model results with the MVBS and custom metric as dependent variables were provided comparison of the fidelity of the two acoustically derived biological proxies, and model results for the 70 and 200 kHz channels were compared to examine the different influences of the environmental variables for the two functional groups

discriminated acoustically.

3.2.8 Run Length Analysis

An initial focus was made to determine data types maximizing the detection of coherent scattering layers. The side-looking configuration of our system presents opportunity to examine inhomogeneous features in the horizontal, such as single acoustic targets (i.e. individual animals). The algorithm implemented by Simrad for single target detection relies on confirming the validity of targets via a minimum allowable deviation in angle information [43]. Without robust calibration information, we attempted a simplified derivation of single target information inspired by ‘run length’ analysis, a technique used for lossless data compression [44]. To extract information on isolated targets detrended Sv/TS/or Power ping data is first median filtered over range using a small 1D kernel (3-5 times the raw delta range bin resolution). The initial median filtering of the data helps to render the major scattering layers as coherent single runs, allowing for easier separability of these features, but reduces the detectability of targets smaller than the filter window size. The data is then binarized using an empirically selected threshold value slightly elevated from the noise floor. The total number and length of separatable sequences or ‘runs’ (i.e. continuous ones bounded by zero values) are calculated for each ping.

The derived run length data can be classified using the length and abundance criteria to isolate ping data likely pertaining to single animal targets. A maximum run length size helps identify coherent scattering layer that have long run lengths reflecting a consistent elevation of scattering above the threshold value across long ranges. Setting a minimum for run length size and number per ping allows for removal of less confident targets that may be contributed to by noise or are relatively depopulate.

3.3 Assessment

3.3.1 Model Side-Looking Echosounder Ping Results

We simulated the received backscatter signal from insonified ‘high’ and ‘low’ TS horizontal layers, reflecting the scattering conditions within or outside the scattering layer from the side-looking perspective (Figure 25). The model results show that when a sonar system is not noise limited over the 100 meter acoustic range (i.e. $NL < SL + TS - TL$ for all ranges), there is a fixed offset between the power for the high and low TS pings equal to the delta TS between the scattering environments (Figure 26). When the system is noise limited before 100 meters due to the transmission loss ($NL > SL + TS - TL$), the offset between the power for the high and low TS pings is not fixed over range and reflects instead a convergence to the noise floor affected by the spreading loss, and the power difference between the high and low TS layer signal decays logarithmically.

These model results reflect what is seen in the side-looking Wire Flyer data when the data is ‘detrended’ over range, by subtracting an approximated average return (Figure 27). For high intensity pings recorded at the scattering layers, the detrended data reveals the signal at a maximum (scaled to the scattering layer TS) near the transducer and dropping towards the noise floor as a function of the TL terms. For this reason, excess signal strength for homogenous scattering layers is obtained over range until the SNR reaches 0, and thus higher intensity scattering layers result in a detectable signal over farther ranges than in weaker scattering layers. This also explains related phenomenon seen in Wire Flyer datasets, such as scattering layers recorded before installation of an input power filter (higher NL) being detectable over shorter ranges than in the input power filtered (lower NL) data.

The simulated power approximated the overall trends observed in the real Wire Flyer Power data, but we were unable to match the slopes exactly at both

short and long ranges. More sophisticated modeling efforts may provide an ability to quantify increased signal extinction due to enhanced scattering losses from the side-looking perspective, a phenomenon we imagine is likely to affect the acoustic recordings.

3.3.2 2D Metric for Scattering Layer Results

Backscatter intensity contours across scattering layers are largely coherent as viewed in the 3-dimensional acoustic data and appear to outline the scattering layer intensity gradients, as would be expected from our simulated results. To capture this 3-dimensional signal as a scalar across the full range with the highest fidelity, we first threshold the Scattering Volume data using an empirically selected value. The value selection is constrained by the requirement to exceed the noise floor on the low end and to avoid the saturation of scattering above the threshold across the full sampling range, which would ‘clip’ gradient features in the scattering layers. To convert to a scalar value, we integrate the binarized ping data across range to derive a value representing the percentage of range bins with scattering values exceeding the selected threshold (Figure 28). This method derives data targeting the recording of intensity gradients for apparently coherent/dense scattering layers and is less affected by scattering from single targets and noise than an averaging approach, especially over the full sampling range (Figure 29). Backscatter intensity profiles as represented by this custom metric had smoother shapes than observed in the MVBS data and in other tested derived backscatter data types (e.g. selecting a single or averaged Sv value at a preset range or range window, filtering and contour tracing the Sv data across pings). The fidelity of the custom metric was compared to the MVBS data in greater detail and with statistical criteria in analyzes detailed below.

3.3.3 Edge Layer Shape Metric Results

The layer shape for the 70 and 200 kHz acoustic profiles were derived both from the MVBS data and the custom metric and were roughly an order of magnitude smaller than recorded in the original paper, reflecting the larger vertical thickness of the layers analyzed here. The successful derivation of layer shape metrics from the automated processing decreased roughly two-fold using the MVBS data type, with 32 and 42 profile layer shapes derived from the MVBS data compared to 69 and 70 layer shapes derived from the custom metric for the 70 and 200 kHz channels respectively. Pairwise comparisons of the layer shape metrics with the environmental data and other derived metrics (e.g. layer thickness, layer depth) demonstrated weak and noisy correlations with low R² values (Figure ?? and Figure ??) . Relatively consistent correlations were found between the layer shapes and the layer peak depths, as well as between the 200 kHz layer shapes and the chlorophyll layer shapes. We examined whether the difference in scattering in a 5 and 10 meter depth window above and below the peak chlorophyll layer depth was correlated to the chlorophyll layer shape, as was found in the original study for thin layers. A weak, negative relationship was observed between the data types for the non-thin scattering layers we observed acoustically, curiously opposing the original findings. We found this weak relationship to be unconvincing of a gradient in predation pressure (as derived from scattering difference across the chlorophyll layer) inducing the chlorophyll layer shapes observed in the data, and do not think the layer shape approach as implemented in the original form applies well to our dataset with meter-scale vertical resolutions much coarser than recorded in the original study.

3.3.4 1D Phytoplankton Model Results

While it did not appear that a vertical gradient in predation pressure provided a mechanism for the chlorophyll profile layer shapes observed in our dataset, examination of potential passive physical processes offered a potential mechanism for producing the observed layer shapes with respect to the local water column structure. The chlorophyll layer peaks were consistently observed to occur on or below the peak in buoyancy frequency, with a vertical displacement between the peaks of roughly 0 to 10 meters. The vertical eddy diffusivity profile can be assumed to be inversely proportional to the buoyancy frequency (as related by epsilon and assuming no vertical shear). It is possible that differing gradients in the vertical eddy diffusivity (k) above and below the chlorophyll layer peaks may produce the observed positive (sharper upper gradient) in the dataset.

The model results show that phytoplankton layers with a sharp upper interface and elongated lower interface can result from different vertical gradients in passive diffusion enacted by the proximity of the phytoplankton to the stratified layer, and match well to observed shapes in the 200 kHz Wire Flyer data (Figure 32).

3.3.5 Multivariate Linear Regression Model Results

The best-fit multiple linear regression model using the custom metric as the dependent variable explained 76% and 80% of the variation in the data for the 70 and 200 kHz models respectively, while the MVBS models explained only 30% and 33% of the variation in the biological data. The rank order of included predictor variables selected using the Akaike Information Criteria was conserved among the MVBS and custom metric models, suggesting similar relationships existing between the two biological proxies to the environmental data. Individually strong predictor variables were removed to reduce collinearity and replaced by a single best representative variable (i.e. spice substituting temperature, salinity, depth,

and density). No predictor variables were transformed, as the linear relationships all demonstrated higher R² scores in independent testing than the transformed variables. The best-fit 70 kHz models included in rank order of importance chlorophyll, alongtrack distance, spice, oxygen, and buoyancy frequency (N^2). The best-fit 200 kHz models included in rank order of importance chlorophyll, oxygen, spice, alongtrack distance, and buoyancy frequency.

3.3.6 Run Length Distributions

Valid single target data within the bounds of the size criteria and with sufficient instances of single targets across range demonstrate altered distributions in the data set from the regions of high MVBS scattering. In the 70 kHz data from the Baltimore Canyon, valid single target ping data occurred on the boundaries of the major scattering layers exceeding the maximum length criteria (Figure ??). This likely reflects the decrease in scattering intensity towards the threshold and greater disaggregation of these dense scattering layers towards the vertical boundaries. Abundant valid single target data also defined a region within the deeper canyon environment and with horizontal boundaries corresponding to the tilted distribution of an intermediate water masses. While there may be non-negligible contributions from noise in the run length analysis, the correspondence between the valid single target pings and a specific intermediate water mass bounded within the canyon provides us confidence the derived distribution likely reflects the zonation of abundant single targets within the surveyed mesopelagic environment.

3.4 Discussion

3.4.1 Aspects of the Custom Metric

We have derived a novel biological proxy metric from side-looking acoustic data that maximizes the detection of dense, coherent scattering layers. The custom metric relies on the attenuation of weak scattering returns in the horizontal, and

the detection of intense scattering layers over farther sampling ranges. Simulation of the received acoustic intensity levels from a homogeneously insonified scattering layer demonstrated the logarithmic attenuation of the signal over the sampling range and provided the basic assumptions used to derive the custom data type.

The custom metric demonstrated greater statistical correlations to the environmental data than the range-averaged Scattering Volume data while sharing predictor variables selected by the best-fit criteria. The custom metric maximizes the detection of dense scattering layers and is more invariant to high intensity returns from single targets. For these reasons, the major scattering layer is recorded with higher fidelity in the custom metric, increasing the ability to correlate the scattering layer distributions to the environmental data. Deriving Mean Volume Backscatter Strength over shorter range windows improved the correlation of the MVBS data to the environmental measurements, but still did not exceed the model fits for the custom metric. The custom metric allows for the extraction of high fidelity scattering intensity information derived from the full sampling range, without being affected by added noise.

There are several considerations for analyzing the custom metric data type. The custom metric relies on empirically determined threshold values, which may introduce biases. The thresholding technique was effective for the isolation of the major scattering layer in the dataset used, due to the largely stationary noise floor observed during the survey and the lack of other similarly intense scattering layers. Adaptive techniques would allow for better detection of multiple scattering layers and remove the biases introduced by the threshold selection. We are also not yet accounting for higher order aspects of the survey geometry, such as returns from the side lobes and the increased vertical sampling volume over larger ranges [28]. Close inspection of the acoustic measurements at scattering layers showed that the

intense returns from the layers appear first at short ranges, and not approaching from long ranges as was observed for surface-reflected returns. This provides us reassurance the attenuation of the signal over range has a dominant influence on the receive level than other factors related to the survey geometry. Implementing routines to deconvolve the profiling data from the survey geometry and beam pattern will allow for higher vertical sampling resolutions and improved recordings of the scattering layer gradients.

3.4.2 Efforts to Assess Layer Shapes

The layer shape metric derived as implemented in the original study did not demonstrate statistically strong correlations to the environmental features. These results are due in part to the coarser vertical resolution of the side-looking acoustic measurements. It also appears that the physical processes within the Baltimore Canyon may exert a more dominant role in the structuring of the phytoplankton layer. Relating the water column stratification structure into a simulated diffusivity profile, the 1D phytoplankton growth model showed that differential passive diffusion of the upper and lower boundaries of the phytoplankton layers can produce the shapes observed in the collected data.

3.4.3 Environmental Predictors of the Scattering Layer Distributions

Comparison of the multivariate linear regression model results suggest different relationships to the environment variables between the 70 and 200 kHz acoustic scattering layers. Model fits for the 200 kHz were slightly increased from the 70 kHz models, with a 4% increase in the model fit in the 200 compared to the 70 kHz custom metric models. The difference in the ability to predict the scattering layer distributions from the environmental distributions likely reflects the tighter coupling of the 200 kHz assemblages, likely comprised of zooplankton [45] to the

local environment. Specifically, the association between the 200 kHz scattering and chlorophyll layers accounted for 70% of the observed variance in the custom metric model fit. The deeper association of the 200 kHz zooplankton assemblage to the chlorophyll distributions explains the greater predictive power of the model. Additionally oxygen concentrations demonstrated higher correlations to the 200 kHz data, adding several percentage more explanatory power to the model. It is likely that the scattering layer assemblage detected within the 70 kHz frequency band are larger zooplankton and mobile nekton species with enhanced ability for behavioral responses to influence their fine-scale distributions in the environment. Comparisons between the 70 and 200 kHz model results should be interpreted with caution, however, as the larger beam angle for the 70 kHz transducer invokes coarser vertical sampling resolutions and echo integration values from sampling volumes with greater vertical areas. The different vertical resolution owing to the different beam geometries may have impacted the goodness of fit of the 70 kHz model relative to the 200 kHz dataset.

3.4.4 Interpretation of Run Length Data

The distribution of classified ‘single target’ data derived from run length analysis was distinct from the echo-integration and custom metric echograms. Abundant run length data delineated the boundaries of the dense scattering layers and a unique mesopelagic region within the Baltimore Canyon tracking the intermediate water mass. Visual inspection of the full 3-dimensional acoustic data showed abundant single target-like features in the submarine canyon region matching the run length data. It however is not unlikely that noise may contribute to the classified run length data, as we have observed similar discrete features while in passive mode but recording during a separate and more complicated deployment. Extensive averaging and the selection criteria likely mitigated contributions from noise.

The salient correspondence between the mesopelagic run length distributions and the tilted water mass structure leads us to believe the run length data is in major part identifying regions with abundant single animal targets. There is also potential to use run length information to quantify the homogeneity of the scattering layers and to further classify the density of regions across the scattering layers. Implementing Simrad’s single target algorithm for split beam systems will allow us to compare the run length data to the formally derived data pertaining to single acoustic targets [46].

3.4.5 Taxonomic Information

In general, our analyzes were limited by the lack of net tow data that could provide baseline taxonomic information and groundtruth the identity of the assemblages discriminated acoustically [47]. For this reason, effort was made to derive simple data types determining the distributions of dense scattering layers and abundant single targets. An assumption has been made that the 200 kHz data resolves zooplankton, while the 70 kHz channel resolves nekton and larger zooplankton. Groundtruth taxonomic data collected by net tows or imaging systems will be invaluable to improve these assumptions and better define the ‘functional groups’ discriminated acoustically.

3.4.6 Spectral Information and System Noise

To fully exploit the broadband acoustic information from the system, frequency dependent Scattering Volume, $Sv(f)$, was derived following [46]. In theory, the echosounder should directly measure spectral response information useful for discriminating various taxonomic and functional animal groups [48, 49]. Spectral data was derived across a sliding window from 5 to 10 meters in range with 50% overlap, with a Fast Fourier Transform (FFT) resolution of 512 frequency points

(corresponding to a frequency resolution of 68 and 137 Hz for the 70 and 200 kHz channels respectively). Several passive 70 and 200 kHz acoustic profiles obtained during cruise work in the Baltimore Canyon were isolated for spectral analysis to provide baseline characterization of the noise spectrum from our system. The spectral response shapes from the passive profiles were compared to $S_v(f)$ data calculated from active profiling in depth bands corresponding to the major scattering layers. The active $S_v(f)$ data was elevated in magnitude from the passive $S_v(f)$ data but did not demonstrate altered response shapes (Figure 34). Further subsetting of meso and epi-pelagic scattering layers did not reveal discernable differences in response shapes. This preliminary spectral analysis provided baseline information on the systems noise content. In general our system is affected by a noticeably elevated noise floor [50]. An overall flat response shape and magnitude spikes in narrow frequency bands were consistently observed in the 200 kHz data, whereas the 70 kHz spectral response decreased over the frequency range. Further characterization and dedicated mitigation of the various noise sources in the Wire Flyer acoustic system, specifically with respect to potential electrical and flow noise induced by the vehicles profiling motion, is required to fully exploit the broadband potential of our system.

3.5 Summary

Using basic acoustic assumptions we have derived simple and diverse metrics from side looking echo integrated Scattering Volume data. The simulation of side-looking echosounder data within homogenous scattering layers matched trends observed in the Wire Flyer data and illustrated the mechanisms of the attenuation of the signal strength over range at dense scattering layers. Our intention to maximize the detection of dense scattering layers and disaggregated targets was achieved by targeting information pertaining to the homogeneity of elevated scat-

tering intensities over the horizontal sampling range. We were able to confirm the efficacy of these metrics using model fits between the standard range-averaged Mean Volume Backscattering Strength (MVBS) or custom metric to the same environmental data. These model fits diverged between the 70 and 200 kHz acoustic channels, showing the stronger coupling of the 200 kHz scattering layer to the environmental distributions, especially chlorophyll.

3.6 Acknowledgments

We thank the captain and crew of the R/V Endeavor for assistance in the field. Lars Anderson provided guidance with the spectral analysis. Joe Warren and Kelly Benoit-Bird provided helpful discussion about the side-looking acoustic data.

3.7 Figures



Figure 23. Wire Flyer survey waypoints overlaid on Google Earth bathymetry. The major portion of the observed shallow water front is indicated by the green waypoints

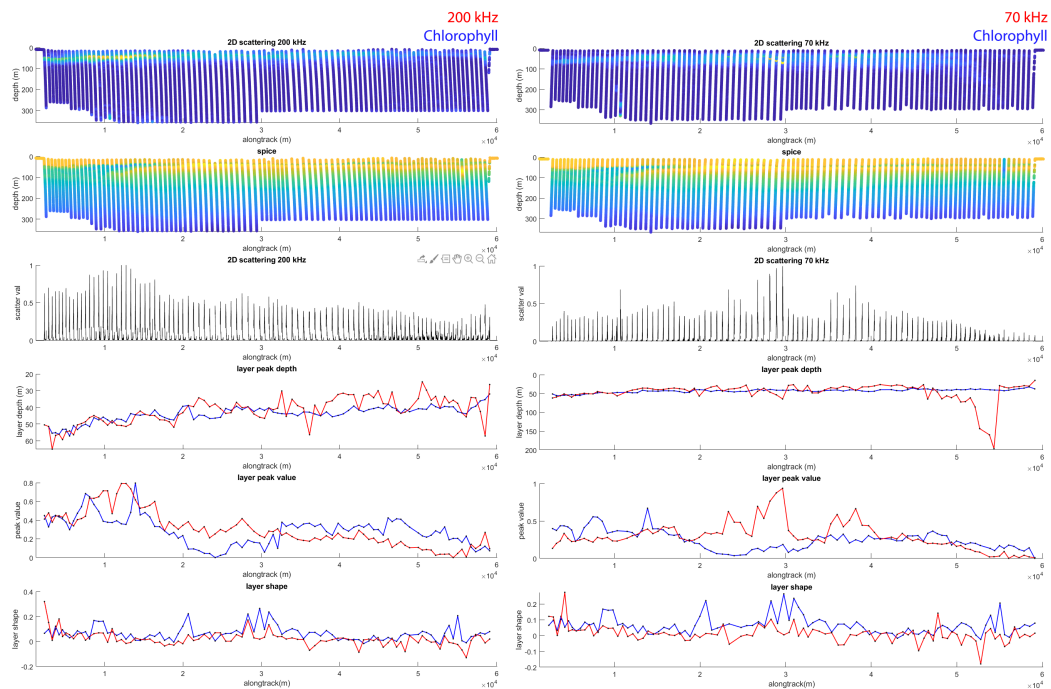


Figure 24. Environmental and layer shape associated per-profile metrics from the 70 and 200 kHz custom metric data (red line plots) plotted alongside the chlorophyll layer shape data (blue) for the complete Baltimore Canyon Survey. The 200 kHz scattering layer reaches maximum intensities at the front. The 70 kHz layer shape data types track the downward migrating layer at dusk.

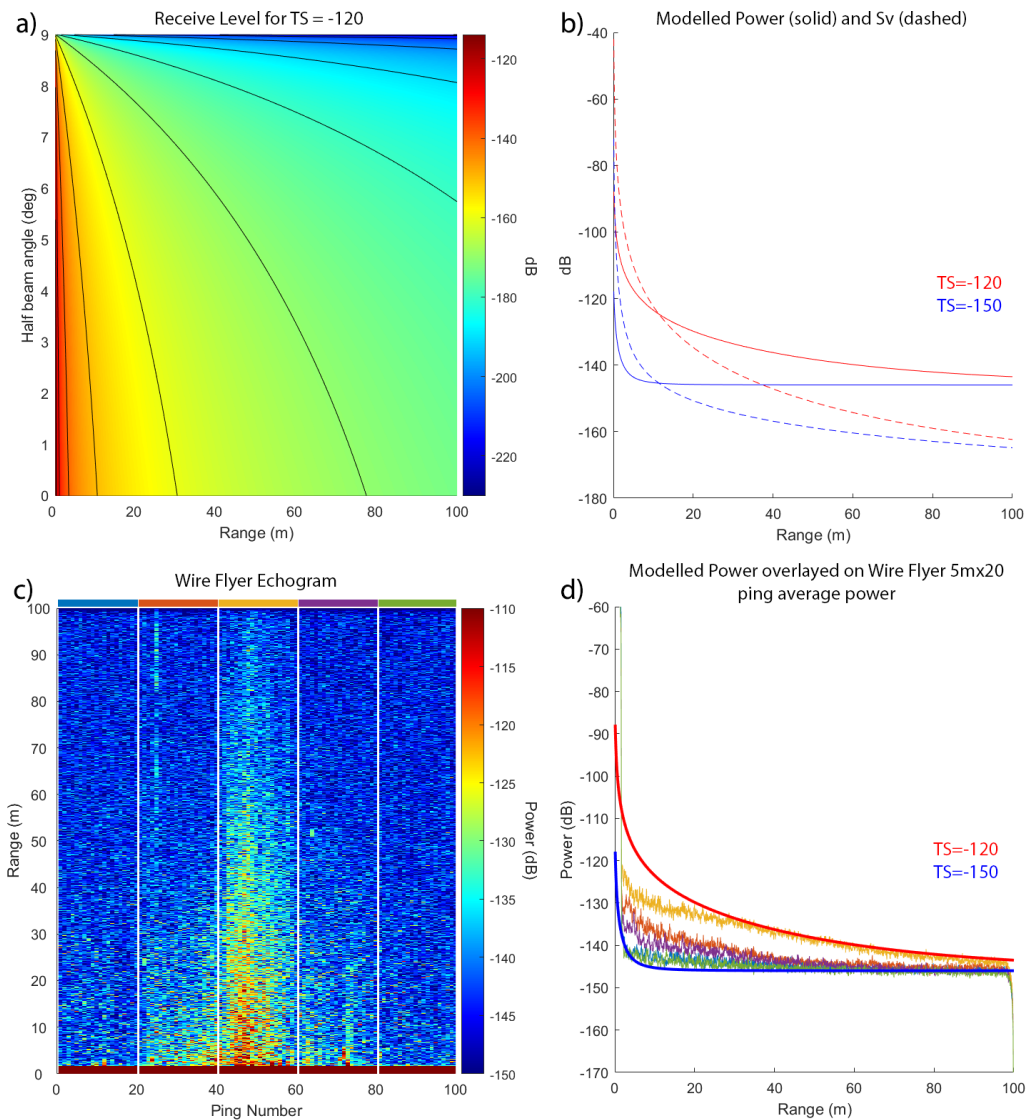


Figure 25. Simulated side-looking echosounder Power and Sv data (Theta = 18 deg, SL = 15 dB, NL=-146 dB, AbsCo=20 dB/km) matches the Wire Flyer data. A) Receive level distribution for a homogeneous scattering layer of -120 dB Target Strength across range angle cells. B) Modelled Power and Sv ping data for scattering layers of -120 and -150 dB Target Strength. C) Wire Flyer 100 ping power echogram showing bounded scattering feature. The colored bars atop show the 20 pings averaged for comparison to the model power data. D) Simulated power pings for TS=-120 dB and TS=-150 dB overlaid on Wire Flyer 20 ping power averages showing good alignment at far ranges.

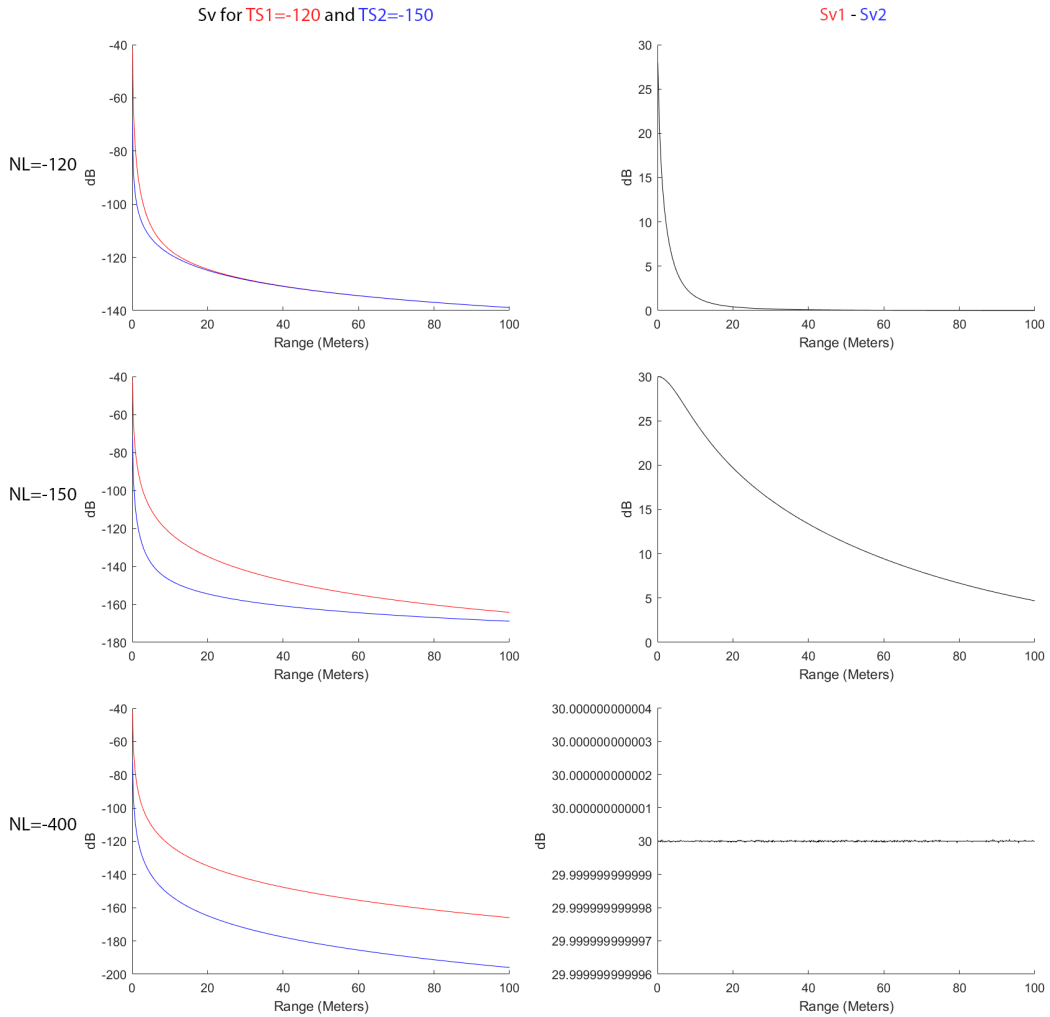


Figure 26. Modelled Scattering Volume for two scattering layers with TS=-120 and TS=-150 dB on the left panels, and the difference between the Sv for the high minus low TS pings on the right panel, under increasing Noise Levels (-120 dB top row, -150 dB middle row, -400 dB bottom row).

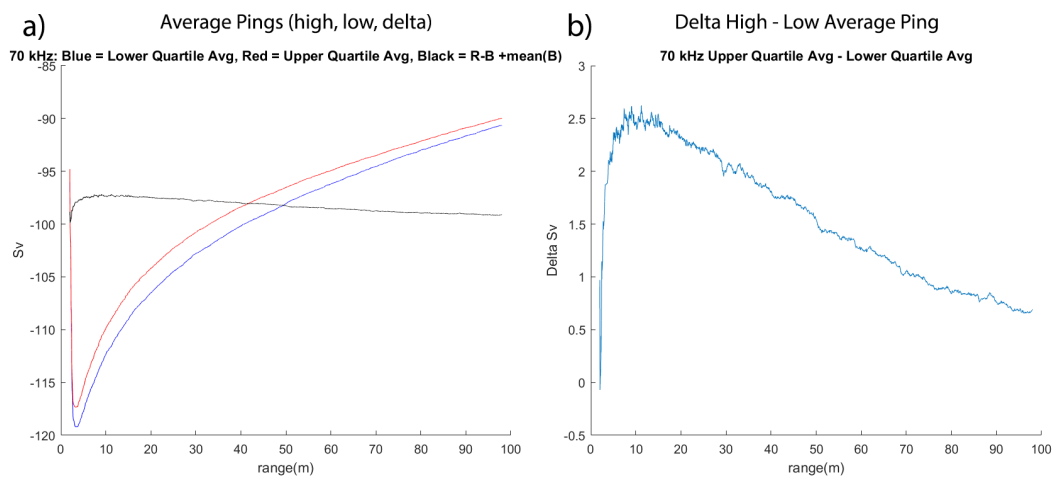
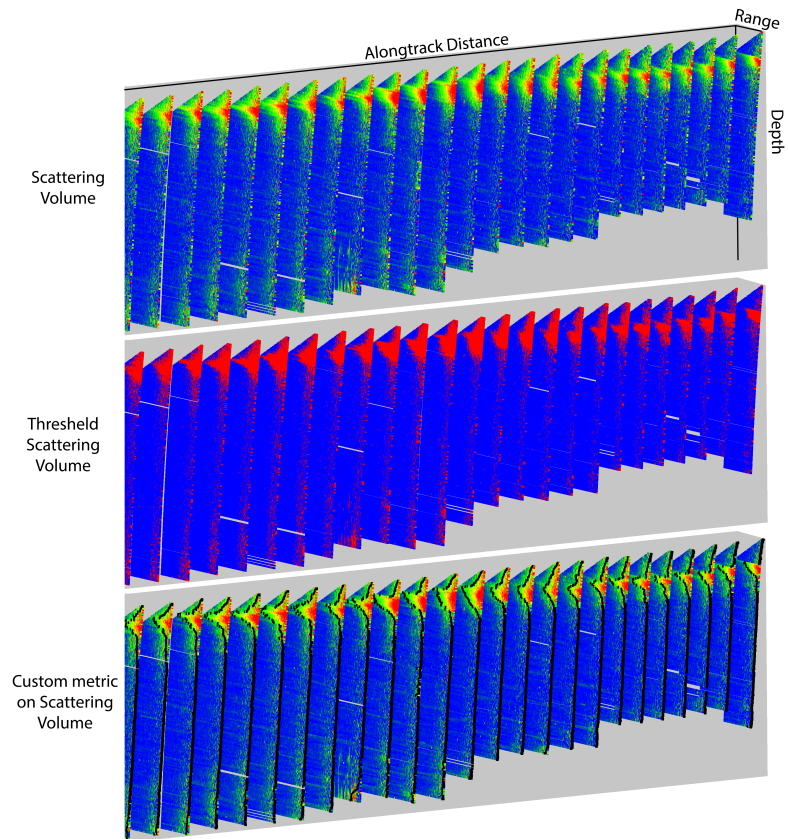
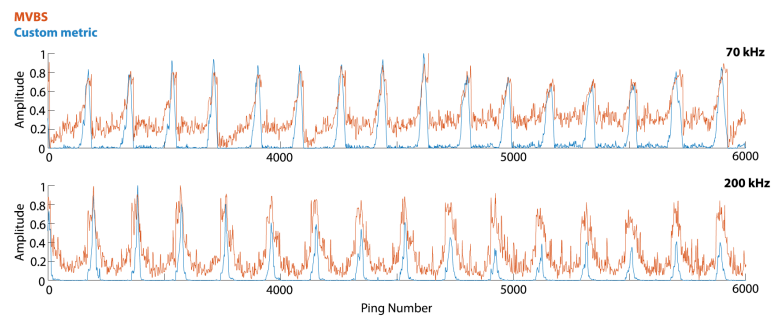


Figure 27. Averaged Wire Flyer Sv data from the Baltimore Canyon deployment demonstrating the raw and detrended Sv curves over range. A) Averaged 0-25% (blue) and 75-100% (red) Sv quartile averages. The difference between the high and low quantiles with an average value added back is shown in black and represents the detrended Sv data. B) The raw difference between the upper and lower Sv quantiles matches the logarithmic decay observed in the simulated Sv data.



(a) Derivation of custom metric



(b) Custom metric vs MVBS signals

Figure 28. Comparison of the custom metric, Sv, and MVBS signals. A) Custom metric normalized to sampling range plotted as black line over the 3-dimensional Sv data. The custom metric effectively traces contours in Scattering Volume across scattering layers. B) Normalized custom metric data plotted alongside normalized MVBS. The custom metric signal is smoother and captures more of the scattering layer intensity gradients.

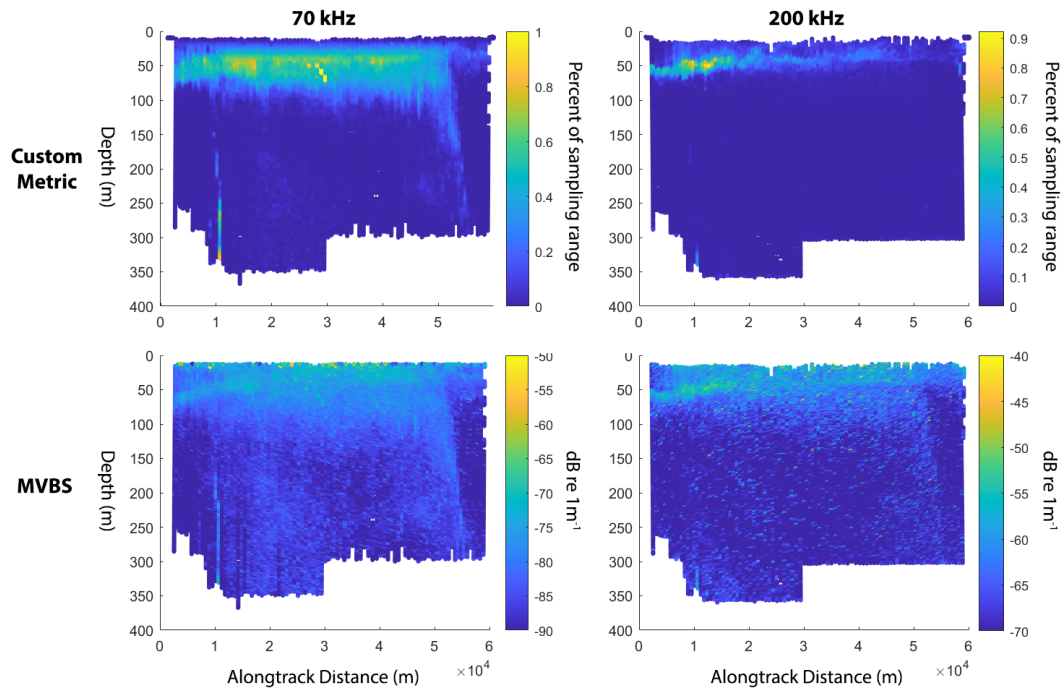


Figure 29. 70 and 200 kHz Wire Flyer echogram sections showing the custom metric data type versus MVBS derived from the full sampling range. The custom metric demonstrates better detection of the major scattering layers.

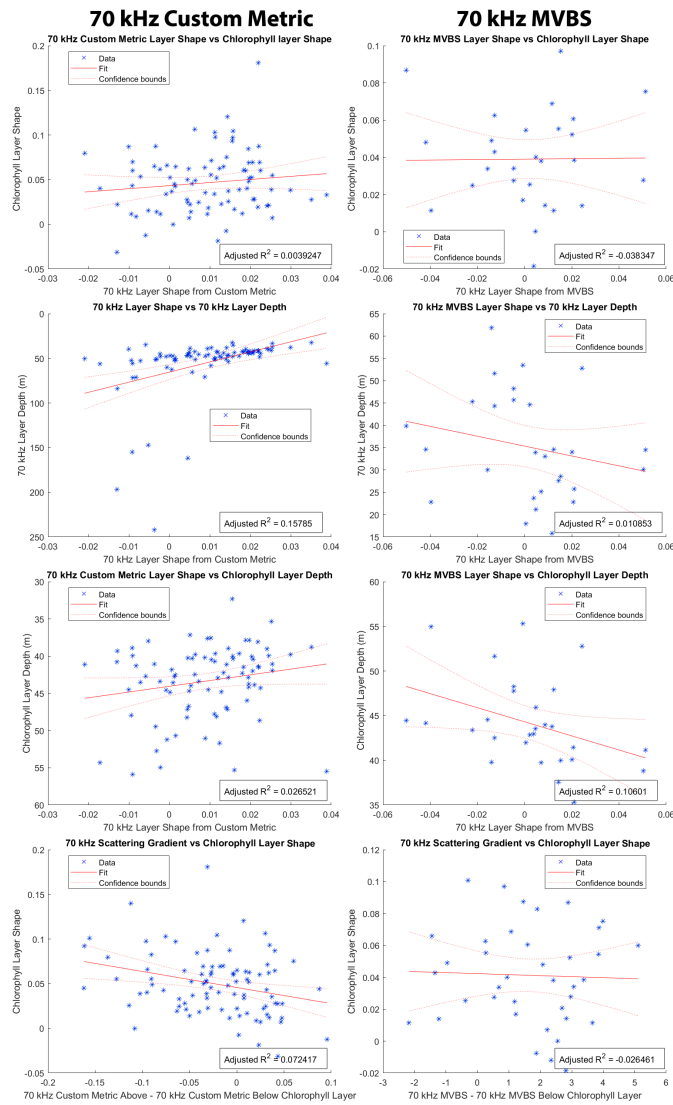


Figure 30. Pairwise linear regressions for layer shape based data types derived from the 70 kHz custom metric (left panels) and 70 kHz MVBS (right panels). The top panel shows chlorophyll layer shapes plotted against the scattering layer shapes. The second row shows the scattering layer depth plotted against the scattering layer shape. The third row shows the chlorophyll layer depth plotted against the scattering layer shape. The last row shows the chlorophyll layer shape as a function of the scattering difference above and below the chlorophyll layer.

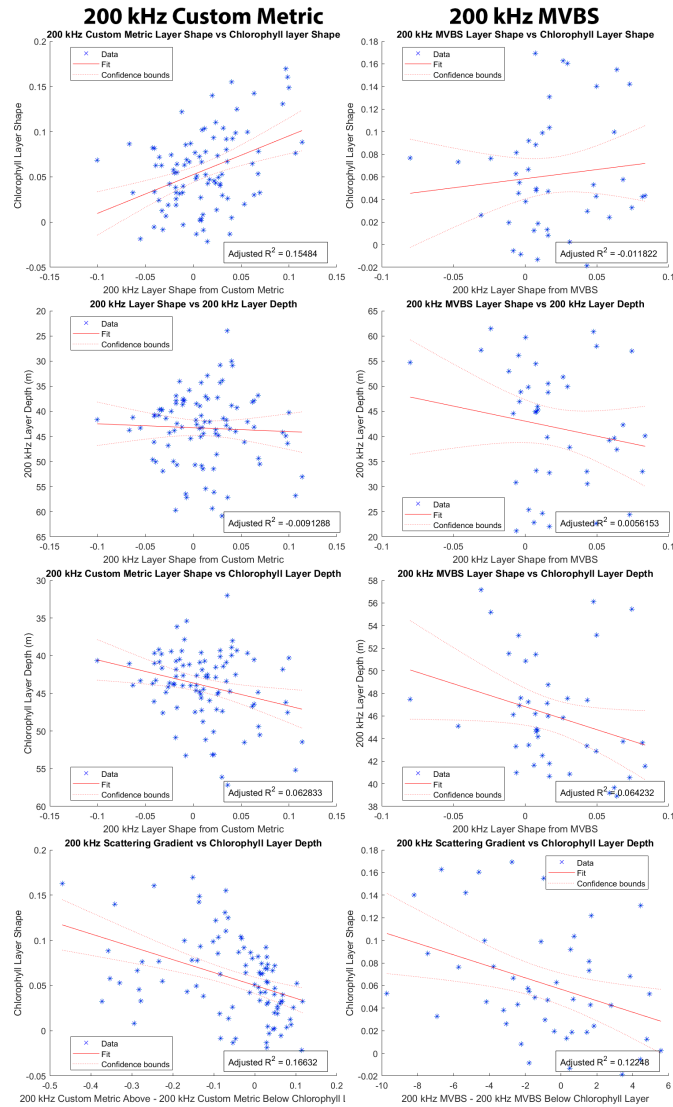


Figure 31. Pairwise linear regressions for layer shape based data types derived from the 200 kHz custom metric (left panels) and 200 kHz MVBS (right panels). The top panel shows chlorophyll layer shapes plotted against the scattering layer shapes. The second row shows the scattering layer depth plotted against the scattering layer shape. The third row shows the chlorophyll layer depth plotted against the scattering layer shape. The last row shows the chlorophyll layer shape as a function of the scattering difference above and below the chlorophyll layer.

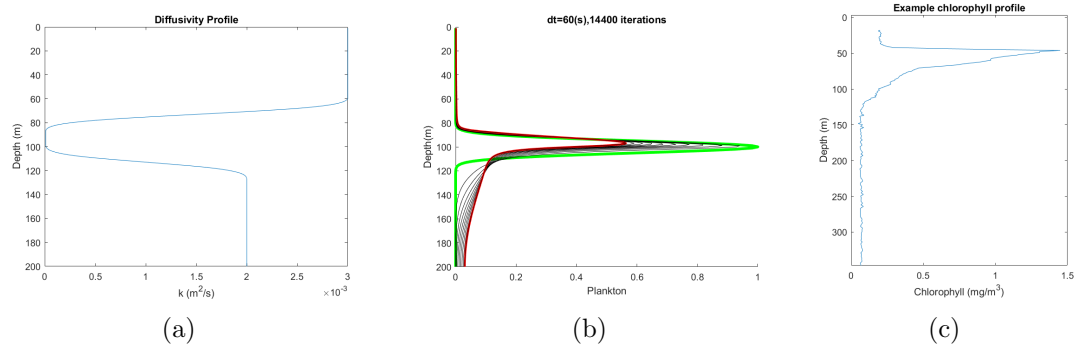


Figure 32. 1D phytoplankton model results. A) The simulated diffusivity profile. B) Phytoplankton model output for 10 days of run time. The phytoplankton starting distributions are shown in green. The final distributions are shown in red and demonstrate a dispersed lower gradient. C) Example 200 kHz chlorophyll profile demonstrating a similar shape to the model output.

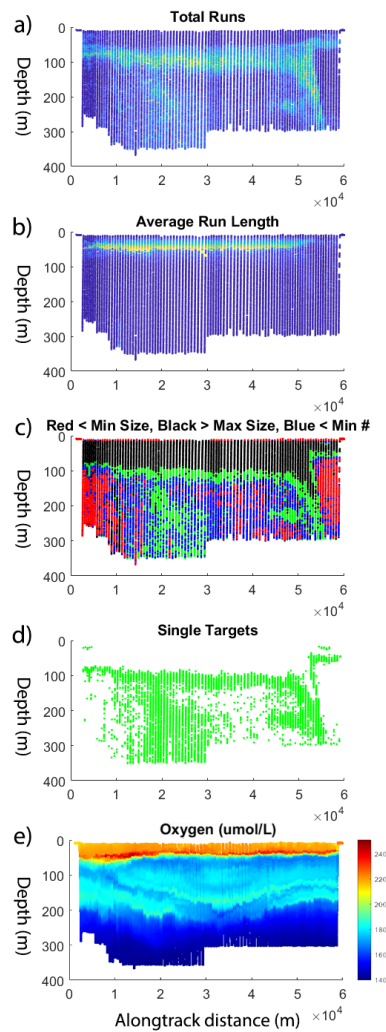


Figure 33. Run length data section plots derived from the 70 kHz Scattering Volume profiles. A) Total number of runs detected per ping. The most abundant runs were observed in pings delineating the lower boundary of the mixed layer associated scattering layer and the migrating assemblage departing the surface at dawn. B) Average run length data (percentage of sampling range). Long runs visible in the color scale at lengths beyond that expected for individual animals corresponds directly to the dense nighttime scattering layer. C) Selection criteria showing the classification of valid single target data. Pings in black exceed the maximum run length criteria and denote the dense scattering layers. Ping data show in red and blue did not exceed the minimum run length size and number of runs per ping respectively. D) Valid single target data corresponds to the boundaries of the dense scattering layers and a unique region within the canyon. E) Oxygen section shows intermediate water mass distributions matching the mesopelagic single target distributions.

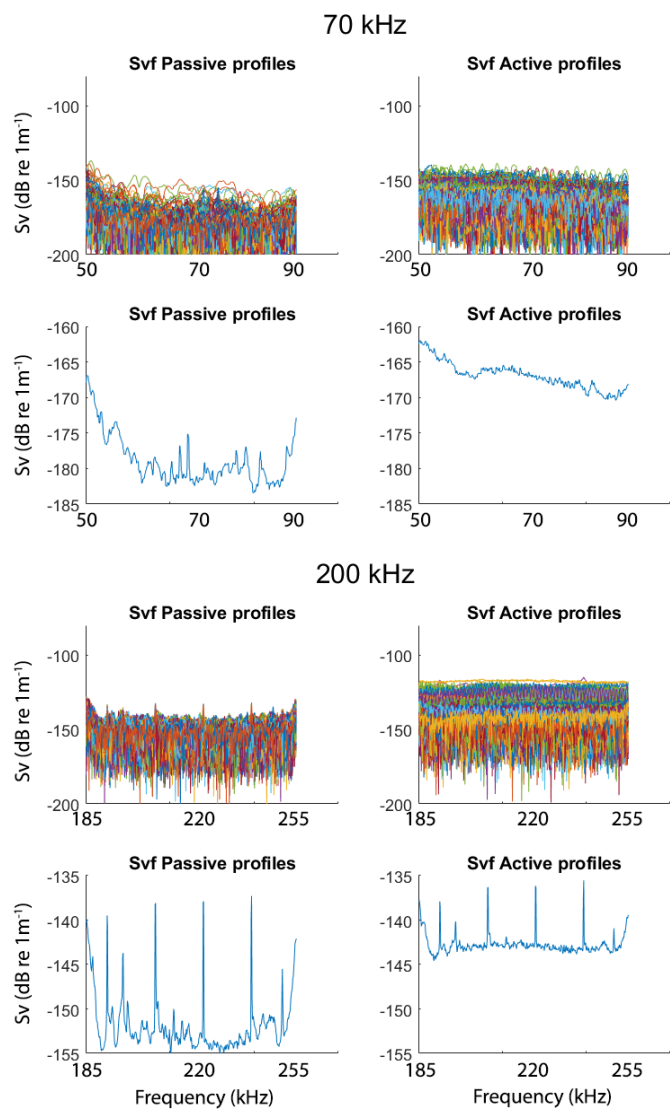


Figure 34. Frequency dependent Scattering Volume data from active and passive mode Wire Flyer profiles. The top two rows and bottom two rows show $S_v(f)$ data from the 70 kHz channel and 200 kHz channel respectively. The left and right panels show $S_v(f)$ data collected during passive and active acoustic profiling respectively. The colored line plots show $S_v(f)$ data for all pings in the profiles while the blue line plots show the average $S_v(f)$ response shapes. The active mode $S_v(f)$ demonstrates similar response shapes to the passive noise spectrum with elevated amplitude.

List of References

- [1] S. Kaartvedt, A. Staby, and D. L. Aksnes, “Efficient trawl avoidance by mesopelagic fishes causes large underestimation of their biomass,” *Marine Ecology Progress Series*, vol. 456, pp. 1–6, 2012.
- [2] X. Irigoien, T. A. Klevjer, A. Røstad, U. Martinez, G. Boyra, J. L. Acuña, A. Bode, F. Echevarria, J. I. Gonzalez-Gordillo, S. Hernandez-Leon, *et al.*, “Large mesopelagic fishes biomass and trophic efficiency in the open ocean,” *Nature communications*, vol. 5, no. 1, pp. 1–10, 2014.
- [3] R. Proud, N. O. Handegard, R. J. Kloser, M. J. Cox, and A. S. Brierley, “From siphonophores to deep scattering layers: uncertainty ranges for the estimation of global mesopelagic fish biomass,” *ICES Journal of Marine Science*, vol. 76, no. 3, pp. 718–733, 04 2018. [Online]. Available: <https://doi.org/10.1093/icesjms/fsy037>
- [4] J. A. Koslow, P. Davison, A. Lara-Lopez, and M. D. Ohman, “Epipelagic and mesopelagic fishes in the southern california current system: Ecological interactions and oceanographic influences on their abundance,” *Journal of Marine Systems*, vol. 138, pp. 20–28, 2014.
- [5] E. Sinclair and P. Stabeno, “Mesopelagic nekton and associated physics of the southeastern bering sea,” *Deep Sea Research Part II: Topical Studies in Oceanography*, vol. 49, no. 26, pp. 6127–6145, 2002.
- [6] P. H. Wiebe and M. C. Benfield, “From the hensen net toward four-dimensional biological oceanography,” *Progress in Oceanography*, vol. 56, no. 1, pp. 7–136, 2003.
- [7] J. H. Steele, “Can ecological theory cross the land-sea boundary?” *Journal of Theoretical Biology*, vol. 153, no. 3, pp. 425–436, 1991.
- [8] T. T. Sutton, M. R. Clark, D. C. Dunn, P. N. Halpin, A. D. Rogers, J. Guinotte, S. J. Bograd, M. V. Angel, J. A. A. Perez, K. Wishner, *et al.*, “A global biogeographic classification of the mesopelagic zone,” *Deep Sea Research Part I: Oceanographic Research Papers*, vol. 126, pp. 85–102, 2017.
- [9] L. Haury, J. McGowan, and P. Wiebe, “Patterns and processes in the time-space scales of plankton distributions,” in *Spatial pattern in plankton communities*. Springer, 1978, pp. 277–327.
- [10] A. T. Greer, A. D. Boyette, V. J. Cruz, M. K. Cambazoglu, B. Dzwonkowski, L. M. Chiaverano, S. L. Dykstra, C. Briseño-Avena, R. K. Cowen, and J. D. Wiggert, “Contrasting fine-scale distributional patterns of zooplankton driven by the formation of a diatom-dominated thin layer,” *Limnology and Oceanography*, vol. 65, no. 9, pp. 2236–2258, 2020.

- [11] R. C. Hooff and W. T. Peterson, “Copepod biodiversity as an indicator of changes in ocean and climate conditions of the northern california current ecosystem,” *Limnology and Oceanography*, vol. 51, no. 6, pp. 2607–2620, 2006.
- [12] O. J. Schmitz, J. R. Miller, A. M. Trainor, and B. Abrahms, “Toward a community ecology of landscapes: predicting multiple predator–prey interactions across geographic space,” *Ecology*, vol. 98, no. 9, pp. 2281–2292, 2017.
- [13] R. K. Cowen, A. T. Greer, C. M. Guigand, J. A. Hare, D. E. Richardson, and H. J. Walsh, “Evaluation of the in situ ichthyoplankton imaging system (isiis): Comparison with the traditional (bongo net) sampler,” 2013.
- [14] A. T. Greer, R. K. Cowen, C. M. Guigand, J. A. Hare, and D. Tang, “The role of internal waves in larval fish interactions with potential predators and prey,” *Progress in Oceanography*, vol. 127, pp. 47–61, 2014.
- [15] K. J. Benoit-Bird, “Dynamic 3-dimensional structure of thin zooplankton layers is impacted by foraging fish,” *Marine Ecology Progress Series*, vol. 396, pp. 61–76, 2009.
- [16] K. J. Benoit-Bird, T. J. Cowles, and C. E. Wingard, “Edge gradients provide evidence of ecological interactions in planktonic thin layers,” *Limnology and Oceanography*, vol. 54, no. 4, pp. 1382–1392, 2009.
- [17] K. J. Benoit-Bird and M. A. McManus, “A critical time window for organismal interactions in a pelagic ecosystem,” *PLoS One*, vol. 9, no. 5, p. e97763, 2014.
- [18] J. V. Gartner Jr, W. J. Conley, and T. L. Hopkins, “A case study using lanternfishes (pisces: Myctophidae),” *Fishery Bulletin*, vol. 87, no. 1, p. 213, 1989.
- [19] D. Bianchi, C. Stock, E. D. Galbraith, and J. L. Sarmiento, “Diel vertical migration: Ecological controls and impacts on the biological pump in a one-dimensional ocean model,” *Global Biogeochemical Cycles*, vol. 27, no. 2, pp. 478–491, 2013.
- [20] T. Klevjer, D. Torres, and S. Kaartvedt, “Distribution and diel vertical movements of mesopelagic scattering layers in the red sea,” *Marine Biology*, vol. 159, 08 2012.
- [21] K. F. Wishner, M. M. Gowing, and C. Gelfman, “Mesozooplankton biomass in the upper 1000 m in the arabian sea: overall seasonal and geographic patterns, and relationship to oxygen gradients,” *Deep Sea Research Part II: Topical Studies in Oceanography*, vol. 45, no. 10-11, pp. 2405–2432, 1998.
- [22] K. F. Wishner, D. M. Outram, B. A. Seibel, K. L. Daly, and R. L. Williams, “Zooplankton in the eastern tropical north pacific: Boundary effects of oxygen

- minimum zone expansion,” *Deep Sea Research Part I: Oceanographic Research Papers*, vol. 79, pp. 122–140, 2013.
- [23] T. T. Sutton, “Vertical ecology of the pelagic ocean: classical patterns and new perspectives,” *Journal of Fish Biology*, vol. 83, no. 6, pp. 1508–1527, 2013. [Online]. Available: <https://onlinelibrary.wiley.com/doi/abs/10.1111/jfb.12263>
- [24] T. A. Klevjer, X. Irigoien, A. Røstad, E. Fraile-Nuez, V. M. Benítez-Barrios, and S. Kaartvedt, “Large scale patterns in vertical distribution and behaviour of mesopelagic scattering layers,” *Scientific Reports*, vol. 6, no. 1, pp. 1–11, 2016.
- [25] D. Bianchi and K. Mislan, “Global patterns of diel vertical migration times and velocities from acoustic data,” *Limnology and Oceanography*, vol. 61, no. 1, pp. 353–364, 2016.
- [26] S. S. Urmy and K. J. Benoit-Bird, “Fear dynamically structures the ocean’s pelagic zone,” *Current Biology*, vol. 31, no. 22, pp. 5086–5092, 2021.
- [27] J. Simmonds and D. N. MacLennan, *Fisheries acoustics: theory and practice*. John Wiley and Sons, 2008.
- [28] N. Diner, “Correction on school geometry and density: approach based on acoustic image simulation,” *Aquatic Living Resources*, vol. 14, no. 4, pp. 211–222, 2001.
- [29] E. J. Katz and W. E. Witzell Jr, “A depth controlled tow system for hydrographic and current measurements with applications,” *Deep Sea Research Part A. Oceanographic Research Papers*, vol. 26, no. 5, pp. 579–596, 1979.
- [30] R. J. Kloser, “Improved precision of acoustic surveys of benthopelagic fish by means of a deep-towed transducer,” *ICES Journal of Marine Science*, vol. 53, no. 2, pp. 407–413, 1996.
- [31] P. Wiebe, T. Stanton, C. Greene, M. Benfield, H. Sosik, T. Austin, J. Warren, and T. Hammar, “BIOMAPER-II: An integrated instrument platform for coupled biological and physical measurements in coastal and oceanic regimes,” *IEEE Journal of Oceanic Engineering*, vol. 27, pp. 700 – 716, 08 2002.
- [32] A. C. Lavery, T. K. Stanton, J. M. Jech, and P. Wiebe, “An advanced sensor platform for acoustic quantification of the ocean twilight zone,” *The Journal of the Acoustical Society of America*, vol. 145, no. 3, pp. 1653–1653, 2019. [Online]. Available: <https://doi.org/10.1121/1.5101063>

- [33] K. Benoit-Bird, C. Waluk, P. Welch, J. A. Barth, I. Wangen, P. McGill, C. Okuda, G. Hollinger, M. Sato, and S. Mccammon, “Equipping an underwater glider with a new echosounder to explore ocean ecosystems,” *Limnology and oceanography, methods*, 09 2018.
- [34] C. Roman, D. S. Ullman, D. Hebert, and S. Licht, “The Wire Flyer Towed Profiling System,” *Journal of Atmospheric and Oceanic Technology*, vol. 36, no. 2, pp. 161–182, 2019. [Online]. Available: <https://doi.org/10.1175/JTECH-D-17-0180.1>
- [35] K. F. Wishner, B. A. Seibel, C. Roman, C. Deutsch, D. Outram, C. T. Shaw, M. A. Birk, K. A. S. Mislan, T. J. Adams, D. Moore, and S. Riley, “Ocean deoxygenation and zooplankton: Very small oxygen differences matter,” *Science Advances*, vol. 4, no. 12, 2018. [Online]. Available: <http://advances.sciencemag.org/content/4/12/eaau5180>
- [36] K. Iida, T. Mukai, and D. Hwang, “Relationship between acoustic backscattering strength and density of zooplankton in the sound-scattering layer,” *ICES Journal of Marine Science*, vol. 53, no. 2, pp. 507–512, 1996.
- [37] A. L. Alldredge, T. J. Cowles, S. MacIntyre, J. E. Rines, P. L. Donaghay, C. F. Greenlaw, D. Holliday, M. M. Dekshenieks, J. M. Sullivan, and J. R. V. Zaneveld, “Occurrence and mechanisms of formation of a dramatic thin layer of marine snow in a shallow pacific fjord,” *Marine Ecology Progress Series*, vol. 233, pp. 1–12, 2002.
- [38] O. Cheriton, M. McManus, M. Stacey, and J. Steinbuck, “Physical and biological controls on the maintenance and dissipation of a thin phytoplankton layer,” *Marine Ecology Progress Series*, vol. 378, pp. 55–69, 2009.
- [39] D. A. Birch, W. R. Young, and P. J. Franks, “Plankton layer profiles as determined by shearing, sinking, and swimming,” *Limnology and Oceanography*, pp. 397–399, 2009.
- [40] H. Akaike, “Information theory and an extension of the maximum likelihood principle,” in *Selected papers of hirotugu akaike*. Springer, 1998, pp. 199–213.
- [41] M. O. Akinwande, H. G. Dikko, A. Samson, *et al.*, “Variance inflation factor: as a condition for the inclusion of suppressor variable (s) in regression analysis,” *Open Journal of Statistics*, vol. 5, no. 07, p. 754, 2015.
- [42] R. D. Cook, “Influential observations in linear regression,” *Journal of the American Statistical Association*, vol. 74, no. 365, pp. 169–174, 1979.
- [43] “Hydroacoustic data processing.” [Online]. Available: <https://echoview.com/>
- [44] S. D. Bradley, “Optimizing a scheme for run length encoding,” *Proceedings of the IEEE*, vol. 57, no. 1, pp. 108–109, 1969.

- [45] A. S. Brierley, P. Ward, J. L. Watkins, and C. Goss, “Acoustic discrimination of southern ocean zooplankton,” *Deep Sea Research Part II: Topical Studies in Oceanography*, vol. 45, no. 7, pp. 1155–1173, 1998.
- [46] L. N. Andersen, D. Chu, H. Heimvoll, R. Korneliussen, G. J. Macaulay, and E. Ona, “Quantitative processing of broadband data as implemented in a scientific splitbeam echosounder,” *arXiv preprint arXiv:2104.07248*, 2021.
- [47] C. H. Greene, P. H. Wiebe, A. J. Pershing, G. Gal, J. M. Popp, N. J. Copley, T. C. Austin, A. M. Bradley, R. G. Goldsborough, J. Dawson, *et al.*, “Assessing the distribution and abundance of zooplankton: a comparison of acoustic and net-sampling methods with d-bad mocness,” *Deep Sea Research Part II: Topical Studies in Oceanography*, vol. 45, no. 7, pp. 1219–1237, 1998.
- [48] A. C. Lavery, C. Bassett, G. L. Lawson, and J. M. Jech, “Exploiting signal processing approaches for broadband echosounders,” *ICES Journal of Marine Science*, vol. 74, no. 8, pp. 2262–2275, 2017.
- [49] K. J. Benoit-Bird and C. M. Waluk, “Exploring the promise of broadband fisheries echosounders for species discrimination with quantitative assessment of data processing effects,” *The Journal of the Acoustical Society of America*, vol. 147, no. 1, pp. 411–427, 2020.
- [50] D. Demer, L. Andersen, C. Bassett, L. Berger, D. Chu, J. Condiotty, and G. Cutter, “Evaluation of a wideband echosounder for fisheries and marine ecosystem science,” *ICES Cooperative Research Report*, no. 336, 2017.

.1 Appendix

.1.1 Chapter 1 Software Overview

A software library to batch-process water column image datasets was written in C++, using the OpenCV computer vision library and a custom directory manager and memory buffer. The goals of this software library were to normalize image data collected in the epi and mesopelagic ocean and autonomously perform combined image segmentation and stereo feature matching routines on large stereo image datasets (1000s of paired images). The software is configurable by the user, and multithreaded to operate on several image pairs simulatenously. A directory of paired segmented image data and a compiled datasets containing the relevant segmentation and 3-d reprojection information for the extracted regions is output for analysis or further processing.

.1.2 Ch1 Lighting Normalizations

The collected stereo imaging datasets are affected by two sources of variable lighting that can bias image segmentation and feature extraction performance for the image data. The primary source of lighting variability is due by the attenuation of the active strobe lighting away from the image sensor. The strobe lighting generates a basal intensity gradient across the image plane that is conserved among all image data collected by each of the cameras in the calibrates stereo camera. A secondary lighting signal is produced by ambient lighting conditions in situ as the stereo camera profiles through the epipelagic depths. Ambient illumination changes overall image brightness and produces a variable intensity gradient opposing the gradient of the strobe lighting in the imaging plane. To normalize the collected imagery for image segmentation and data extraction routines, an initial two-step correction is applied to decimate the variable lighting. The lighting correction software was is semi-autonomous, with several settings prescribed by the user



Figure .35. Results of the two step image lighting normalization. A) Raw image from the color camera in the stereo pair. B) Flattened image data after subtracting the signed strobe lighting representation. C) Foreground isolated image data after subtracting the calculated ambient background lighting.

to allow optimization for operating on diverse stereo imagery datasets collected by the system. The dedicated decimation of the fixed and variable illumination acts to isolate the foreground and the efficacy of segmentation routines.

.1.3 Ch1 Strobe illumination decimation

A representation of the strobe illumination is obtained by averaging normalized images minimally influenced by ambient lighting and objects in the field of view. A desired image subset used to render the strobe lighting gradient is determined autonomously from simple image statistic calculations. The standard deviation of the image intensities and the mean image intensities are calculated for each image in the profile. Standard deviations are then calculated for the image intensity standard deviation and the mean image intensities. The two vectors of standard deviation values are sorted along with the index to the image. The image subset is then selected from the two sorted vectors, where images occurring below a user set proportion of both vectors are marked for inclusion in the strobe lightfield correction. The histograms for the selected images are then normalized by subtracting their mean intensity. A vector of intensity values for every pixel is

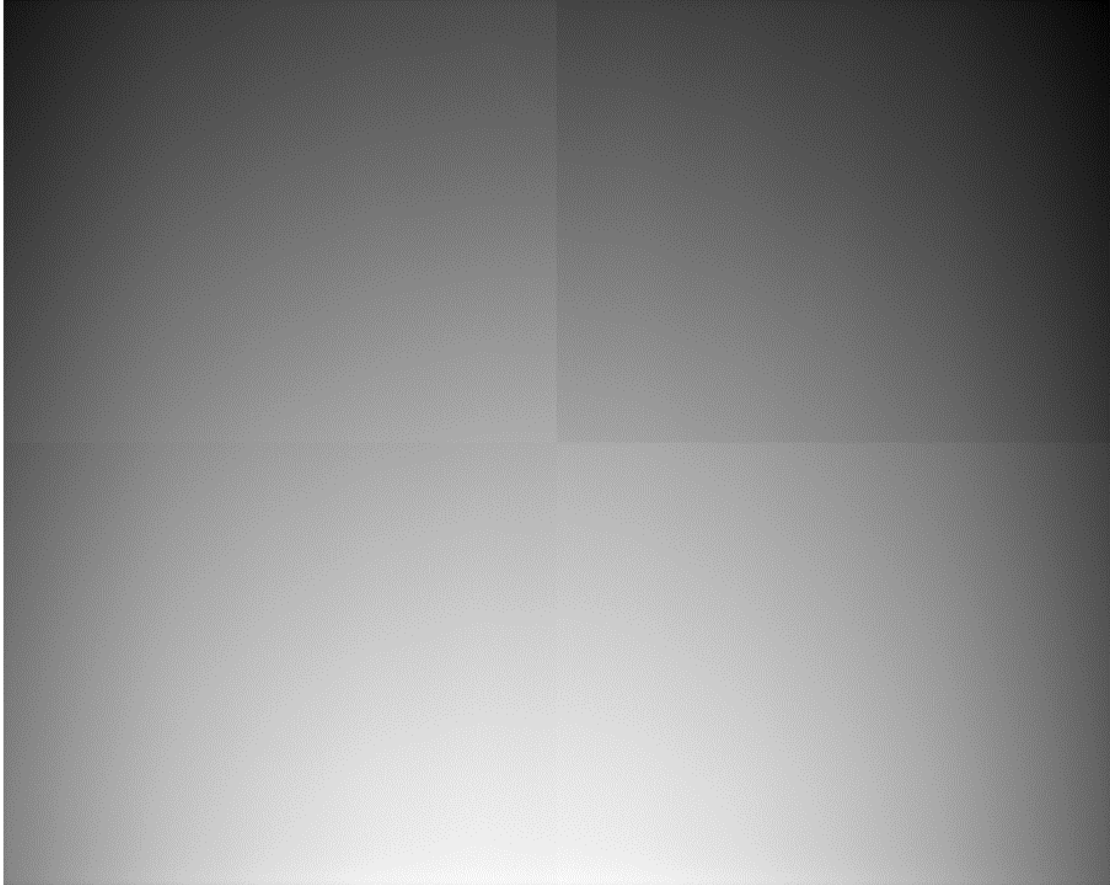


Figure .36. Fixed lighting gradient calculated for the strobe lighting. Quadrant gain variation is evident and reflects the composite sensor design.

constructed from the autonomously subset zero-mean intensity images. The strobe lighting image is constructed by averaging the lower 50 image intensity values from the sorted intensity vectors for every pixel. The pixel-specific calculation works to minimize averaging of image regions affected by particulates and organisms. The derived strobe lighting image captures gain differences due to the sensor design. A flatfield correction is performed on the raw images by subtracting the signed zero mean intensity lightfield image derived by the pixelwise averaging of the normalized inlier images [1]. This lightfield calculation and correction routine is performed separately for each camera in the stereo pair.

.1.4 Ch1 Ambient illumination decimation

A similar technique is used to calculate the variable ambient lighting subtracted to normalize specific images in the imaging profiles, but instead the routine operates on a sliding window of images nearby in time and space. A specific representation of the ambient lighting is generated for each image in the profile using data from a prescribed number of raw images (5 for the datasets shown here) centered about the relevant image. Each pixel of the ambient lightfield is populated independently as the minimum intensity pixel value from the images in the sliding window. A gaussian blur is applied to the generated ambient lightfield and subtracted from raw image centered around the sequence of images used for the calculation. Several versions of sliding window ambient lighting operations were built and tested, including averaging a variable numbers of images adaptively determined by the image statistics. We however found the sliding image window calculation to work well with only a few images when operating on a pixel-by-pixel basis and was specifically useful minimizing the influence of a baited squid mantle in the field of view for one of the datasets.

.1.5 Ch1 Image Segmentation

Regions of interest were defined in the image data using simple thresholding and connected-component routines supported in OpenCV [2]. The lighting corrected image data were convolved with an adaptive gaussian threshold kernel, where a threshold value is determined by the weighted sum of neighboring values within the kernel. A kernel size was selected to maximize the search radius for the average representation of the target species. The adaptive thresholding routing was found to be more effective on the lighting corrected imagery than static value thresholding operations that can result in over or under segmentation due to slight variabilities in the mean intensities of the normalized image data. A morphological

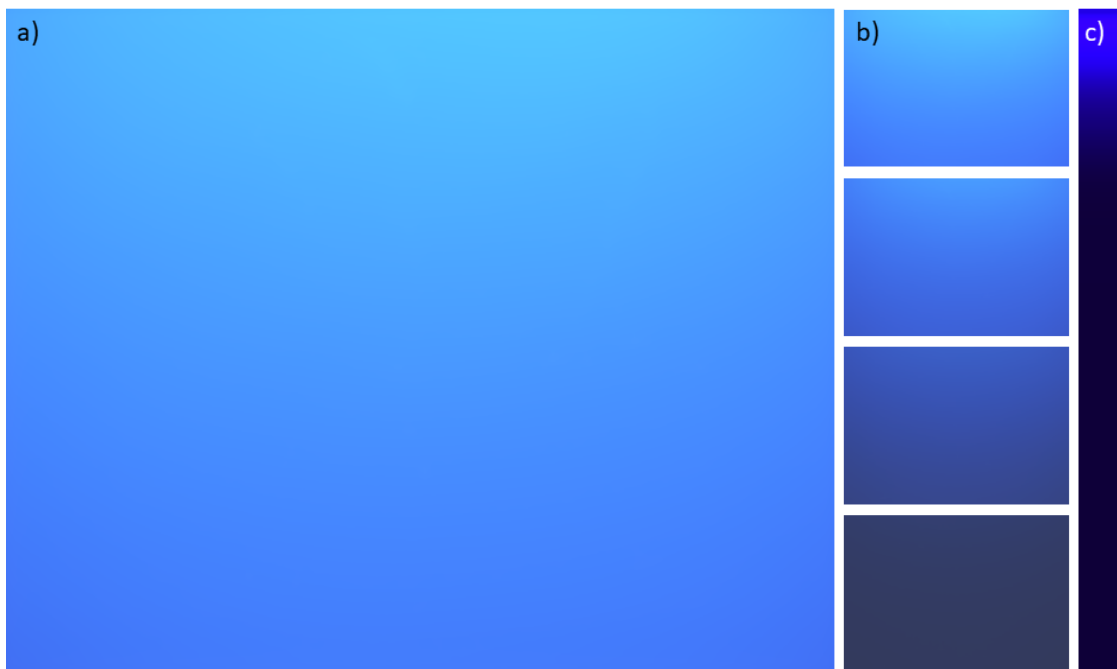


Figure .37. Images generated by the sliding window ambient lighting correction. A) Ambient lighting generated for an image near the surface. B) Nearby ambient lighting images generated for images 10 m apart. C) Scalar mean intensity representation of the ambient lighting images generated for a whole profile.



Figure .38. Bounding contours detected and reprojected from the stereo image pair.

opening of the binarized image data (erosion followed by dilation) was performed to remove noise and smooth the border of larger objects. The binarized objects in the image plane were then defined using OpenCV's contour detection routine, which simply defines the continuous points along the boundary of the thresholded foreground objects. From this routine, a vector is populated for each image in the stereo pair containing the boundary definitions for all detected objects in the image plane. The bounding contour data is referenced during feature detection and stereo matching operations to define paired regions between the cameras for quantification and extraction.

.1.6 Ch1 Feature Detection

The lighting corrected images are adjusted by a fixed brightness and contrast value selected to improve the average intensity distribution over the available bits. The greyscale image of the stereo pair is first convolved with a gaussian filter (sigma of 5) to better match the resolution of the color image when converted to grayscale. The stereo pair is then convolved with a gaussian filter (sigma of 7 pixels) blurring the images to remove noise. These image processing operations were used for the image data processed for this study but the functions, filter values, and order of operations are configurable by the user from a suite of basic image processing and morphological operations, and the settings are logged in a YAML file for reuse. A feature detection routine is then applied to each image in the pair. We used the Scale Invariant Feature Transform (SIFT) which identifies pixel-centered regions by defining intensity gradients that retain saliency across a range of scale space representations (i.e. varying intensities of Gaussian image blurring). The identified ‘keypoints’ are stored in vectors for each image in the pair. The 128-element descriptor vectors are calculated for the surviving SIFT keypoints to be used for feature matching between the stereo image pair.

.1.7 Ch1 Stereo Matching and Definition of Paired Regions of Interests

The two arrays of keypoint descriptors for stereo image pairs were matched in a one vs. all manner using the brute force feature matching algorithm. Each keypoint was assigned the strongest 6 keypoint matches from the stereo pair. The keypoint and the 6 matching keypoints were reprojected onto the undistorted and rectified image plane defined by the stereo calibration parameters and trimmed using constraints defined by the stereo geometry. Keypoint match pairs not distributed on the same epipolar lines were removed, and match pairs having horizontal disparities defining triangulated distances greater than 7 m or less than

.1 m from the optical center were removed. The keypoint and surviving matches were then assigned to an overlapping contours defined by the segmentation routine for each image in the pair. Keypoints detected in regions without contour definitions were removed. Two selection criteria enforced unique match pair for each contour object. If a majority of ROI keypoint matches are indexed to a single stereo pair ROI contour, the ROI match is selected from this mode. If a match ID mode does not exist, similarity metrics between contour shapes were calculated from the Hu-moment values and the ROI with the lowest distance matching shape was selected. The contours and assigned keypoints provided the basic definition of regions of interest. Bounding boxes are calculated for the ROI and normalized by comparing the displacement between the bounding edges and keypoint matches between the ROI pairs.

.1.8 Ch1 Manual Identification and Data Processing

The stereo image processing pipeline creates a directory of segmented image pairs that are indexed to a datasheet with the fused sensor data and derived 3-D information. The Pleuroncondes planipes regions of interest were manually identified and sorted into a folder. A script read the folder of identified P planipes and assigned the identifications to the datasheet. The datasheet was imported to R for data analysis. Crab abundances were averaged by depth bins and image aspect ratios were calculated to provide a proxy metric for the animal orientation. The derived image data was registered to the 70 and 200 kHz Continuous Wave Scattering Volume echograms recorded from the shipboard echosounder.

.1.9 Chapter 2 Software Overview

The first thing you do is use “proc_raw_ek80” to parse in and process the .raw files. This creates a .mat file directory with an indexing file (“global_index.mat”).



Figure .39. Screenshot of manually identified *Pleuronectes planipes* image region pairs segmented autonomously.

Typically, the flyer merged file is loaded automatically from this directory for processing. Instead you will need to load in an rov log file that at minimum contains a good ‘timestamp’, ‘timestamp_ek80’, and ‘depth.’

Once step 1 is done, you can create datasets from the .mat file directory. I am showing/ suggesting two main ways to do this. Option 1 is using the “proc_ek80” script to create datasets that you can further process and play around with in matlab. Option 2 “pointcloud_exporter” is a script to create a pointcloud file from the data, using the main tools you would want. Detrending the data (esp. important for Sv and TS data), range averaging (the raw range bins, or anything less than ~5 m will be huge files, so you want to do this).

Step 1 Processing RAW Files, ”proc_raw_ek80”

- This script will create a .mat directory of processed acoustic data from .raw files.
- Before running, populate the output and rovd data filepath.

- When running script, a file browser will open. Select all .raw files to process..
- Uses functions in (/rawparser) to parse in the files and (/powerprocs) to perform the calculations.

Need to populate:

- Outpath (line 7) = string for output directory path
- Rovdata(line 6) = string to rov data (.mat or .csv).
- Needs to contain timestamp, ek_timestamp, and depth
- Any additional vars can be added by adding below line 97.
- `global_indexer(global_counter).VAR = interp1(double([rovdata.timestamp]), double([rovdata.VAR]),double(newTime), 'linear','extrap');`
- Leave save_files and save.index as 1, to save these files (0 if you are just testing etc).

Step 2: Generating data

(Option 1) Overview, “prok_ek80”

- This function is meant to make prescribed datasets from the processed .mat directory, and then you can prescribe further processing or plotting below
- Simply calls “ek80” which uses “generate_data” to make prescribed 70 and 200 kHz datasets.
- The variables (value types, index types, index) to prescribe datasets are described below
- The call to ‘ek80’ will return the generated data “procdata”.
- 70 kHz data is “procdata.chan70”, 200 kHz is “procdata.chan200”

- The acoustic data is stored as a matrix in “[procddata.chanX.val]”
- The range values are stored as a matrix in “[procddata.chanX.range]”
- The interpolated variables are stored as a table in “[procddata.chanX.vars]”

Need to Populate: 'Value' type

- ‘power_cw’ = Continuous Wave power
- ‘power_pc’ = Frequency Modulated power
- ‘power_pc1’-‘power_pc4’ = Element-specific power, (1:4 for 70 and 1:3 for 200)
- ‘alongship’ = alongship power angle (70 kHz only)
- ‘athwartship’ = athwartship power angle (70 kHz only)
- ‘sv_pc’ = FM scattering volume
- ‘ts_pc’ = FM target strength
- ‘sv_cw’ = CW scattering volume
- ‘ts_cw’ = CW target strength

Need to Populate: 'Index' type

- The range of Index Type values to generate data from. For instance:
- index = ‘depth’; indexes = ‘100:500’;
- will generate data for all pings between 100 to 500 m.
- set min/max for an index type as ‘max([global_indexer.THE CHOSEN VAR])’;

- ‘cast’= 1 for all pings made for the rovd dataset, setting indexes to 1 will extract all data
- ‘max([global_indexer.timestamp]) - 2 : max([global_indexer.timestamp])’, would give you the back half of the dataset

3D plots

- plot_ek80_3D(procdata.chan_x, min power, max power, point size)
- takes procdata channel, set min and max power values, point size
- Will plot ping number by depth by range

2D plots

- Range average data and plot vs vars or
- Imagesc([procdata.chanX.val]) will make an echogram, range vs ping number

(Option 2) Overview, “pointcloud_exporter”:

- This is an all in one script to generate/process data that is exported to a pointcloud file.
- Set dir_path (line5) = ‘path\to\.mat\directory”
- Set out_path (line5) = ‘path\to\save”
- Set ‘name’ (line7) = ‘name of point cloud file’
- Set ‘var_name (line8) = one of the acoustic variables described above (e.g. ‘sv_pc’)
- Set ‘index_type’ and ‘indexes’ (line 8,9) as described above. Setting cast and 1 will use all the data.

- Set range averaging params (line 8-10)= min range, max range, range bin size (meters)
- Set detrend to 1 if you want to detrend the data. The default settings (line 30/31) are 50 m cutoff depth for averaging and a median filter size of 100
- Running the script will export a point cloud name_70 and name_200 in the output path

Some Useful Processing Tools

Detrending the data:

- **detrend_data_divewise(data, mindepth, filter_size)**
- procddata, the cutoff depth to avoid averaging surface returns, and the median filter size.
- Typically: detrend_data_divewise(data, 50, 100)

Range averaging:

- **rangeds(indata, minrange, maxrange, binsize)**
- binsize is in meters
- To get scalar average, binsize =maxrange-minrange.

Ping averaging:

- **pingds(data, mindepth, maxdepth, ds)**
- ds = Number of sequential pings to average together.
- can also be used to subset depth with mindepth, maxdepth, ds=1.

TVG:

- **apply_TVG(indata, logfactor)**
- give it `procdatan.chan_x` and log factor (e.g. 10, 20), and it will TVG the values.

Rejecting surface return/ triangle:

- **reject_surface_reverb(datain, tri_min_depth, tri_max_depth)**
- I typically use the `get_type_vectors` (described below) to perform this, but this function can be called to perform and return this on a “`procdatan.chanX`”.

Median Difference filter:

- **modem_reject_filter(in_data, start_range, filter_k, std_limit)**
- Start range is the range from x – 100m you want to average
- Filter_k is the median filter size, # pings.
- Std_limit is the std deviation cutoff for the median difference standard deviation
- Useful for removing modem interfenced pings

Making data vectors (here timestamp x depth):

- **get_timestamp_vectors(data, minp, maxp, scale_range, scale_depth, tri_min_depth, tri_max_depth)**
- makes/ returns a matrix of 4 XYZC vectors
- x=timestamp, y=range, z=depth, c=acoustic value
- These vectors are used to make pointclouds or plot 3D data

- Populating the variables in sequence after ‘data’ will perform the relevant functions, but you don’t have too.
- Data= procddata.chan70 or procddata.chan200
- minp/maxp = acoustic value cutoffs
- scale_range/scale_depth= scale factors
- tri_min_depth/tri_max depth = For rejecting along the hypotenuse of a triangle near the surface. Min sets starting depth where all ranges are removed. Max is depth where all values over range are preserved. i.e. if min =0 and max = 50, at 25 m depth data in 50-100m range is removed.
- There are also functions to make vectors using alongtrack distance (get_alongtrack_vectors), or lat/lon (get_localtrack_vectors) if available.

Exporting a pointcloud from a data vector set:

- **export_pointcloud(data_vectors, out_directory, name)**
- Takes in the vectorized data and writes a point cloud file from it.
- You specify the out directory path and the name if the file

Per Element Power Trends

Example 1

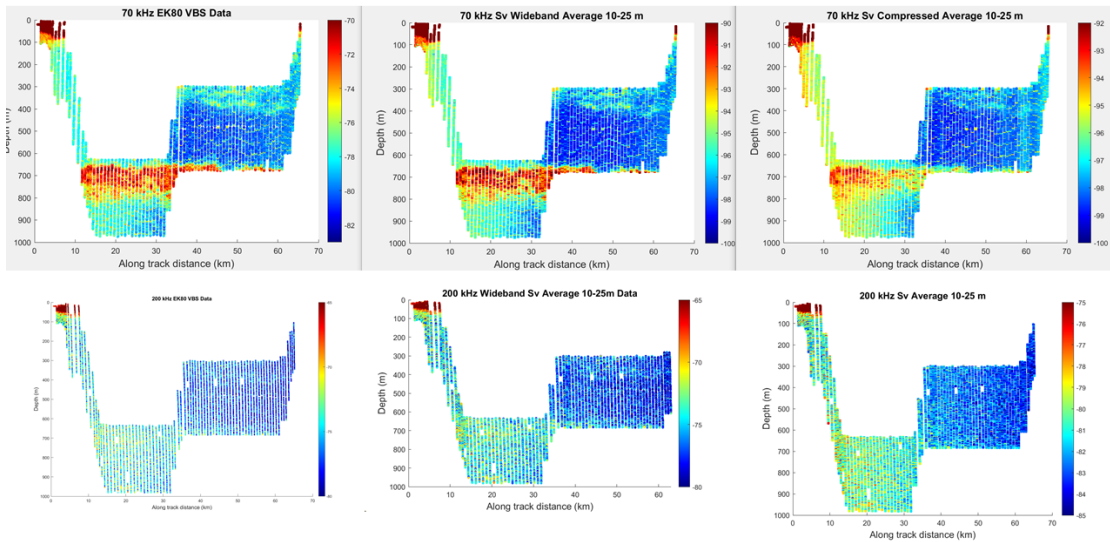


Figure .40. Comparison between Simrad’s VBS data, the processed Sv Continuous Wave data, and the processed Sv Frequency Modulated data before installation of the input power filter.

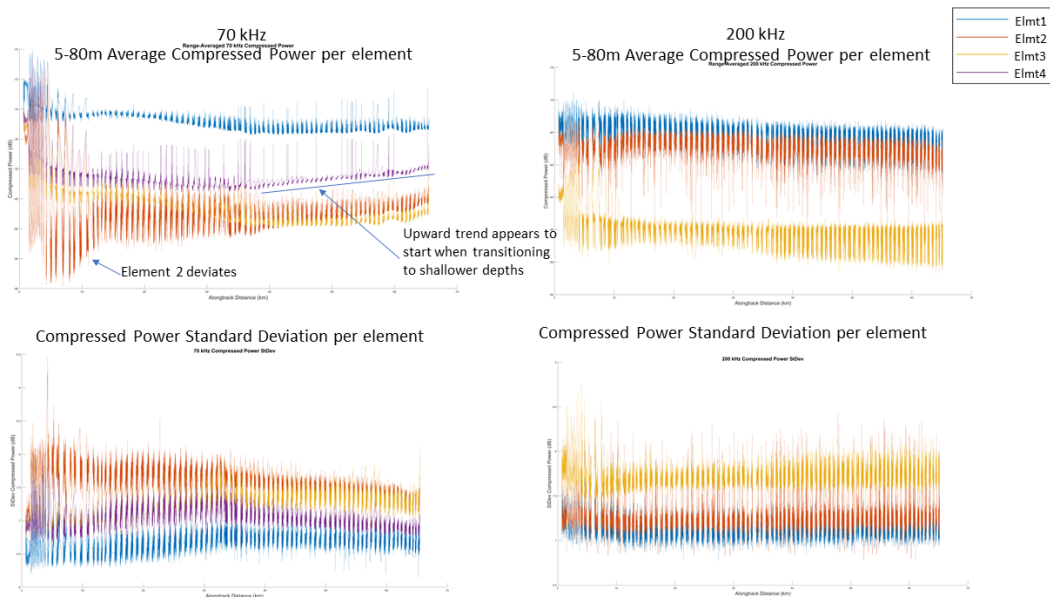


Figure .41. Per element power plots showing deviating trends among the sectors.

Alongtrack 70 kHz Compressed Power Pointclouds

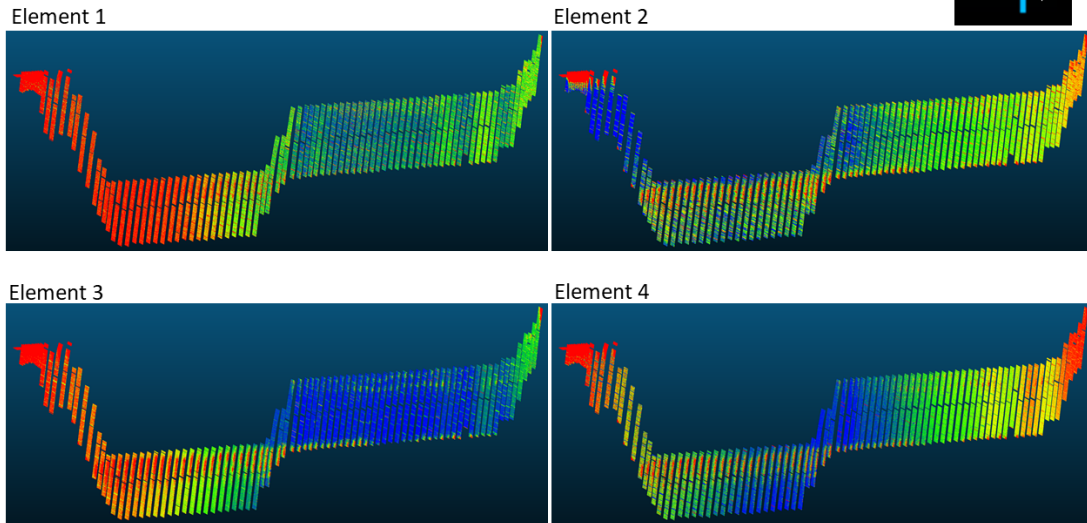


Figure .42. Per element power point clouds showing non-stationary and diverging trends.

Example 2

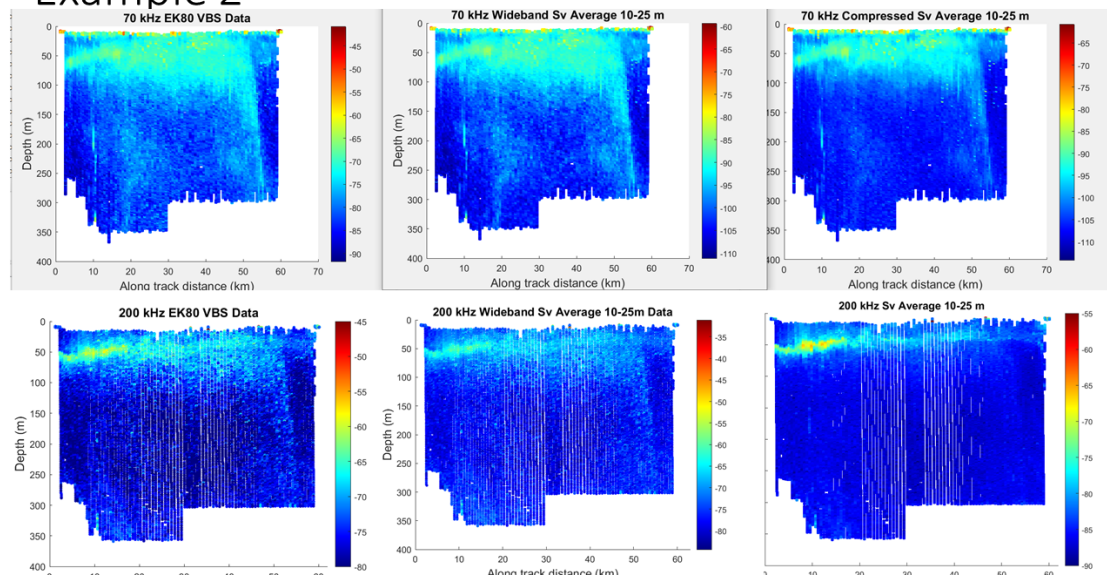


Figure .43. Comparison between Simrad's VBS data, the processed Sv Continuous Wave data, and the processed Sv Frequency Modulated data after installation of the input power filter.

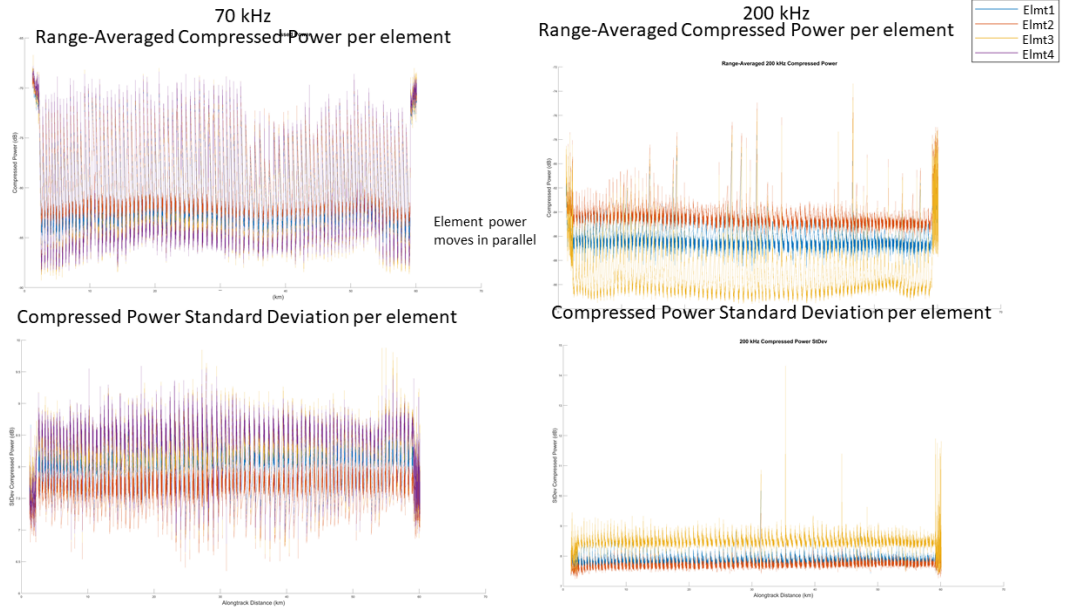


Figure .44. Per element power plots showing largely consistent trends among the sectors.

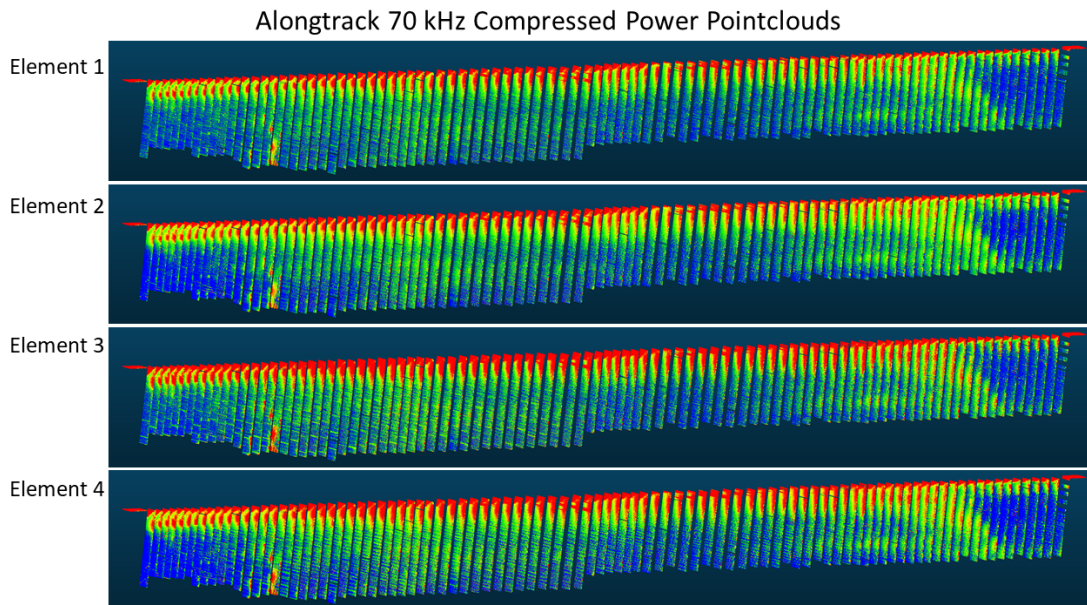


Figure .45. Per element power point clouds showing consistent power distributions

List of References

- [1] J. A. Seibert, J. M. Boone, and K. K. Lindfors, “Flat-field correction technique for digital detectors,” in *Medical Imaging 1998: Physics of Medical Imaging*, vol. 3336. SPIE, 1998, pp. 348–354.
- [2] G. Xie and W. Lu, “Image edge detection based on opencv,” *International Journal of Electronics and Electrical Engineering*, vol. 1, no. 2, pp. 104–106, 2013.

BIBLIOGRAPHY

- “Hydroacoustic data processing.” [Online]. Available: <https://echoview.com/>
- Akaike, H., “Information theory and an extension of the maximum likelihood principle,” in *Selected papers of hirotugu akaike*. Springer, 1998, pp. 199–213.
- Akinwande, M. O., Dikko, H. G., Samson, A., *et al.*, “Variance inflation factor: as a condition for the inclusion of suppressor variable (s) in regression analysis,” *Open Journal of Statistics*, vol. 5, no. 07, p. 754, 2015.
- Allredge, A. L., Cowles, T. J., MacIntyre, S., Rines, J. E., Donaghay, P. L., Greenlaw, C. F., Holliday, D., Deksheniaks, M. M., Sullivan, J. M., and Zaneveld, J. R. V., “Occurrence and mechanisms of formation of a dramatic thin layer of marine snow in a shallow pacific fjord,” *Marine Ecology Progress Series*, vol. 233, pp. 1–12, 2002.
- Aloisi, G., Bouloubassi, I., Heijs, S. K., Pancost, R. D., Pierre, C., Damsté, J. S. S., Gottschal, J. C., Forney, L. J., and Rouchy, J.-M., “Ch4-consuming microorganisms and the formation of carbonate crusts at cold seeps,” *Earth and Planetary Science Letters*, vol. 203, no. 1, pp. 195–203, 2002.
- Andersen, L. N., Chu, D., Heimvoll, H., Korneliussen, R., Macaulay, G. J., and Ona, E., “Quantitative processing of broadband data as implemented in a scientific splitbeam echosounder,” *arXiv preprint arXiv:2104.07248*, 2021.
- Anderson, T. R. and Tang, K. W., “Carbon cycling and poc turnover in the mesopelagic zone of the ocean: Insights from a simple model,” *Deep Sea Research Part II: Topical Studies in Oceanography*, vol. 57, no. 16, pp. 1581–1592, 2010.
- Åström, E. K., Carroll, M. L., Ambrose Jr, W. G., Sen, A., Silyakova, A., and Carroll, J., “Methane cold seeps as biological oases in the high-arctic deep sea,” *Limnology and Oceanography*, vol. 63, no. S1, pp. S209–S231, 2018.
- Aurioles-Gamboa, D., “Inshore-offshore movements of pelagic red crabs pleuroncodes planipes (decapoda, anomura, galatheaidae) off the pacific coast of baja california sur, mexico,” *Crustaceana*, pp. 71–84, 1992.
- Benfield, M. C., Grosjean, P., Culverhouse, P. F., Irigoien, X., Sieracki, M. E., Lopez-Urrutia, A., Dam, H. G., Hu, Q., Davis, C. S., Hansen, A., *et al.*, “Rapid: research on automated plankton identification,” *Oceanography*, vol. 20, no. 2, pp. 172–187, 2007.

- Benoit-Bird, K., Waluk, C., Welch, P., A. Barth, J., Wangen, I., McGill, P., Okuda, C., Hollinger, G., Sato, M., and Mccammon, S., “Equipping an underwater glider with a new echosounder to explore ocean ecosystems,” *Limnology and oceanography, methods*, 09 2018.
- Benoit-Bird, K. J., “Dynamic 3-dimensional structure of thin zooplankton layers is impacted by foraging fish,” *Marine Ecology Progress Series*, vol. 396, pp. 61–76, 2009.
- Benoit-Bird, K. J. and Au, W. W., “Echo strength and density structure of hawaiian mesopelagic boundary community patches,” *The Journal of the Acoustical Society of America*, vol. 114, no. 4, pp. 1888–1897, 2003.
- Benoit-Bird, K. J., Battaile, B. C., Heppell, S. A., Hoover, B., Irons, D., Jones, N., Kuletz, K. J., Nordstrom, C. A., Paredes, R., Suryan, R. M., *et al.*, “Prey patch patterns predict habitat use by top marine predators with diverse foraging strategies,” *PloS one*, vol. 8, no. 1, p. e53348, 2013.
- Benoit-Bird, K. J., Cowles, T. J., and Wingard, C. E., “Edge gradients provide evidence of ecological interactions in planktonic thin layers,” *Limnology and Oceanography*, vol. 54, no. 4, pp. 1382–1392, 2009.
- Benoit-Bird, K. J. and McManus, M. A., “A critical time window for organismal interactions in a pelagic ecosystem,” *PLoS One*, vol. 9, no. 5, p. e97763, 2014.
- Benoit-Bird, K. J., Moline, M. A., and Southall, B. L., “Prey in oceanic sound scattering layers organize to get a little help from their friends,” *Limnology and Oceanography*, vol. 62, no. 6, pp. 2788–2798, 2017. [Online]. Available: <https://aslopubs.onlinelibrary.wiley.com/doi/abs/10.1002/lno.10606>
- Benoit-Bird, K. J. and Waluk, C. M., “Exploring the promise of broadband fisheries echosounders for species discrimination with quantitative assessment of data processing effects,” *The Journal of the Acoustical Society of America*, vol. 147, no. 1, pp. 411–427, 2020.
- Benoit-Bird, K. J., Zirbel, M. J., and McManus, M. A., “Diel variation of zooplankton distributions in hawaiian waters favors horizontal diel migration by midwater micronekton,” *Marine Ecology Progress Series*, vol. 367, pp. 109–123, 2008.
- Bianchi, D. and Mislán, K., “Global patterns of diel vertical migration times and velocities from acoustic data,” *Limnology and Oceanography*, vol. 61, no. 1, pp. 353–364, 2016.
- Bianchi, D., Stock, C., Galbraith, E. D., and Sarmiento, J. L., “Diel vertical migration: Ecological controls and impacts on the biological pump in a one-dimensional ocean model,” *Global Biogeochemical Cycles*, vol. 27, no. 2, pp. 478–491, 2013.

- Birch, D. A., Young, W. R., and Franks, P. J., “Plankton layer profiles as determined by shearing, sinking, and swimming,” *Limnology and Oceanography*, pp. 397–399, 2009.
- Boswell, K. M., D’Elia, M., Johnston, M. W., Mohan, J. A., Warren, J. D., Wells, R., and Sutton, T. T., “Oceanographic structure and light levels drive patterns of sound scattering layers in a low-latitude oceanic system,” *Frontiers in Marine Science*, vol. 7, p. 51, 2020.
- Boyd, C. M., “The benthic and pelagic habitats of the red crab, pleuroncodes planipes,” 1967.
- Bradley, S. D., “Optimizing a scheme for run length encoding,” *Proceedings of the IEEE*, vol. 57, no. 1, pp. 108–109, 1969.
- Brierley, A. S., Ward, P., Watkins, J. L., and Goss, C., “Acoustic discrimination of southern ocean zooplankton,” *Deep Sea Research Part II: Topical Studies in Oceanography*, vol. 45, no. 7, pp. 1155–1173, 1998.
- Cheriton, O., McManus, M., Stacey, M., and Steinbuck, J., “Physical and biological controls on the maintenance and dissipation of a thin phytoplankton layer,” *Marine Ecology Progress Series*, vol. 378, pp. 55–69, 2009.
- Chu, D. and Stanton, T. K., “Statistics of echoes from a directional sonar beam insonifying finite numbers of single scatterers and patches of scatterers,” *IEEE journal of oceanic engineering*, vol. 35, no. 2, pp. 267–277, 2010.
- Colbo, K., Ross, T., Brown, C., and Weber, T., “A review of oceanographic applications of water column data from multibeam echosounders,” *Estuarine, Coastal and Shelf Science*, vol. 145, pp. 41–56, 2014. [Online]. Available: <https://www.sciencedirect.com/science/article/pii/S0272771414000900>
- Cook, R. D., “Influential observations in linear regression,” *Journal of the American Statistical Association*, vol. 74, no. 365, pp. 169–174, 1979.
- Corgnati, L., Marini, S., Mazzei, L., Ottaviani, E., Aliani, S., Conversi, A., and Griffa, A., “Looking inside the ocean: Toward an autonomous imaging system for monitoring gelatinous zooplankton,” *Sensors*, vol. 16, no. 12, p. 2124, 2016.
- Cowen, R. K., Greer, A. T., Guigand, C. M., Hare, J. A., Richardson, D. E., and Walsh, H. J., “Evaluation of the in situ ichthyoplankton imaging system (isiis): Comparison with the traditional (bongo net) sampler,” 2013.
- Culverhouse, P. F., Williams, R., Benfield, M., Flood, P. R., Sell, A. F., Mazzocchi, M. G., Buttino, I., and Sieracki, M., “Automatic image analysis of plankton: future perspectives,” *Marine Ecology Progress Series*, vol. 312, pp. 297–309, 2006.

- Cushman-Roisin, B. and Beckers, J.-M., “Stratification,” in *International Geophysics*. Elsevier, 2011, vol. 101, pp. 347–364.
- Davis, C. S., Gallagher, S. M., Marra, M., and Stewart, W. K., “Rapid visualization of plankton abundance and taxonomic composition using the video plankton recorder,” *Deep Sea Research Part II: Topical Studies in Oceanography*, vol. 43, no. 7-8, pp. 1947–1970, 1996.
- Davison, P., Checkley Jr, D., Koslow, J., and Barlow, J., “Carbon export mediated by mesopelagic fishes in the northeast pacific ocean,” *Progress in Oceanography*, vol. 116, pp. 14–30, 2013.
- De Robertis, A. and Higginbottom, I., “A post-processing technique to estimate the signal-to-noise ratio and remove echosounder background noise,” *ICES Journal of Marine Science*, vol. 64, no. 6, pp. 1282–1291, 2007.
- De Robertis, A., Jaffe, J. S., and Ohman, M. D., “Size-dependent visual predation risk and the timing of vertical migration in zooplankton,” *Limnology and Oceanography*, vol. 45, no. 8, pp. 1838–1844, 2000.
- Dekshenieks, M. M., Donaghay, P. L., Sullivan, J. M., Rines, J. E., Osborn, T. R., and Twardowski, M. S., “Temporal and spatial occurrence of thin phytoplankton layers in relation to physical processes,” *Marine Ecology Progress Series*, vol. 223, pp. 61–71, 2001.
- D’elia, M., Warren, J. D., Rodriguez-Pinto, I., Sutton, T. T., Cook, A., and Boswell, K. M., “Diel variation in the vertical distribution of deep-water scattering layers in the gulf of mexico,” *Deep Sea Research Part I: Oceanographic Research Papers*, vol. 115, pp. 91–102, 2016.
- Demer, D., Andersen, L., Bassett, C., Berger, L., Chu, D., Condiotty, J., and Cutter, G., “Evaluation of a wideband echosounder for fisheries and marine ecosystem science,” *ICES Cooperative Research Report*, no. 336, 2017.
- Demer, D. A., Berger, L., Bernasconi, M., Bethke, E., Boswell, K., Chu, D., Domokos, R., Dunford, A., Fassler, S., Gauthier, S., *et al.*, “Calibration of acoustic instruments.” 2015.
- Demer, D. A. and Renfree, J. S., “Variations in echosounder–transducer performance with water temperature,” *ICES Journal of Marine Science*, vol. 65, no. 6, pp. 1021–1035, 2008.
- Denman, K. L. and Powell, T. M., “Effects of physical processes on planktonic ecosystems in the coastal ocean,” *Oceanogr. Mar. Biol. Ann. Rev.*, vol. 22, pp. 125–168, 1984.
- Diner, N., “Correction on school geometry and density: approach based on acoustic image simulation,” *Aquatic Living Resources*, vol. 14, no. 4, pp. 211–222, 2001.

- Easson, C. G., Boswell, K. M., Tucker, N., Warren, J. D., and Lopez, J. V., “Combined edna and acoustic analysis reflects diel vertical migration of mixed consortia in the gulf of mexico,” *Frontiers in Marine Science*, 2020.
- Fernandes, P. G., Stevenson, P., Brierley, A. S., Armstrong, F., and Simmonds, E. J., “Autonomous underwater vehicles: future platforms for fisheries acoustics,” *ICES Journal of Marine Science*, vol. 60, no. 3, pp. 684–691, 2003.
- Fu, L.-L. and Ferrari, R., “Observing oceanic submesoscale processes from space,” *Eos, Transactions American Geophysical Union*, vol. 89, no. 48, pp. 488–488, 2008.
- Gallager, S. M., Yamazaki, H., and Davis, C. S., “Contribution of fine-scale vertical structure and swimming behavior to formation of plankton layers on georges bank,” *Marine Ecology Progress Series*, vol. 267, pp. 27–43, 2004.
- Gartner Jr, J. V., Conley, W. J., and Hopkins, T. L., “A case study using lantern-fishes (pisces: Myctophidae),” *Fishery Bulletin*, vol. 87, no. 1, p. 213, 1989.
- Gawarkiewicz, G. and Chapman, D. C., “The role of stratification in the formation and maintenance of shelf-break fronts,” *Journal of Physical Oceanography*, vol. 22, no. 7, pp. 753–772, 1992.
- González, P., Álvarez, E., Díez, J., López-Urrutia, Á., and del Coz, J. J., “Validation methods for plankton image classification systems,” *Limnology and Oceanography: Methods*, vol. 15, no. 3, pp. 221–237, 2017.
- Greene, C. H., Wiebe, P. H., Pershing, A. J., Gal, G., Popp, J. M., Copley, N. J., Austin, T. C., Bradley, A. M., Goldsborough, R. G., Dawson, J., *et al.*, “Assessing the distribution and abundance of zooplankton: a comparison of acoustic and net-sampling methods with d-bad mocness,” *Deep Sea Research Part II: Topical Studies in Oceanography*, vol. 45, no. 7, pp. 1219–1237, 1998.
- Greer, A. T., Boyette, A. D., Cruz, V. J., Cambazoglu, M. K., Dzwonkowski, B., Chiaverano, L. M., Dykstra, S. L., Briseño-Avena, C., Cowen, R. K., and Wiggert, J. D., “Contrasting fine-scale distributional patterns of zooplankton driven by the formation of a diatom-dominated thin layer,” *Limnology and Oceanography*, vol. 65, no. 9, pp. 2236–2258, 2020.
- Greer, A. T., Cowen, R. K., Guigand, C. M., and Hare, J. A., “Fine-scale planktonic habitat partitioning at a shelf-slope front revealed by a high-resolution imaging system,” *Journal of Marine Systems*, vol. 142, pp. 111–125, 2015.
- Greer, A. T., Cowen, R. K., Guigand, C. M., Hare, J. A., and Tang, D., “The role of internal waves in larval fish interactions with potential predators and prey,” *Progress in Oceanography*, vol. 127, pp. 47–61, 2014.

- Guihen, D., Fielding, S., Murphy, E. J., Heywood, K. J., and Griffiths, G., “An assessment of the use of ocean gliders to undertake acoustic measurements of zooplankton: the distribution and density of antarctic krill (*euphausia superba*) in the weddell sea.” *Limnology and Oceanography: Methods*, vol. 12, no. 6, pp. 373–389, 2014.
- Haris, K., Kloser, R. J., Ryan, T. E., and Malan, J., “Deep-water calibration of echosounders used for biomass surveys and species identification,” *ICES Journal of Marine Science*, vol. 75, no. 3, pp. 1117–1130, 2018.
- Haury, L., McGowan, J., and Wiebe, P., “Patterns and processes in the time-space scales of plankton distributions,” in *Spatial pattern in plankton communities*. Springer, 1978, pp. 277–327.
- Herman, A. W., Beanlands, B., Chin-Yee, M., Furlong, A., Snow, J., Young, S., and Phillips, T., “The Moving Vessel Profiler (MVP): In-situ sampling of plankton and physical parameters at 12 kts and the integration of a new laser/optical plankton counter,” in *Proceedings of Oceanology International*, vol. 102, 1998, pp. 123–135.
- Hernández-Hernández, N., Arístegui, J., Montero, M. F., Velasco-Senovilla, E., Baltar, F., Marrero-Díaz, Á., Martínez-Marrero, A., and Rodríguez-Santana, Á., “Drivers of plankton distribution across mesoscale eddies at submesoscale range,” *Frontiers in Marine Science*, vol. 7, p. 667, 2020.
- Holliday, D. and Pieper, R., “Bioacoustical oceanography at high frequencies,” *ICES Journal of marine Science*, vol. 52, no. 3-4, pp. 279–296, 1995.
- Holliday, D., Pieper, R., Greenlaw, C., and Dawson, J., “Acoustical sensing of small-scale vertical structures in zooplankton assemblages,” *Oceanography*, vol. 11, no. 1, pp. 18–23, 1998.
- Holliday, D., Pieper, R., and Kleppel, G., “Determination of zooplankton size and distribution with multifrequency acoustic technology,” *ICES Journal of Marine Science*, vol. 46, no. 1, pp. 52–61, 1989.
- Hooff, R. C. and Peterson, W. T., “Copepod biodiversity as an indicator of changes in ocean and climate conditions of the northern california current ecosystem,” *Limnology and Oceanography*, vol. 51, no. 6, pp. 2607–2620, 2006.
- Houghton, R. W., Olson, D. B., and Celone, P. J., “Observation of an anticyclonic eddy near the continental shelf break south of new england,” *Journal of Physical Oceanography*, vol. 16, no. 1, pp. 60–71, 1986.
- Iida, K., Mukai, T., and Hwang, D., “Relationship between acoustic backscattering strength and density of zooplankton in the sound-scattering layer,” *ICES Journal of Marine Science*, vol. 53, no. 2, pp. 507–512, 1996.

- Irigoién, X., Klevjer, T. A., Røstad, A., Martínez, U., Boyra, G., Acuña, J. L., Bode, A., Echevarría, F., González-Gordillo, J. I., Hernández-León, S., *et al.*, “Large mesopelagic fishes biomass and trophic efficiency in the open ocean,” *Nature communications*, vol. 5, no. 1, pp. 1–10, 2014.
- Kaartvedt, S., Staby, A., and Aksnes, D. L., “Efficient trawl avoidance by mesopelagic fishes causes large underestimation of their biomass,” *Marine Ecology Progress Series*, vol. 456, pp. 1–6, 2012.
- Katz, E. J. and Witzell Jr, W. E., “A depth controlled tow system for hydrographic and current measurements with applications,” *Deep Sea Research Part A. Oceanographic Research Papers*, vol. 26, no. 5, pp. 579–596, 1979.
- Kelly, T. B., Davison, P. C., Goericke, R., Landry, M. R., Ohman, M. D., and Stukel, M. R., “The importance of mesozooplankton diel vertical migration for sustaining a mesopelagic food web,” *Frontiers in Marine Science*, vol. 6, p. 508, 2019.
- Klevjer, T., Torres, D., and Kaartvedt, S., “Distribution and diel vertical movements of mesopelagic scattering layers in the red sea,” *Marine Biology*, vol. 159, 08 2012.
- Klevjer, T. A., Irigoien, X., Røstad, A., Fraile-Nuez, E., Benítez-Barrios, V. M., and Kaartvedt, S., “Large scale patterns in vertical distribution and behaviour of mesopelagic scattering layers,” *Scientific Reports*, vol. 6, no. 1, pp. 1–11, 2016.
- Kloser, R. J., “Improved precision of acoustic surveys of benthopelagic fish by means of a deep-towed transducer,” *ICES Journal of Marine Science*, vol. 53, no. 2, pp. 407–413, 1996.
- Kloser, R. J., Ryan, T. E., Keith, G., and Gershwin, L., “Deep-scattering layer, gas-bladder density, and size estimates using a two-frequency acoustic and optical probe,” *ICES Journal of Marine Science*, vol. 73, no. 8, pp. 2037–2048, 01 2016. [Online]. Available: <https://doi.org/10.1093/icesjms/fsv257>
- Koslow, J. A., Davison, P., Lara-Lopez, A., and Ohman, M. D., “Epipelagic and mesopelagic fishes in the southern california current system: Ecological interactions and oceanographic influences on their abundance,” *Journal of Marine Systems*, vol. 138, pp. 20–28, 2014.
- Kubilius, R., Ona, E., and Calise, L., “Measuring in situ krill tilt orientation by stereo photogrammetry: examples for euphausia superba and meganyctiphanes norvegica,” *ICES Journal of Marine Science*, vol. 72, no. 8, pp. 2494–2505, 2015.

- Lavery, A. C., Bassett, C., Lawson, G. L., and Jech, J. M., “Exploiting signal processing approaches for broadband echosounders,” *ICES Journal of Marine Science*, vol. 74, no. 8, pp. 2262–2275, 2017.
- Lavery, A. C., Stanton, T. K., Jech, J. M., and Wiebe, P., “An advanced sensor platform for acoustic quantification of the ocean twilight zone,” *The Journal of the Acoustical Society of America*, vol. 145, no. 3, pp. 1653–1653, 2019. [Online]. Available: <https://doi.org/10.1121/1.5101063>
- Legendre, L. and Demers, S., “Towards dynamic biological oceanography and limnology,” *Canadian Journal of Fisheries and Aquatic Sciences*, vol. 41, no. 1, pp. 2–19, 1984.
- Lévy, M., Franks, P. J., and Smith, K. S., “The role of submesoscale currents in structuring marine ecosystems,” *Nature communications*, vol. 9, no. 1, pp. 1–16, 2018.
- Longhurst, A. R. and Harrison, W. G., “The biological pump: profiles of plankton production and consumption in the upper ocean,” *Progress in Oceanography*, vol. 22, no. 1, pp. 47–123, 1989.
- Luo, J. Y., Grassian, B., Tang, D., Irisson, J.-O., Greer, A. T., Guigand, C. M., McClatchie, S., and Cowen, R. K., “Environmental drivers of the fine-scale distribution of a gelatinous zooplankton community across a mesoscale front,” *Marine Ecology Progress Series*, vol. 510, pp. 129–149, 2014.
- Maas, A. E., Frazar, S. L., Outram, D. M., Seibel, B. A., and Wishner, K. F., “Fine-scale vertical distribution of macroplankton and micronekton in the eastern tropical north pacific in association with an oxygen minimum zone,” *Journal of plankton research*, vol. 36, no. 6, pp. 1557–1575, 2014.
- Marouchos, A., Sherlock, M., Kloser, R. J., Ryan, T., and Cordell, J., “A profiling acoustic and optical system (paos) for pelagic studies; prototype development and testing,” *OCEANS 2016 - Shanghai*, pp. 1–6, 2016.
- McManus, M., Alldredge, A., Barnard, A., Boss, E., Case, J., Cowles, T., Donaghay, P., Eisner, L., Gifford, D., Greenlaw, C., *et al.*, “Characteristics, distribution and persistence of thin layers over a 48 hour period,” *Marine Ecology Progress Series*, vol. 261, pp. 1–19, 2003.
- Moline, M. A., Benoit-Bird, K., O’Gorman, D., and Robbins, I. C., “Integration of scientific echo sounders with an adaptable autonomous vehicle to extend our understanding of animals from the surface to the bathypelagic,” *Journal of Atmospheric and Oceanic Technology*, vol. 32, no. 11, pp. 2173–2186, 2015. [Online]. Available: <https://doi.org/10.1175/JTECH-D-15-0035.1>

- Nelson, J. S., Grande, T. C., and Wilson, M. V., *Fishes of the World*. John Wiley and Sons, 2016.
- Netburn, A. N. and Anthony Koslow, J., “Dissolved oxygen as a constraint on daytime deep scattering layer depth in the southern california current ecosystem,” *Deep Sea Research Part I: Oceanographic Research Papers*, vol. 104, pp. 149 – 158, 2015. [Online]. Available: <http://www.sciencedirect.com/science/article/pii/S0967063715001107>
- Ortner, P. B., Wiebe, P. H., Haury, L., and Boyd, S., “Variability in zooplankton biomass distribution in the northern sargasso sea: the contribution of gulf stream cold core rings,” *Fishery Bulletin*, vol. 76, no. 2, pp. 323–334, 1978.
- O’Driscoll, R., Oeffner, J., Ross, O., Dunford, A., and McMillan, P., “Pilot acoustic survey for jack mackerel on the west coast new zealand (jma7),” *New Zealand Fisheries Assessment Report*, vol. 1, pp. 1–53, 2013.
- Pascual, A., Ruiz, S., Olita, A., Troupin, C., Claret, M., Casas, B., Mourre, B., Poulain, P.-M., Tovar-Sanchez, A., Capet, A., *et al.*, “A multiplatform experiment to unravel meso-and submesoscale processes in an intense front (al-borex),” *Frontiers in Marine Science*, vol. 4, p. 39, 2017.
- Patel, R., Handegard, N. O., and Godø, O. R., “Behaviour of herring (*clupea harengus* l.) towards an approaching autonomous underwater vehicle,” *ICES Journal of Marine Science*, vol. 61, no. 7, pp. 1044–1049, 2004.
- Pollard, R., “Frontal surveys with a towed profiling conductivity/temperature/depth measurement package (SeaSoar),” *Nature*, vol. 323, p. 433–435, 1986.
- Proud, R., Handegard, N. O., Kloser, R. J., Cox, M. J., and Brierley, A. S., “From siphonophores to deep scattering layers: uncertainty ranges for the estimation of global mesopelagic fish biomass,” *ICES Journal of Marine Science*, vol. 76, no. 3, pp. 718–733, 04 2018. [Online]. Available: <https://doi.org/10.1093/icesjms/fsy037>
- Remsen, A., Hopkins, T. L., and Samson, S., “What you see is not what you catch: a comparison of concurrently collected net, optical plankton counter, and shadowed image particle profiling evaluation recorder data from the northeast gulf of mexico,” *Deep Sea Research Part I: Oceanographic Research Papers*, vol. 51, no. 1, pp. 129–151, 2004.
- Rienecker, M. M. and Mooers, C. N., “Mesoscale eddies, jets, and fronts off point arena, california, july 1986,” *Journal of Geophysical Research: Oceans*, vol. 94, no. C9, pp. 12 555–12 569, 1989.

- Robinson, C. J. and Goómez-Gutierrez, J., “The red-crab bloom off the west coast of baja california, mexico,” *Journal of plankton research*, vol. 20, no. 10, pp. 2009–2016, 1998.
- Robinson, C., Steinberg, D. K., Anderson, T. R., Aristegui, J., Carlson, C. A., Frost, J. R., Ghiglione, J.-F., Hernández-León, S., Jackson, G. A., Koppelman, R., *et al.*, “Mesopelagic zone ecology and biogeochemistry—a synthesis,” *Deep Sea Research Part II: Topical Studies in Oceanography*, vol. 57, no. 16, pp. 1504–1518, 2010.
- Roman, C., Ullman, D. S., Hebert, D., and Licht, S., “The Wire Flyer Towed Profiling System,” *Journal of Atmospheric and Oceanic Technology*, vol. 36, no. 2, pp. 161–182, 2019. [Online]. Available: <https://doi.org/10.1175/JTECH-D-17-0180.1>
- Roman, M. R., Holliday, D. V., and Sanford, L. P., “Temporal and spatial patterns of zooplankton in the chesapeake bay turbidity maximum,” *Marine Ecology Progress Series*, vol. 213, pp. 215–227, 2001.
- Rousselet, L., De Verneil, A., Doglioli, A. M., Petrenko, A. A., Duhamel, S., Maes, C., and Blanke, B., “Large-to submesoscale surface circulation and its implications on biogeochemical/biological horizontal distributions during the outpace cruise (southwest pacific),” *Biogeosciences*, vol. 15, no. 8, 2018.
- Rudnick, D. L. and Klinke, J., “The Underway Conductivity Temperature Depth Instrument,” *Journal of Atmospheric and Oceanic Technology*, vol. 24, pp. 1910–1923, 2007.
- Scalabrin, C., Marfia, C., and Boucher, J., “How much fish is hidden in the surface and bottom acoustic blind zones?” *ICES J. Mar. Sci.*, vol. 66, 06 2009.
- Schmitz, O. J., Miller, J. R., Trainor, A. M., and Abrahms, B., “Toward a community ecology of landscapes: predicting multiple predator–prey interactions across geographic space,” *Ecology*, vol. 98, no. 9, pp. 2281–2292, 2017.
- Seibel, B. A., Luu, B. E., Tessier, S. N., Towanda, T., and Storey, K. B., “Metabolic suppression in the pelagic crab, pleuroncodes planipes, in oxygen minimum zones,” *Comparative Biochemistry and Physiology Part B: Biochemistry and Molecular Biology*, vol. 224, pp. 88–97, 2018.
- Seibert, J. A., Boone, J. M., and Lindfors, K. K., “Flat-field correction technique for digital detectors,” in *Medical Imaging 1998: Physics of Medical Imaging*, vol. 3336. SPIE, 1998, pp. 348–354.
- Siegelman, L., O’toole, M., Flexas, M., Rivière, P., and Klein, P., “Submesoscale ocean fronts act as biological hotspot for southern elephant seal,” *Scientific reports*, vol. 9, no. 1, pp. 1–13, 2019.

- Sieracki, M. E., Benfield, M., Hanson, A., Davis, C., Pilskaln, C. H., Checkley, D., Sosik, H. M., Ashjian, C., Culverhouse, P., Cowen, R., *et al.*, “Optical plankton imaging and analysis systems for ocean observation,” *Proc. Ocean Obs*, vol. 9, pp. 21–25, 2010.
- Simmonds, J. and MacLennan, D. N., *Fisheries acoustics: theory and practice*. John Wiley and Sons, 2008.
- Sinclair, E. and Stabeno, P., “Mesopelagic nekton and associated physics of the southeastern bering sea,” *Deep Sea Research Part II: Topical Studies in Oceanography*, vol. 49, no. 26, pp. 6127–6145, 2002.
- St John, M. A., Borja, A., Chust, G., Heath, M., Grigorov, I., Mariani, P., Martin, A. P., and Santos, R. S., “A dark hole in our understanding of marine ecosystems and their services: perspectives from the mesopelagic community,” *Frontiers in Marine Science*, vol. 3, p. 31, 2016.
- Stanton, T. K., Lee, W.-J., and Baik, K., “Echo statistics associated with discrete scatterers: A tutorial on physics-based methods,” *The Journal of the Acoustical Society of America*, vol. 144, no. 6, pp. 3124–3171, 2018.
- Steele, J. H., “Can ecological theory cross the land-sea boundary?” *Journal of Theoretical Biology*, vol. 153, no. 3, pp. 425–436, 1991.
- Suberg, L., Wynn, R. B., Van Der Kooij, J., Fernand, L., Fielding, S., Guihen, D., Gillespie, D., Johnson, M., Gkikopoulou, K. C., Allan, I. J., *et al.*, “Assessing the potential of autonomous submarine gliders for ecosystem monitoring across multiple trophic levels (plankton to cetaceans) and pollutants in shallow shelf seas,” *Methods in Oceanography*, vol. 10, pp. 70–89, 2014.
- Sullivan, J. M., Donaghay, P. L., and Rines, J. E., “Coastal thin layer dynamics: consequences to biology and optics,” *Continental shelf research*, vol. 30, no. 1, pp. 50–65, 2010.
- Sundermeyer, M. A. and Ledwell, J. R., “Lateral dispersion over the continental shelf: Analysis of dye release experiments,” *Journal of Geophysical Research: Oceans*, vol. 106, no. C5, pp. 9603–9621, 2001.
- Sutton, T. T., “Vertical ecology of the pelagic ocean: classical patterns and new perspectives,” *Journal of Fish Biology*, vol. 83, no. 6, pp. 1508–1527, 2013. [Online]. Available: <https://onlinelibrary.wiley.com/doi/abs/10.1111/jfb.12263>
- Sutton, T. T., Clark, M. R., Dunn, D. C., Halpin, P. N., Rogers, A. D., Guinotte, J., Bograd, S. J., Angel, M. V., Perez, J. A. A., Wishner, K., *et al.*, “A global biogeographic classification of the mesopelagic zone,” *Deep Sea Research Part I: Oceanographic Research Papers*, vol. 126, pp. 85–102, 2017.

- Underwood, M. J., García-Seoane, E., Klevjer, T., Macaulay, G. J., and Melle, W., “An acoustic method to observe the distribution and behaviour of mesopelagic organisms in front of a trawl,” *Deep Sea Research Part II: Topical Studies in Oceanography*, p. 104873, 2020.
- Urmy, S. S. and Benoit-Bird, K. J., “Fear dynamically structures the ocean’s pelagic zone,” *Current Biology*, vol. 31, no. 22, pp. 5086–5092, 2021.
- Urmy, S. S., Benoit-Bird, K. J., Ryan, J. P., and Horne, J. K., “Mesopelagic predator-prey interactions revealed by joint passive and active acoustic observations,” *The Journal of the Acoustical Society of America*, vol. 146, no. 4, pp. 2899–2899, 2019.
- Wiebe, P., Stanton, T., Greene, C., Benfield, M., Sosik, H., Austin, T., Warren, J., and Hammar, T., “BIOMAPER-II: An integrated instrument platform for coupled biological and physical measurements in coastal and oceanic regimes,” *IEEE Journal of Oceanic Engineering*, vol. 27, pp. 700 – 716, 08 2002.
- Wiebe, P. H. and Benfield, M. C., “From the hensen net toward four-dimensional biological oceanography,” *Progress in Oceanography*, vol. 56, no. 1, pp. 7–136, 2003.
- Wiebe, P. H., Copley, N. J., and Boyd, S. H., “Coarse-scale horizontal patchiness and vertical migration of zooplankton in gulf stream warm-core ring 82-h,” *Deep Sea Research Part A. Oceanographic Research Papers*, vol. 39, pp. S247–S278, 1992.
- Wiebe, P. H., Stanton, T. K., Greene, C. H., Benfield, M. C., Sosik, H. M., Austin, T. C., Warren, J. D., and Hammar, T., “Biomaper-ii: an integrated instrument platform for coupled biological and physical measurements in coastal and oceanic regimes,” *IEEE Journal of Oceanic Engineering*, vol. 27, no. 3, pp. 700–716, 2002.
- Wishner, K. F., Seibel, B. A., Roman, C., Deutsch, C., Outram, D., Shaw, C. T., Birk, M. A., Mislán, K. A. S., Adams, T. J., Moore, D., and Riley, S., “Ocean deoxygenation and zooplankton: Very small oxygen differences matter,” *Science Advances*, vol. 4, no. 12, 2018. [Online]. Available: <http://advances.sciencemag.org/content/4/12/eaau5180>
- Wishner, K. F., Gowing, M. M., and Gelfman, C., “Mesozooplankton biomass in the upper 1000 m in the arabian sea: overall seasonal and geographic patterns, and relationship to oxygen gradients,” *Deep Sea Research Part II: Topical Studies in Oceanography*, vol. 45, no. 10-11, pp. 2405–2432, 1998.
- Wishner, K. F., Outram, D. M., Seibel, B. A., Daly, K. L., and Williams, R. L., “Zooplankton in the eastern tropical north pacific: Boundary effects of oxygen

minimum zone expansion,” *Deep Sea Research Part I: Oceanographic Research Papers*, vol. 79, pp. 122–140, 2013.

Xie, G. and Lu, W., “Image edge detection based on opencv,” *International Journal of Electronics and Electrical Engineering*, vol. 1, no. 2, pp. 104–106, 2013.

Yamamoto, T. and Nishizawa, S., “Small-scale zooplankton aggregations at the front of a kuroshio warm-core ring,” *Deep Sea Research Part A. Oceanographic Research Papers*, vol. 33, no. 11-12, pp. 1729–1740, 1986.